Studies on Power Generation in Water Lettuce (*Pistia stratiotes*) Assisted Sediment Microbial Fuel Cell

A Thesis

Submitted in the partial fulfilment of the requirements for the degree of

Doctor of Philosophy

by

ARUP DUTTA

School of Energy Science and Engineering

Indian Institute of Technology Guwahati

Guwahati-781039, Assam, India

April 2025

INDIAN INSTITUTE OF TECHNOLOGY GUWAHATI
School of Energy Science and Engineering
Guwahati – 781039, Assam, India

STATEMENT

I do hereby declare that the matter incorporated in this thesis is the result of investigations carried out by me in the School of Energy Science and Engineering, Indian Institute of Technology Guwahati, India, under the guidance of Prof. Pranab Goswami and Dr. Lepakshi Barbora.

In keeping with the general practice of reporting scientific observations, due acknowledgements have been made wherever the work described is based on the findings of other investigations.

April 2025

Arup Dutta
Roll no. 186151002

INDIAN INSTITUTE OF TECHNOLOGY GUWAHATI
School of Energy Science and Engineering
Guwahati – 781039, Assam, India

CERTIFICATE

This is to certify that the thesis entitled **"Studies on Power Generation in Water Lettuce (*Pistia stratiotes*) Assisted Sediment Microbial Fuel Cell"** that is being submitted by **Arup Dutta** (Roll no. 186151002) for the award of the degree of Doctor of Philosophy is an authentic record of the results obtained from the research work carried out under my supervision in the School of Energy Science and Engineering, Indian Institute of Technology Guwahati, Assam, India.

The results incorporated in this thesis have not been submitted to any other University or Institute for the award of any degree.

April 2025

Prof. Pranab Goswami
Department of Biosciences and Bioengineering
(Research Supervisor)

Dr. Lepakshi Barbora
School of Energy Science and Engineering
(Research Co-Supervisor)

ACKNOWLEDGEMENT

I am obliged to take the opportunity of this column to acknowledge all those whose contribution and support helped me immensely in successful completion of my PhD.

I am deeply indebted for the invaluable guidance, constant encouragement, countless help and support of my supervisor Prof. Pranab Goswami, Department of Biosciences and Bioengineering, IIT Guwahati and my co-supervisor Dr. Lepakshi Barbora, School of Energy Science and Engineering, IIT Guwahati.

I would like to express my sincere gratitude to Prof. Vaibhav Vasant Goud, HoS School of Energy Science and Engineering and my doctoral committee Prof. Vijayanand S. Moholkar, Prof. Sisir Kumar Nayak and Dr. Pankaj Kalita for their guidance and encouragement during the thesis work.

I am grateful to all the former and current staff members of School of Energy Science and Engineering and research scholars of School of Energy Science and Engineering for their constant help and support.

I thank Centre for Excellence facility of Department of Biosciences and Bioengineering, Central Instruments Facility, IIT Guwahati for proving the access to the various facilities for conducting the research work smoothly.

I thank Ministry of Human Resource and Development (MHRD), Govt. of India, Department of Science and Technology (DST), Govt. of India, and Department of Biotechnology (DBT), Govt. of India for providing all the financial assistance and the platform for the smooth conduction of the research work.

I am obliged to receive help, support and encouragement from my seniors Dr. Priyanki Das, Dr. Mohd. Golam Abdul Quadir, Dr. Smita Das; juniors Nabajyoti, Aparupa, Mohit, Malaya, Kangkana; and friends Barlina, Rashmi, Gaurav, Sayantan for the successful accomplishment of my PhD work.

Lastly, I would like to express my deep sense of gratitude to my parents, my brother and my wife for their unconditional love and moral support during the course of the PhD journey. Thanks to the Almighty for bestowing all his blessings to complete the thesis work.

Arup Dutta

April 2025

ABSTRACT

Sediment microbial fuel cells (SMFCs) are emerging as a promising green energy technology with enormous application potential for wastewater treatment and linked electrical energy production. However, the practical application of these devices is challenged by their low-performance factors pertaining to the imbalanced electrolyte and oxygen levels and weak cathodic functions in open environment conditions. This study explored to address the poor performance of the SMFC by coupling it with a free-floating aquatic plant, Water lettuce. Growth of the plant balanced the catholyte pH in the range of 7.2–7.6, increased the ionic conductivity by 60%, stabilized the sub-surface water oxygen level, and boosted the cathodic potential by ~ 102 mV and ~ 49 mV in open and close circuit operations mode, respectively. The cumulative effect of these inputs led to producing a power density of 22.45 mW/m^2 and a current density of 136.84 mA/m^2 at 2 kΩ and 50 Ω loads, respectively. The enhanced cathodic performance was also attributed to the colonization of Water lettuce root bacteria as biofilm on the cathode that supported catalytic oxygen reduction on the graphite electrode. Metagenomic analysis indicated the biofilm is created mostly by aerobic microbes such as *Ferrovibrio terrae, Comamonas aquatic, Achromobacter xylosoxidans, Hydrogenophaga taeniospiralis* etc. bearing catalase enzyme, *Pannonibacter phragmitetus, Streptococcus pyogenes*, *Streptococcus mutans* etc. bearing heme enzyme and these microbes synergistically catalysed cathodic reduction reactions. This study demonstrated the positive role of Water lettuce in boosting the power performance of SMFC mainly by activating the cathodic functions of the setup. The progress of this innovative green energy technology destined for open environment applications is also mired by their inherent low voltage generation. A solution to improve the voltage level is to stack several unit cells through series or parallel connections. Paradoxically, such stacks frequently encounter voltage reversal (VR), which grossly affects their performance. Thus this study also presents strategy to mitigate VR in stacked water lettuce-assisted SMFCs (WL-SMFCs) by tuning the anodic surface area. A theoretical framework was first developed to relate electrical parameters to anodic surface area, predicting that increasing the anodic surface area of the terminal unit would enhance the overall stack voltage. This prediction was experimentally validated using a laboratory-scale stack of series-connected WL-SMFC units. When the anodic surface area of the terminal unit was increased to match the total anodic surface area of all other units combined, VR was significantly reduced. In two-, three-, and four-unit stacks, VR decreased by 70%, 57%, and 54%, respectively. Electrochemical impedance spectroscopic analysis

confirms the corresponding increase in anodic storage charge (C) to 318.25±12.35 (670±26), 453.08±12.12 (964±26), and 422.92±9.39 (872±19) from the unit value of 240.58±25.65 (523±55) with respective capacitance (pF) values shown in brackets. This anodic surface area tuning approach offers a technically simple, self-sustaining, and cost-effective solution for alleviating VR, thereby enhancing the feasibility of SMFCs for open-environment applications. Herein, another effort has been made to increase the power output of plant-assisted sediment MFCs, using a power management system (PMS). Water lettuce-assisted sediment MFCs with a reactor volume of 500 ml were constructed, and four stacks were made, each with two cell units connected in series. When each of the stacks was connected to a charge pump, the voltage increased to double with an efficiency of 97.15±0.01%. The output of the four charge pumps was cascaded for charging a pair of 3300 µF capacitors, which were then discharged in series through a 0.5 F supercapacitor. With the input from the capacitors, the time for charging the supercapacitor was 35 hours that generated 3.5 V, which is ~61.5% of its maximum voltage limit (5.69 V). At the maximum operating point for the stacks (10 kΩ load), the PMS delivers ~0.92 mW, which is 7.13 times the total power delivered by the stacks. The maximum power conversion efficiency of the PMS was 81.76%. This study demonstrated powering a 1 W LED using the fabricated PMS. The power efficiency for the PMS can be further increased by allowing additional charging time for the supercapacitor and increasing the supercapacitor's value. These results would be informative for designing a self-powered PMS topology to boost power in MFC stacks for their practical applications.

CONTENTS

LIST OF ABBREVIATIONS

SMFC	Sediment microbial fuel cell
WL	Water lettuce (*Pistia stratiotes*)
WL-SMFC	Water lettuce assisted SMFC
C-SMFC	Control SMFC (SMFC without WL)
OC	Open circuit
CC	Close circuit
WL-SMFC(CC)	WL-SMFC operated in CC condition
WL-SMFC(OC)	WL-SMFC operated in OC condition
C-SMFC(CC)	C-SMFC operated in CC condition
C-SMFC(OC)	C-SMFC operated in OC condition
DO	Dissolved oxygen
OCP	Open circuit potential
NGS	Next generation sequencing
CV	Cyclic voltammetry
DPV	Differential pulse voltammetry
GCE	Glassy carbon electrode
ORR	Oxygen reduction reaction
EDX	Energy dispersive X-ray
EC	Ionic conductivity
NaPBS	Sodium phosphate buffer solution
EIS	Electrochemical impedance spectroscopy
VR	Voltage reversal
PMS	Power management system
IC	Integrated circuit
DC	Direct current
SC	Supercapacitor
MPPT	Maximum power point tracking
LED	Light emitting diode

LIST OF UNITS

g/L	Gram per liter
mS/cm	MilliSiemens per centimeter
µS/cm	MicroSiemens per centimeter
mW/m^2	Milliwatt per square meter
mA/m^2	Milliampere per square meter
mV	Millivolt
kΩ	Killo-Ohm
V	Volt
mV	Millivolt
mg/L	Milligram per liter
mg/day	Milligram per day
cm^2	Centimeter square
AU	Absorbance unit
mW	Milliwatt
µW	Microwatt
F	Farad
µF	Microfarad
pF	Picofarad
C	Coulomb
pF/g	Picofarad per gram
mA	Milliampere
µA	Microampere

LIST OF SYMBOLS

E	Redox potential
C	DO concentration
p	Partial pressure of DO
E^0	Standard redox potential
ΔH_r^0	Standard molar enthalpy of reduction
ΔH_{sol}	Molar enthalpy change of solution
K_H^0	Henry's law constant
R	Universal gas constant
n	Number of e^-(s)
F	Faraday constant
T	Normal temperature
T^0	Standard state temperature
V	Potential
q	Charge
C	Capacitance
I	Current
t	Time
ε	Permittivity of the electrolyte
δ	Distance between the centre of the capacitance layer to the surface of the electrode
A	Surface area of electrode
η_{act}	Activation over potential
η_{con}	Concentration over potential
R_{ext}	External resistance
R_{int}	Internal resistance
P_{in}	Input power
P_{out}	Output power
P_{total}	Total power
E_{SC}	Energy stored in supercapacitor
P_{SC}	Power of supercapacitor
η_P	Power efficiency
V_D	Discharging voltage

V_C	Charging voltage
T_C	Charging time
T_D	Discharging time
V_B	Diode barrier potential

LIST OF FIGURES

LIST OF TABLES

CHAPTER 1

INTRODUCTION AND REVIEW OF LITERATURE

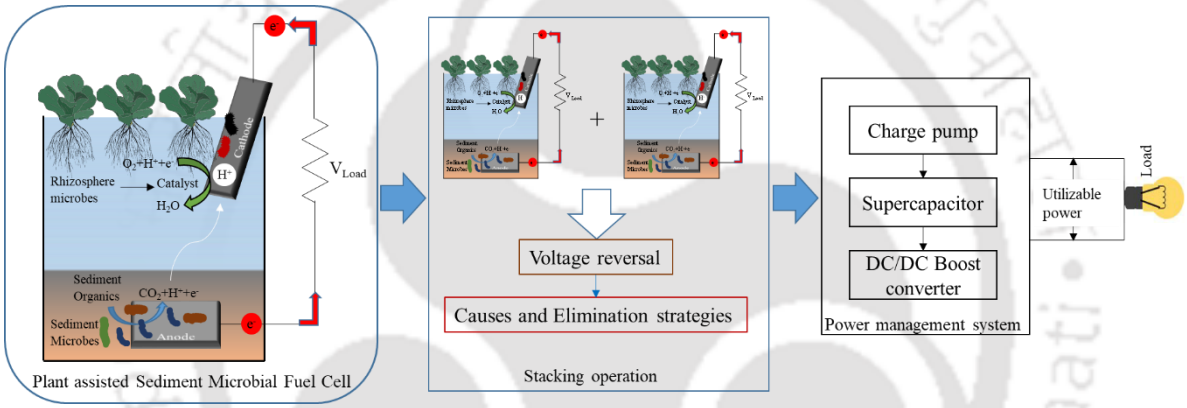

1.1 Introduction

In the pursuit of sustainable and clean energy sources to support a global low-carbon economy, the scientific community emerged with an innovative concept termed microbial fuel cell (MFC). The foundational idea of exploiting the catalytic activity of microbial species to produce electrical current was first proposed by M.C. Potter (Potter, 1911) , who laid down the groundwork for MFC technology. This concept gained practical momentum when Suzuki et al. (1976) developed the first MFC design. In recent years, significant progress has been achieved in understanding the fundamental principles underlying the MFC operation. The effectiveness of MFCs relies primarily on the presence of an active microbial population and the availability of organic minerals to ensure sustained energy production. Installation of MFCs in natural environment settings facilitates continuous electrochemical activity by maintaining a natural supply of organic substrates. A noteworthy progression in this direction is the development of plant-assisted MFCs, which integrate vegetation into the system to enhance organic matter availability and improve overall performance. The concept of plant-assisted MFCs, made well known by a group of researchers from Wageningen university of research, Netherlands in 2008, is rhizosphere-mediated generation of bioelectricity, effectively coupling plant activity with microbial electrochemical processes.

Over the past decade, plant-assisted MFCs have evolved with the understanding of plant-microbe interactions in various environmental settings such as floating water bodies, marshy wetlands, and paddy fields (Regmi et al., 2018) These studies exploring different plant species for bioelectricity generation convey the scope for further investigations in this domain. Another promising version of MFC technology for both energy generation and environmental remediation is the sediment microbial fuel cell (SMFC). Primarily, SMFCs are bioenergy generators that harvest energy from the chemical energy stored in the organic-rich sediment of natural water bodies such as rivers, lakes, ponds, etc. These aquatic ecosystems typically exhibit a columnar structure, where the uppermost zone is saturated with oxygen and the bottommost zone is anaerobic and serves as a sink for organic matter, both separated by a water column. This natural redox gradient is ideal for MFC operation: the exoelectrogenic microorganisms in the sediment act as the electron donor by oxidizing organic matter, and the oxygen-rich surface layer acts as the unlimited electron sink/acceptor. Thus, by implementing a solid anode in the sediment and a solid cathode near the water surface, this redox difference can be harnessed to generate electricity.

These considerations motivated us to conduct an investigation into the influence of floating aquatic plants on key performance parameters of sediment microbial fuel cells (SMFCs), with a particular focus on plant–system interaction mechanisms. The selection of a suitable aquatic floating plant for this study was guided by criteria such as natural availability, resilience to climatic variability, and adaptability to the physicochemical dynamics of the host aquatic ecosystem. Water lettuce (*Pistia stratiotes*, WL), which was chosen for this investigation, is a freshwater, free-floating small aquatic plant belonging to the family of monocotyledons and is the sole species of its genus, *Pistia* (Buzgo, 1994; Schmid, 2000). Typically forming dense green colonies on water surfaces, WL extends its submerged roots beneath the floating fronds. These morphological features allow it to interact directly with both the water column and sediment interface, potentially influencing the electrochemical dynamics of SMFCs. WL thrives within a temperature range of 22–30 °C and can tolerate conditions up to 35 °C, with an optimal pH range of 6.5–7.2 (Tamada et al., 2015). These environmental tolerances, combined with its rapid growth and structural characteristics, are expected to address several technical challenges associated with plant integration in SMFC systems, making it a viable candidate for this application.

In addition to the challenge of scaling up the inherently low power output of SMFCs, the issue of voltage reversal (VR) in series-connected configurations poses a significant barrier to their practical application. VR refers to a condition in which the voltage of an individual MFC unit reverses polarity within a stack, thereby diminishing the total voltage and output of the entire series system (Aelterman et al., 2006; Oh and Logan, 2007). This phenomenon makes stacking strategy less feasible to address the high power demand in practical applications. Open-filed SMFC operate under fluctuating environmental conditions, these dynamic conditions increase the susceptibility of the system to VR, complicating long-term and scalable deployment. Previous research has suggested that increasing the anodic surface area can enhance SMFC performance (Ewing et al., 2014). However, this strategy has not yet been thoroughly examined as a potential solution for mitigating VR in stacked configurations. This gap in understanding motivated us to investigate the influence of anodic surface area on the occurrence of VR in series-connected SMFCs, with the goal of improving stack performance and enabling more reliable power delivery in practical applications.

Under optimal operating conditions, sediment microbial fuel cells (SMFCs) typically produce an open circuit potential (OCP) of less than 1 V. To improve the voltage output, SMFCs can be stacked in series using voltage reversal (VR) elimination strategies. However, in natural

ecosystems, where SMFCs are often deployed, the physical size constraints make it impractical to connect a large number of cells in series. To address this, integrating a power management system (PMS) with SMFCs can enhance power delivery to meet application-specific requirements and support practical implementations. The efficiency of the PMS is therefore a critical factor in realizing the real-world potential of SMFCs. From an energy sustainability perspective, it is essential to design a PMS that consumes only a minimal portion of the SMFC's output for its own operation while effectively converting the harvested energy for practical use. Existing PMS designs that rely heavily on passive components can significantly increase internal power consumption, leading to lower overall energy conversion efficiency. As such, there is a strong need to develop self-powered, high-efficiency PMS architectures capable of boosting the SMFC output voltage for practical applications. This motivation underpins our focus on designing a self-powered PMS that maximizes conversion efficiency and enables SMFCs to be viable power sources in natural environments.

1.2 Microbial fuel cell

1.2.1 Theory of operation

Microbial cells (bacteria) function as biocatalysts that drive biotransformation processes and enable the synthesis of value-added chemicals (Beygmoradi and Homaei, 2017; Ladkau et al., 2014; Wohlgemuth, 2010). These cells host a collection of enzymes that facilitate cascaded metabolic reactions essential for their survival on organic minerals. When integrated with an electrochemical system, this microbial metabolism can be harnessed for biologically driven electricity generation, a concept known in the literature as microbial fuel cells (MFCs) (Schröder et al., 2015). In this context, microbial cells are referred to as electrochemically active microorganisms, which serve as biocatalysts in MFCs, playing a critical role in energy recovery and organic waste degradation, primarily through anaerobic oxidation processes (Yang and Chen, 2021). An ideal MFC operates through effective electrical communication between these electrochemical biocatalysts and solid electrodes. The microorganisms donate electrons to the electrochemically polarized anode as part of their respiration process, oxidizing complex organic substrates (Kaushik and Goswami, 2018). A counter electrode, the cathode, is placed in a separate ionic environment to support the complementary reduction reactions and facilitate extraction of electrical energy. These anode and cathode chambers are typically separated by a semi-permeable ion exchange membrane to maintain electrolyte

continuity (Figure 1.1A). The system can be operated in either open-circuit (OC) or closed-circuit (CC) mode across a fixed load (Abdul Quadir et al., 2025). In OC mode, electrons accumulate at the anode, generating a negative potential. When a load is connected, electron flow reduces the anode's negative potential and equilibrates it with the cathode through the resistor. The overall MFC voltage (EMFC) is measured as the potential difference between the cathode (Ecathode) and the anode (Eanode), as shown in Equation 1.1. By varying the external resistance and recording the corresponding voltage (V) and current (I), the power output (P) can be calculated using the equation P = VI (Logan et al., 2006a). A microbial community that generates high current at low resistance will yield high power density at that resistance. Conversely, communities producing lower currents at higher resistances may still yield high power at those resistance levels. MFCs can be configured in either single- or dual-chamber designs. A sediment microbial fuel cell (SMFC) is a type of single-chamber MFC. In addition to structural design, MFCs are also classified by the resources they utilize. Environmental MFCs include plant-MFCs and SMFCs, while photosynthetic MFCs utilize photosynthetic microorganisms to generate electricity in response to light (Kaushik and Goswami, 2018; Sarma et al., 2016). This study focuses on evaluating the power performance of SMFCs due to their capability to produce electrical energy from the microbial metabolism of sediment organic matter, highlighting their versatility and potential for sustainable energy applications (Zabihallahpoor et al., 2015).

$$E_{MFC} = E_{cathode} - E_{anode} \quad (1.1)$$

1.2.2 SMFC

Sediment microbial fuel cells (SMFCs) are ecosystem-based MFC configurations that can be deployed directly in natural environments with minimal construction material requirements (Gupta et al., 2023). The sediment bed in such environments is inherently rich in organic matter, enabling sustainable energy generation. SMFCs are thus considered a promising green energy technology, offering the dual benefits of renewable electricity production and bioremediation of pollutants in aquatic ecosystems (Sun et al., 2023). Additionally, the fabrication of SMFCs demands relatively low energy input, contributing to a favorable net energy balance. Tommasi and Lombardelli (2017) reported that an SMFC setup using graphite electrodes could recover its energy investment within 2.7 years, making it one of the most sustainable MFC types. Despite their sustainability advantages, SMFCs currently face limitations in both power output and contaminant removal efficiency, restricting their

practical real-world applications (Ewing et al., 2017; Li et al., 2023; Tommasi and Lombardelli, 2017; Wang et al., 2019). Various studies have attempted to address the issue of low power generation from multiple perspectives (Feregrino-Rivas et al., 2023; Wang et al., 2023). However, SMFCs operate in open natural environments where key factors such as the availability of sedimentary organics, microbial community structure, dissolved solids, minerals, and nutrient content vary significantly based on climatic, geographic, and anthropogenic influences (Feregrino-Rivas et al., 2023). Critical environmental parameters such as dissolved oxygen (DO), ionic conductivity (EC), pH, and microbial interactions at the electrode interfaces substantially influence SMFC performance (Domínguez-Garay et al., 2013; Parot et al., 2011; Rismani-Yazdi et al., 2008a; Song et al., 2019; Zhao et al., 2006). Suboptimal DO levels, large anode–cathode separation, and low EC contribute to elevated internal resistance. Specifically, increased electrode spacing and reduced conductivity lead to higher ohmic losses; insufficient cathodic oxygen levels result in mass transfer limitations; and inadequate organic matter leads to reduced exoelectrogenic activity and increased activation losses (Logan et al., 2006a).

Unlike controlled laboratory conditions, field-deployed SMFCs are challenged by the difficulty of maintaining optimal biotic and abiotic parameters (He et al., 2007; Najafgholi et al., 2015). These issues are particularly pronounced in the cathodic region, where performance is heavily influenced by oxygen availability (for oxygen reduction reaction, ORR), electrolyte conductivity (to reduce internal resistance), and pH (impacting microbial activity and catalyst stability) (Zhao et al., 2006). To overcome cathodic limitations, some efforts have focused on enhancing the ORR through noble metal catalysts (Clauwaert et al., 2009), bacterial catalysts (Milner et al., 2016; Parot et al., 2011), metal-organic framework (MOF) derived electrocatalysts (You et al., 2016), and increased cathode surface area (Freguia et al., 2007a). However, these strategies remain fragmented and lack a unified, scalable approach. A recent and promising development involves coupling plants with SMFCs to boost performance (Wang et al., 2023). Preliminary research indicates that plant root exudates can serve as additional substrates for electroactive biofilms at both electrodes. Furthermore, plants contribute oxygen through their roots, which supports ORR at the cathode (Li et al., 2023; Nitisoravut and Regmi, 2017; Regmi et al., 2018). While initially considered a strategy for enhancing SMFC power output, plant-coupled SMFCs have evolved into a distinct research subcategory. A detailed review of the historical background and development of plant-integrated SMFCs is presented in a later section of this chapter.

1.3 Enhancement of SMFC power performance

The main elements of an SMFC setup are the anode and cathode electrodes, the sediment organic content, the microbial community in the sediment and the overlying water above the sediment (Figure 1.1B). The physicochemical parameters associated with these elements are the performance decisive factors of the SMFC. Improving the power performance of SMFC is subject to improve sediment and water characteristics, anodic and cathodic reaction kinetics, and internal resistance. To date, the strategies mainly introduce electrode modification, exogenous organic and inorganic salt addition to adjust electrolyte characteristics, SMFC configuration improvements and energy harvesting technology (He et al., 2007; Najafgholi et al., 2015; Prasad and Tripathi, 2021a; Shi et al., 2021).

1.3.1 Causes of limited SMFC power performance

SMFCs are open environment systems, the higher anode cathode displacement due to higher separation between the sediment and the water surface causes higher ohmic losses. Moreover, suboptimal electrolyte characteristics such as low electrolyte conductivity, acidic or alkaline pH, and low dissolved oxygen contribute to higher ohmic and mass transport losses, leading to increased internal resistance of the SMFC system (Domínguez-Garay et al., 2013; Logan et al., 2006b). In addition to this, the limited organic content and sluggish anodic reaction are responsible for higher activation losses in SMFCs (Domínguez-Garay et al., 2013). Also, higher cathodic oxygen reduction over potential contributes to the low power performance of SMFC (Rismani-Yazdi et al., 2008b).

Now, to address the low ionic strength of electrolytes, Hong et al. (2005) showed the possibilities of increasing the ionic strength with the addition of exogenous inorganic salt and phosphate buffer in microbial fuel cell setup, which strategy was also implemented by others (Alipanahi and Rahimnejad, 2018; De Schamphelaire et al., 2010; He et al., 2007) in their studies with SMFCs. The power performance precincts caused by organic content limitation can also be addressed with the addition of exogenous organic salts or plant biomass (Danhassan et al., 2023). However, these techniques of conductivity and organic content enhancement are limited to laboratory-scale setups, as implementing these strategies in an onsite SMFC plant is practically challenging. Moreover, the sediment of aquatic ecosystems is a significant reservoir of organic content and according to the studies of Zhao et al. (2016), higher organic content in the sediment does not necessarily influence power performance.

Another power performance-influencing feature is the uniform distribution of sediment organic and nutrients. For example, Bombelli et al. (2013) demonstrated sediment depth-dependent chemical access to the electro-active microorganisms and its relation with output power.

Next, the major dominant limitation in SMFC is the cathodic oxygen reduction reaction (ORR) over potential. The higher ORR over potential can also contribute to internal resistance value and so can deteriorate power performance. Incomplete oxygen reduction attributed to less efficient cathode catalysts raises ORR over potential (Logan and Rabaey, 2012). Studies have explored the utilization of noble metal catalysts, bacterial catalysts, and enlarged cathode surface areas to address ORR over potential (Babauta et al., 2013; Clauwaert et al., 2009; Freguia et al., 2007b). However, metal catalysts diminish the cost-effectiveness of the technology; the bacteria-endorsed enzymatic catalysis of ORR is sustainable and cost-effective. Although, the bacterial catalysis of ORR is sustainable and cost-effective the efficiency of catalysis is limited and needs adequate enhancement.

In brief, the limited SMFC power performance is a consequence of sluggish biodegradation kinetics due to complex substrate in sediment, higher ohmic losses, ORR overpotential, and suboptimal operating conditions such as pH, conductivity, and DO, especially for SMFCs deployed in aquatic ecosystems.

1.4 SMFC's power performance improvement strategies

1.4.1 Anodic performance enhancement strategies

The anodic performance of an SMFC is primarily dependent on the bacterial reaction kinetics. In an attempt to enlarge the anode surface area with the objective of providing more extent for electroactive biofilm growth, studies have revealed that power density does not depend on the surface area of the current limiting electrode (Hsu et al., 2013). Whereas, for a significant enhancement in power density, a very high enlargement of the surface area of the anode is required and that will induce constructional challenges and high costs for the system (Ewing et al., 2014). In addition to this challenge, non-uniform colonization of the electroactive microbial community on the electrode surface while steady-state current is reached limits current production for large anodes and is reported as the reason that constrains power enhancement using a large surface area anode (Harrington et al., 2015). However, increasing the total anode surface area of anode with multiple small-sized anodes

in parallel configuration within a single setup and single cathode is proven beneficial for power enhancement (Ewing et al., 2014; Zhao et al., 2017). Use of multiple anodes contributes to current production in SMFC to improve power density (Hsu et al., 2013). The horizontal or vertical placement of multiple anode configurations can produce higher power densities with uniform distribution of organic compounds in the sediments, which, however, is reported to be the physicochemical characteristics of sediment change with depth, leading to uneven anodic reactions in the anodes (An et al., 2013; Nam et al., 2020). Although with more burial depth of the anode electrode, the anodic performance increases, more anode to cathode displacement is attributed to more anode burial depth, and this leads to higher internal resistance (Tavakolian et al., 2020). The enhancement of anode performance with burial depth cannot be attributed to the stricter anaerobic condition since Reimers et al. (2001) concluded that oxygen level is completely depleted within the top 1-2 mm of the sediment layer, and there are no differences in the anaerobic condition beyond that depth (Reimers et al., 2001). Moreover, with burial depth the other sediment environmental conditions, such as the access of organic substances and microbial diversity, maintain the thermodynamically and kinetically favorable conditions for the anodic reactions (An et al., 2015b; Bombelli et al., 2013). It is also reported that the microbial diversity reduces with depth in the sediment, and in contrast, studies have revealed that power performance deteriorates when the anode is buried beyond the depth of 3 cm from the water/sediment interface (Najafgholi and Rahimnejad, 2016). Based on these contradictory results, it can be concluded that the optimal depth for the anode is dependent on the sediment properties (An et al., 2015b).

The choice of anode electrode material is crucial since the physicochemical characteristics of the electrode material attribute to different bacterial enrichments, electron transfer resistances, and contaminant removal performance (Karra et al., 2014; Yu et al., 2021). For a sustainable SMFC function, the anode electrode material must possess the characteristics of chemical stability, electrical conductivity, specific surface area, and biocompatibility. Moreover, the mechanical strength, corrosion resistance, and long-term stability are the additional properties that the electrode material must possess if the SMFC is installed in adverse environmental conditions such as acidic or alkaline conditions, high temperature variations, and high salinity (Dopson et al., 2016; Guo et al., 2021). Studies have presented that the use of noble metals, carbon cloth, carbon fibre, or carbon felt to build anode electrodes contributes to the high cost of the system, whereas graphite-based materials such

as graphite plate, graphite rod, and graphite granule are better choice from economic standpoint (Yaqoob et al., 2020).

Lastly, the manipulation of sediment characteristics such as the organic content, conductivity, pH, and moisture is reported to be beneficial for power density enrichment. A sufficient carbon source and nutrient availability in the sediment can promote electroactive biofilm acclimation on the anode surface, resulting in improved power performance (Song and Jiang, 2018). The strategies reported so far to adjust sediment characteristics include exogenous addition of biochar, zero-valent iron, nano zero-valent iron, and organic carbon sources. The addition of these sources decreases sediment resistivity, enhances electroactive biofilm, and provides additional electron donors (Chen et al., 2016; Domínguez-Garay et al., 2013; Matsumoto et al., 2020; Wu et al., 2019). However, along with the addition of exogenous carbon and iron-based sources, proper mixing is required, which is impractical for SMFCs installed in aquatic ecosystems. Moreover, optimization of sediment characteristics is also required since excess organic content in the sediment may deteriorate power performance (Zhao et al., 2016).

1.4.2 Cathodic performance enhancement strategies

The power performance of the SMFC largely influenced by the cathodic reduction reaction kinetics. In SMFCs, oxygen reduction on the cathode is essential, and this creates a situation where installation configuration of the cathode is crucial for increasing oxygen availability at the cathode vicinity for achieving desirable cathodic reaction kinetics. Studies have revealed that for optimal contact of oxygen, horizontal placement of the cathode at the air/water interface is a viable approach. Moreover, studies by Morris and Jin (2012) and Wang et al. (2017) have shown that a partially submerged (wicking) air cathode can produce higher power density (Morris and Jin, 2012; Wang et al., 2017). It was reported that 75% exposure of the cathode to open air can produce 6.44 times higher power density compared to a fully submerged cathode (Wang et al., 2017).

It may be mentioned that, the material property of the cathode is also critical for MFC performance. Carbon-based materials are the most suitable for electrode; a detailed summary on cathode electrode materials has been discussed by Qiu et al. (2021) in their studies (Qiu et al., 2021).

In open environment SMFCs, the sluggish oxygen reduction kinetics at the cathode is one of the major factors for low power generation. This concern of slow ORR kinetics has been

addressed with noble and non-noble metals, carbon-based materials, and biological catalysts for cathode. Amongst the noble metal catalysts, platinum is the most promising catalyst for catalysing ORR in SMFCs. However, the high cost of platinum constrains its use for scale-up applications. Studies have been conducted to innovate substitutes for noble metal catalysts, chitosan based electrocatalysts, activated carbon are some of the cost-effective ORR catalysts. The effectiveness of these catalysts has also been tested for improved power generation in the SMFC setups. For example, Türker et al. (2020) produced 15 times higher power density with novel chitosan based smart cathode electrocatalysts (Türker et al., 2020). Zhang et al. (2009) utilized activated carbon as cathode catalysts to produce higher power densities (Zhang et al., 2009). Further studies have shown the stability and sustainable power generation with activated carbon mixed with polytetrafluoroethylene as cathode catalysts (Karra et al., 2014). The microbial bio-cathodes are also cost-effective and eco-friendly for their non-toxic catalysis of cathodic reaction. The microbial metabolism of biofilm on the cathode surface can be utilized to reduce oxygen and other compounds such as nitrite, nitrate, and sulfate (Du et al., 2014; Kabutey et al., 2020; Rusli et al., 2019). Studies have shown that SMFCs with biocathodes can produce similar or even better power density compared to platinum-coated abiotic cathodes (Wang et al., 2012). Commault et al. (2014) demonstrated that a photosynthetic biofilm can increase oxygen availability at the cathode surface compared to an aerated cathode (Commault et al., 2014). However, one area that is yet to be explored is the open environment-based biofilms, their colonization pathway, and mechanisms of catalysing the cathodic ORR.

The physicochemical characteristics of the overlying water of the SMFC also decide the cathodic ORR. As discussed previously, the cathodic reaction and hence the SMFC power performance greatly depend on the key properties of the overlying water. Dissolved oxygen, pH, conductivity, and temperature are the factors of the overlying water that greatly influence the power density of SMFC. Studies have shown the effect of conductivity on the power performance of the SMFC (Grattieri and Minteer, 2018; Guo et al., 2021). The conductivity greatly affects the mass transport and internal resistance of the system (Alipanahi and Rahimnejad, 2018). However, the effect of these overlying water parameters on the SMFC power performance has received limited investigation (Grattieri and Minteer, 2018; Guo et al., 2021).

1.4.3 Aquatic plant-coupled SMFCs

The aquatic plant-coupled SMFC is the concept of hybridization of conventional SMFCs with aquatic plants. With this concept, the photosynthetic food production process and the rhizosphere microbial diversity are utilized for the power production benefits of the SMFC. For example, the slow mass transfer of dissolved oxygen at the cathode of an SMFC can be addressed with the radial oxygen released by the plant to the cathode; simultaneously, the rhizodeposits maintain the organic content in the sediment (Nitisoravut and Regmi, 2017). Moreover, the coupling of aquatic plants in SMFC also contributes to the contaminants removal.

In an aquatic plant-coupled SMFC, the first concern is the selection of the plant. The plants with immoderately long roots can transfer oxygen via the roots to the anode immerged in the sediment and can interrupt the anode environment. Therefore, the selection of the plant is crucial for the stable and long-term operation of the SMFC. Moreover, the choice of plant is subject to their availability in the local environment. Studies have explored the role of floating macrophytes planted in the cathode with an inference that the macrophytes release more oxygen to increase dissolved oxygen in the cathode and hence improve the power performance (Kabutey et al., 2020). Studies have also been conducted on the use of submerged aquatic plants in SMFC (Xu et al., 2021), where *Ceratophyllum demersum L*, *Vallisneria natans*, and *Hydrilla verticillate* contributed to the power density enhancement of SMFC. The simultaneous contaminant removal efficiency enhancement through the coupling of aquatic plants with SMFCs has also been explored. For example, Kabutey et al. (2019) and Zhao et al. (2019) in their corresponding studies, reported remediation of phenanthrene and pyrene and heavy metals such as Pb, Cd, Hg, Cr, As, and Zn. In the following studies by Xu et al. (2021) efficient remediation of phosphorus from contaminated soil and water was reported (Kabutey et al., 2019a; Xu et al., 2021; Zhao et al., 2019). However, beyond these advantages of aquatic plant-coupled SMFCs, there is a requirement for conducting substantial investigations on the effect of the aquatic plant on the SMFC performance decisive parameters for further advancement in the power production of aquatic plant-coupled SMFCs.

1.4.4 Stacking of SMFCs

The theoretical maximum attainable voltage for a microbial fuel cell is ~1.1 V, while the measured voltage across the anode and cathode electrode is comparatively of lower

magnitude (Logan et al., 2006b). The energy requirement for consumer electronics lies in the range of 3.3 V-12 V (Alipanahi et al., 2019a; Mamun et al., 2023). This introduces a situation where MFCs are required to be stacked to meet the voltage requirement. The stacking of fuel cells is a system structure that contains isolated fuel cell units connected in series or parallel to expand the fuel cell size and boost the electrical power production of the overall system (Kim et al., 2020). In general, the voltage or current output is expected to increase when multiple MFC/SMFC units are connected in series or parallel. With the stacked system, it is also expected to increase the overall power output of the system. However, studies have demonstrated that power output deteriorates poorly when SMFCs installed in the same environment are connected directly in series or parallel configurations (Ewing et al., 2014; Prasad and Tripathi, 2021b). SMFCs deployed in the same electrolyte environment cannot be connected in series or parallel, since all similar-type electrodes share the same electrolyte and form a short circuit when connected (Dutta et al., 2022a; Tang et al., 2015). This issue can be addressed with the isolation of anodic and cathodic environments of individual SMFCs.

Similar to the short circuit issue, the occurrence of voltage reversal (VR) in series stacking of MFCs restricts continuous supply of power at the desired level. Incorporation of a power management system with MFCs may enable MFCs as a power source for small-scale electronics (Dutta et al., 2022a). A power management system is a combination of several electronic components that also require input voltage in the range of 0.3 V-3.3V (Dutta et al., 2022a; Gao et al., 2015). Hence, the riddance of voltage reversal in the series stacking of MFCs is imperative, although challenging. Several concepts have been reported to eliminate VR hitherto (An et al., 2015c, 2016; Gurung and Oh, 2012; Kim et al., 2015b, 2020; Kim and Chang, 2018). These techniques to eliminate VR can be categorized at the micro-scale and macro-scale levels. Improving the MFC redox kinetics through improved microbial response, optimal biofilm growth, and improved electron transfer systems are the micro-scale approach. On the other hand, the elimination of VR with external electronic circuits and components is the macro-scale approach (Kim et al., 2020).

1.4.5 Occurrence of VR: Definition and reasons

Theoretically, a series connection can increase the power produced from an MFC or SMFC by increasing the voltage without increasing the current. VR is the phenomenon where the voltage of a unit MFC is reversed in a system operating in series, and this reversal reduces the overall voltage and output of the entire stack system (Aelterman et al., 2006; Oh and Logan,

2007). In a severe situation, the output voltage of a stack system of several unit MFCs connected in series may reduce to a voltage level comparable with that of a single unit MFC (Figure 1.2) (Kim et al., 2015b).

The occurrence of VR is not reliant on the reactor size; the occurrence of VR has been reported from microlitre to litre scale MFC reactor size. The VR effect on the microbial fuel cell type can affect the functioning of both the anode and cathode. The VR effect reduces the lifetime of the MFC by disrupting the biofilms and also may result in electrode corrosion. Studies have suggested parallel stacking to avoid VR which, however, is not feasible due to inner circuit current losses known as current reversal.

Studies have shown that power performance limitations of stacked MFCs are the primary reason for VR. For example, studies conducted by the group of Oh and Logan in 2007 and 2009, respectively revealed that the occurrence of VR is due to the differences in the performances of unit cells constituting the series stack. The reason for differences in the performance between unit cells is attributed to fuel starvation in unit cells of the stack (Oh et al., 2009; Oh and Logan, 2007). Later, An and Lee demonstrated that the VR is the outcome of kinetic imbalances between unit cells connected in series (An and Lee, 2014). The further studies on VR in the context of kinetic imbalances suggested that the VR also arises from kinetic imbalances between the anode and the cathode (An et al., 2015a). However, a detailed investigation on the reason for the occurrence of VR is yet to be explored.

1.4.5.1 VR elimination strategies

In relation to the previous findings, controlling, preventing, and eliminating VR in the stack of the MFC types are achievable with equivalent reaction kinetics across all cells of the stack unit. However, balancing the reaction kinetics across all unit cells in a stack has been proven to be challenging for all MFC types. Based on the approaches adopted to eliminate VR in literature, the approaches can be categorized into nano, micro, and macro scale approaches. The micro and nanoscale approach for VR removal refers to electroactive microorganisms and redox molecules, respectively (Kim et al., 2015a). These strategies propose control of anodic reactions through controlling enzyme or microbial immobilization at the biofilm growth stage on the anode. For example, Ding et al. (2006) and Fapyane et al. (2016) proposed VR removal with more electroactive strain and functionalizing electrodes with gold nanoparticles to promote direct electron transfer (Ding et al., 2006; Fapyane and Ferapontova, 2016). However, the ORR at the cathode and the charge neutralization rate by

counter-ion transfer also control the overall performance of an MFC (Kim et al., 2007). The micro to nanoscale approaches to improve anodic and reaction kinetics are feasible for lab-scale MFCs; however, they would encounter higher challenges in on-site SMFCs.

The macroscale approaches refer to the external electrical adjustments to regulate power imbalances for the elimination of VR in fuel cell stacked operation. For example, connecting a threshold resistance as shown in Figure 1.3C is used to manipulate the state of current production between two unit cells in a series stack of two MFCs. The resistance required to manipulate the state of current production was calculated by Ohm's law with the current value obtained under the I-V curve. It was reported that the connection of the threshold resistance did not limit the power production; however, a pretest is required for determining the accurate resistance (An et al., 2015c). Notably, SMFCs are open environment systems, and the power performance is regulated by environmental parametric changes, which would enforce continuous monitoring of the threshold resistance. Additionally, studies have shown that connecting an auxiliary fuel cell to provide assistance current can support the low-performing cell and can prevent VR (Figure 1.3B) (Kim et al., 2015b). Manipulating the internal resistance of the stack is another way of regulating the VR. For example, studies conducted by Kim and Chang have suggested connecting an external resistor to the low-performing fuel cell to regulate the current production and then VR (Figure 1.3E). Controlling internal resistance by improving charge and mass transfer resistances is also probable; however, this strategy is not economical, besides being impractical and more difficult than resistor control (Kim and Chang, 2018). Although regulating VR with an external resistor is advantageous, nonetheless, its contribution towards the internal resistance of the stack cannot be ignored. Several studies in the literature have utilized hybrid stacking configurations of MFCs (Figure 1.3A). The hybrid stacking refers to the combination of parallel and series stacking, which increases both the voltage and current rating of the stack configuration (An et al., 2016; Papaharalabos et al., 2017; Zhang et al., 2017). Conceding the fact that MFC in parallel connection would address the current limitation, the current reversal in parallel-connected MFCs should be simultaneously considered. The occurrence of current reversal due to kinetic imbalances would also contribute to the VR in the overall configuration (Wu et al., 2016; Zhang et al., 2017). In parallel to these studies, attempts have also been made to use electronic components as external circuits to address the issue of VR. Capacitors, which can store electrical energy, were utilized to store the energy output from MFC/SMFCs to avoid direct connection between the fuel cell while establishing the series

connection. The use of an external electronic circuit, also termed a power management system (PMS), can address VR and simultaneous boosting of fuel cell power output. A detailed study on the use of PMS to avoid VR and boost MFC/SMFC power has been discussed in the following section.

1.4.6 Power management systems

A PMS is a device that is constituted of some electronic components to work together in order to convert a low electrical input into an utilizable power output. The basic configuration of PMS mainly entails a charge pump, a supercapacitor (SC), and a boost converter (Figure 1.4). The integration of this basic power management system enables the enhancement of the output characteristics of MFCs to intermittently power small-scale appliances. The inability of SMFCs to generate high power performance and their corresponding reasons from the literature have been discussed in the previous section of this chapter. In addition, Degrenne et al. (2012) tried to address the low performance of MFCs from an electrical point of view, few of which are listed in Table 1.1 (Degrenne et al., 2012b). This study also demonstrated the requirement of PMS to boost the power output of MFCs.

Table 1.1: Strategies for addressing the limitations of MFCs as a source of electrical power

Limitations	Detailed explanation	Strategies in power electronics
Limited-power	MFCs can produce power densities (normalized) ranging from 10 $\mu W/cm^2$ to a few mW/cm^2. However, large MFCs fail to deliver better performances.	Low-power-consuming circuit design is the special requirement
Low-voltage	In most cases MFCs can deliver ~0.3 V at maximum power point (MPP).	Require step-up DC/DC converters capable of operating at low input voltage and high energy conversion efficiency (Tehrani et al., 2017).
Hydraulic-association	Serial electric association of MFCs is not possible during hydraulic associations.	Require galvanic isolation by converters in association with each cell, or only a parallel combination of cells can be used.

Dispersion	Many parameters (like physical, chemical, and biological) affect the electrical characteristics.	Individual cell control (voltage balancing) is a must when a stack of several MFCs is considered (Kumar et al., 2018).

The basic operational principle of a PMS is to store the electrical energy generated by a capacitive load (e.g., a SC) and boost the stored energy into another level before releasing it to the load. Devices like DC/DC converters can convert the low potential differences to a required level of potential difference (Alipanahi et al., 2019a; Donovan et al., 2011a; Zhao et al., 2015). Several reports in recent times presented the use of SCs, charge pumps and DC/DC converters to harvest the MFC output power for practical applications. Khaled et al. (2014) deigned a stack of MFCs and a power management system to produce 1.5 mW power for powering sensor applications (Khaled et al., 2014). Bautista et al. (2015) presented a MPPT algorithm based PMS for extracting maximum power from the MFCs (Bautista et al., 2015a). A duty cycle based energy neutral communication protocol for MFC powered wireless networks was proposed by Yang et al. (2015) (Yang et al., 2015). A switched capacitor based converter and a step-up converter simultaneously achieved 85% of power conversion efficiency from a stack of MFCs (Nguyen et al., 2019). Tang et al. (2015) presented that output power can reliably be enhanced if energy is harvested from several SMFCs operating independently with a single PMS (Tang et al., 2015). This PMS utilized the harvested energy for its operation, and hence, the main feature of the PMS was its self-sustainability. Dallago et al. (2016) designed a battery less, programmable device free PMS to convert 8 μA-300 mV MFC output with 55% conversion efficiency (Dallago et al., 2016). Gao et al. (2015) designed a PMS to gather sufficient magnitude of voltage and current output from an MFC generating limited voltage and current for the sensors and communication devices monitoring water quality (Gao et al., 2015). Similarly, a multianode decoupling circuit, a SC, a switching circuit, and a DC/DC converter were used to construct the PMS by Umaz et al. (2017) (Umaz et al., 2017). The function of the multianode decoupling circuit in this system was to eliminate the consequences of weakened anodes in order to expand the heftiness of the Benthic MFC. The SC harvested energy through charging–discharging cycles controlled by the switching circuit. Moreover, the DC/DC converter supplied the required magnitude of voltage to the load. Hence, the general configuration of a PMS can be well thought out to be an electronic circuit configuration,

whereby the primary components included are a SC, a charge pump circuit (acting as a voltage booster) and a DC/DC boost converter. In addition, there are some occasions where a charge control circuit was also used. The charge control circuit works as a controller for harvesting energy at the SC and transferring it to the next component (Alipanahi et al., 2019a; Erbay et al., 2014; Gao et al., 2011; Kim et al., 2014, 2011). Depending on the energy requirement by the load, the circuit configuration for the PMS can be modified by modifying individual components of the circuit. A flyback converter designed by Degrenne and his group (Degrenne et al., 2012b) is such an example. Also, the circuit components, such as the charge pump and the DC/DC boost converter, can be modified to achieve maximum conversion efficiencies.

1.4.6.1 Design for an improved power management system

The MFCs encounter reciprocally low magnitude of voltage and current issues; the concept of a boost converter can be applied to increase the voltage level (Gao et al., 2011; Huang et al., 2013; Kanakasabapathy and Pillai, 2014; Meehan et al., 2009). The straightforward use of boost converters is, however, not always feasible, since most of the converters usually need a minimum of 800 mV potential to start (Meehan et al., 2011, 2009). Again, to increase the current output, high-value capacitors may be used. Initially, the capacitor(s) is charged to a certain value, and then the stored energy is discharged through the load in burst mode (Alipanahi et al., 2019b). SCs can serve the purpose of energy harvesting and current enhancement in most of the cases. However, the MFCs can generate voltage only up to several hundred millivolts, so a charge pump circuit can be connected in between the MFC output and the SC instead of connecting the SC directly to the MFC. The charge pump will boost the MFC voltage up to a level which is necessary to start the DC/DC boost converter (Kanakasabapathy and Pillai, 2014). Hence, from the design perspective of PMSs, MFCs power enhancement can be achieved in two steps: energy harvesting and boosting of the energy. In the PMS process flow, these two steps can be implemented either way, i.e., first energy harvesting and then boosting energy or vice versa. Again, these harvesting of the energy and boosting of the energy may involve different circuitry with varying circuit components (Gao et al., 2011; Kanakasabapathy and Pillai, 2014; Meehan et al., 2009; Schrader et al., 2013). The components that are necessary for a PMS and the latest modifications are discussed in the following sections.

1.4.6.2 PMS circuit components

1.4.6.2.1 Supercapacitors

A SC (also known as ultracapacitor) has a much higher capacitance than the general-purpose capacitors; however, it is limited to subordinate voltage levels. The value of capacitance of SCs is such that it fills the gap between rechargeable batteries and electrolytic capacitors. The SCs have the ability to store energy per unit volume, which is 10–100 times greater in magnitude than that of electrolytic capacitors. In addition, SCs have a faster response towards accepting and delivering charge and tolerance to a greater number of charge/discharge cycles (Häggström and Delsing, 2018). This feature of SCs provides a solution for the circuits which require rapid charge-discharge cycles as a priority instead of only storage of energy (Tehrani et al., 2017). A detailed discussion on the working principle and construction of SCs has been presented in the literature by Dutta et al. (2022).

Coupling of SCs with MFCs may enable these storage units (SC) to serve the purpose of harvesting energy from MFCs and to deliver it on demand (Poli et al., 2020). The exploitation of these storage units for storing charge from MFC also results in higher instantaneous current supply towards the load (Walter et al., 2017). However, the low current levels of MFCs increase the charging time for such high-value capacitors (Donovan et al., 2011a). Also on a few occasions, the MFCs alone cannot charge the SC up to its maximum level of voltage (i.e., its OCP); hence, a supportive circuit such as a charge pump and charge control unit may be required. The storage of energy in SCs is temporary while the load is connected and requires recharging of SC to continue the power dissipation at the load. As a result, this activity requires energy which is supplementary to the capacity of MFCs. An efficient way to utilize the stored energy is to couple a control unit with the SC, which takes care of the threshold limit of stored energy by periodically transferring charge to the load (Umaz, 2020). These capacitors thus can be used as a final charge storage device after boosting the MFC voltage and for direct transmission of charge into the load on requirement. The energy storage can be increased by increasing the SC value. However, this functionality is not feasible in most cases since charging time is a major concern. Typically, a 5 F capacitor was charged up to a magnitude of 3.3 V in 13.6 hours. In this work the SC was charged from multiple MFCs in conjunction with an algorithm that also protects the power ranking as well as the MFC health by means of a PIC24F16KA102 microcontroller and an ultra-low-power DC/DC boost converter (BQ25505), which participated in the function of MPPT with an efficiency ranking of ~50.7% (Reyes et al., 2018). Like the general-purpose capacitors, the

SCs can be utilized to design switch mode charge pumps to enhance voltage to another level with high conversion efficiencies (Kim et al., 2011).

1.4.6.2.2 Charge pump circuits

A charge pump circuit is basically a DC/DC charge converter that raises a lower magnitude of voltage by means of the energy storage feature of capacitors. So far, the reported efficiencies of the charge pump circuits achievable during voltage conversions are up to 90–95%. A charge pump is constructed on the platform of a specific semiconductor technology which is capable of operating at low input voltage. Its preliminary application was to boost the voltage of the MFC (Khaled et al., 2014; Liu et al., 2015; Yang et al., 2015; Zhao et al., 2015). These semiconductor technology-based charge pumps were so designed that they extract a minimum amount of current from the MFC for the conversion of voltage magnitude and to charge a capacitor (or a SC). When the capacitor is charged up to the converted voltage level, it supports the start-up of the boost converter since the MFC voltage is insufficient for starting up this simple electronic device. Hence, the utilization of charge pump in the PMS helps in three different assignments: (1) it makes possible the startup of boost converter in a short interval of time, (2) it can extract nearer to the maximum attainable power by the MFC, since it draws low current from MFCs and finally (3) a power efficient PMS can be built with it (Rossi and Logan, 2020). The energy extracted from the MFC can be harvested by the charge pump while the output is connected to a SC (Liu et al., 2015; Zhao et al., 2015). The process of energy accumulation from MFC by charge pump and capacitors has also been further reported by Donovan et al. (2008). Gao and the group used the S-882Z18 (made by Seiko) charge pump to design the PMS with improved efficiency. This charge pump drew 290 μA at 0.3 V from the MFC and charged a 1 F capacitor up to 1.8 V (Gao et al., 2015). However, the charge pump circuits may cause some drawbacks in PMS. It is to be noted that the loads connected to a source can operate only when a required level of voltage is supplied from the source. The energy requirement for the SC's voltage to rise by a minimum amount, say from V_i to $V_i+\Delta V$, however, would subsequently require a large magnitude of energy for the SC to attain the identical amount if V_i increased. Also, a longer charging time would be needed. These two statements can also be validated by equation 1.2 and 1.3 given below (Dallago et al., 2016).

$$\Delta E_{Store} = \frac{1}{2} C(\Delta V^2 + \Delta V V_i) \quad (1.2)$$

$$\Delta T_i = \frac{C(\Delta V^2 + \Delta V V_i)}{2\eta V_{in} I_{in}} \quad (1.3)$$

Where ΔE_{Store} is the energy required to increase the SC's voltage, η, V_{in} and I_{in} are termed as efficiency of energy conversion, voltage input and current through charge pump, respectively. Since V_{in} and I_{in} are related to the output characteristics of the MFC, an increment in the output voltage Vi of the charge pump, in order to adjust the load requirement, will result in a higher charging time and a reduction in the duty cycle of the load. Since the internal voltage of the charge pump is subject to the number of clock cycles, the above change will also affect the energy conversion efficiency (CMOS IC Datasheet, Seiko Instruments Inc.). Hence, a higher number of stages inside the charge pump can affect the efficiency of the circuit (Dickson, 1976). At the end, a new power management system will be required for the MFC (Huang et al., 2013). According to the requirement of power, multistage charge pump circuits can also be used to charge the SC (Kanakasabapathy and Pillai, 2014). In an algorithm based circuit for tracking the MPP of MFC, a charge pump functions as a generator of control voltage, which in turn modulates a voltage-control oscillator in order to generate a voltage to ensure the MPP (Bautista et al., 2014). The short-circuit effect between the anodes of a multianode MFC setup was addressed with charge pump circuits. Individual charge pump circuits were connected to individual anodes and a common cathode in a multianode and single cathode based benthic MFC. This decoupling circuit, consisting of an equal quantity of charge pumps to that of the anodes and individually connected to them through their negative terminals, also shares one common cathode as their input to the positive terminal, which could solve the issue of bioturbation (Umaz et al., 2017).

1.4.6.2.3 Switching mode capacitor for charge pumping

To address the issue of low efficiency of charge pump, a switched capacitor was designed, which assisted in the boost up of the MFC voltage (Alipanahi et al., 2019b). The elementary principle suggests that capacitors share parallel connections amongst them while extracting charge from MFC, and thereby each individual capacitor gets charged up to the maximum MFC limit; and while the capacitors are fully charged, the parallel connections get swapped with series connections, and the voltages of the capacitors are added up, and the boosted voltage is supplied to the targeted load. Gao et al. (2011) utilized this identical tactic, where capacitors were charged in parallel mode by individual MFCs, and once the charging operation was completed, all capacitors were disconnected from the MFCs, and then the capacitors were connected in series, which resulted in incremented voltage and energy

equivalent to the mathematical sum of the potential energy (voltage) stored in all capacitors. In this practice the quantity of capacitors and MFCs were so chosen that in the power delivery mode the power is sufficient to start the boost converter for further enhancement of the voltage. All the switching operations in the above discussion were controlled by solid-state optical relay switches. An optical relay consists of a light-emitting diode (LED) and a MOSFET, where the light emitted by the LED controls the gate of the MOSFET, and so its drain current decides the on-off state of the switch. In this work the on/off state of the switches was decided by the power supplied from a charge pump and a capacitor (Gao et al., 2011). In another work by Kim et al. (2011) four MFCs and eight 1F SCs were used to design a circuit that charged a group of 4 capacitors from the MFCs in parallel and discharged the other 4 capacitors in series mode at the same time. The switching of the capacitors was established every 1s with 5V DC/1A relays and a programmable Arduino board. In the first stage, one set of 4 capacitors was charged in parallel by four MFCs; the other set of 4 capacitors was discharged through the load after disconnecting them from the source and confirming series connection amongst them. While in the second stage, the configuration was reversed; the set of 4, which was in discharge mode, went to charging mode, and the other set of 4 was connected to the load following series connection. 2.5 V was the maximum achievable voltage in this technique of voltage conversion (Kim et al., 2011). A similar approach was also previously presented where a capacitor-based energy storage circuit powered a microbial electrolysis cell (MEC) (Hatzell et al., 2013). The capacitors were charged in parallel using energy from a MFC and were discharged in series mode to the MEC to increase the hydrogen production rates. Pumping the charge of MFC with the utilization of these circuits may be considered the most efficient way of charge pumping. Notably, the capacitors are the charge storage devices, and in the switching mode, only the connection configuration is altered (i.e., from parallel to series or vice versa); hence, no energy is lost during this process. However, the circuit configuration is simple and the number of capacitors can be increased as per requirement; the increase in the number of capacitors or utilization of larger value capacitors often increases the charging time for such switching circuits. Additionally, the solid-state switches require an external source of supply for their operation (Kim et al., 2011).

1.4.6.2.4 DC/DC boost converters

A DC/DC boost converter is a device or a circuit which can increase the magnitude of an input voltage to a higher magnitude of voltage as its output, and hence is known as a boost

converter. The basic boost converter circuit can be built with an inductor, a capacitor and a switch, which is mostly a transistor or a MOSFET (Figure 1.5). The voltage increment in the circuit is dependent on the on/off period of the switch; the magnitude of voltage increases with a faster on/off cycle. Additionally, for a boost converter, the magnitude of voltage output is limited by the voltage rating characteristics of the MOSFET and/or diode. The maximum output voltage and the minimum input voltage are specified points, which are to be considered in choosing a DC/DC converter. Furthermore, the maximum duty ratio at which the converter can operate is also a practical limitation for the boost converters. Dividing the on-time of the MOSFET by the total switching period defines the duty ratio (Stasi, 2015). Determining the current of the boost converter is to use the power balance equation. This power balance concept for a boost converter states that the current at the output decreases, and it is lesser than the input current if the voltage at the output is greater than the input voltage for balancing the power on both sides of the circuit (Stasi, 2015). Although the boost converter is the last component of the PMS, it is essential, as it serves the purpose of meeting the voltage requirement by the load. The commercially available boost converter (bq25504EVM-674, Texas Instruments) was configured in the PMS to produce a 5 V output voltage from a 2.5 V input from the MFCs in order to charge a mobile phone battery (Walter et al., 2017). The switched mode capacitor-based voltage booster was discharged through a DC/DC boost converter so that 3.3 V output could be achieved from an input of 800 mV of the series-connected capacitors charged by 400 mV of the MFC's output. The boosting of the voltage continued till the series-connected capacitor voltage reduced to 500 mV. Then, the boost converter was disconnected from the capacitors until the voltage across the capacitor reached the magnitude of MFC's voltage. This cycle was repeated continuously (Alipanahi et al., 2019b). The minimum voltage requirement for L6920DB and LTC3429 series boost converters to start was 800 mV (L6920 Datasheet, 2006; LTC3429 Datasheet, 2004). However, 500 mV input voltage was sufficient to start a TPS61200 series boost converter, as claimed by Texas Instruments (TPS61200 Datasheet, 2008). MFCs producing more than 500 mV, if connected directly to such boost converters, begin to draw high current, which is beyond the current limit of the MFC. As a result, the MFC's voltage magnitude reduces, and the MFC cannot rejuvenate its previous voltage level, which is required for starting the boost converter. Hence, these converters are utilized by connecting a charge pump circuit in PMS if the MFC voltage is below the required level. For example, a 2.2 F SC was charged up to 1.8 V, which was further boosted to 3.3 V through a boost converter (Meehan et al., 2009). The PMS built with L6920DB series converters also lags in performance while realizing voltage

boost conversion (Meehan et al., 2011; Umaz, 2020). This induces the requirement for a large SC discharging voltage as its input voltage, and this accordingly demands higher charging time for the SC. Again, the relatively high internal resistance of L6920DB is of concern as its utilization with a low input voltage significantly reduces its efficiency. Furthermore, these voltage converters assume no a priori information about the input voltage/energy signals. Hence, these issues can be addressed with complicated timing circuits, which enable control and synchronization of the switches to accept a dynamic range of input voltage/energy signals. Koffi and Okabe considered a single air-breathing cathode-based MFC as a model source of energy and increased the low voltage of the MFC with a circuit which could boost the low voltage by a process of voltage multiplication. The voltage boosting was implemented with a self-oscillating low-voltage booster prepared on transistor technology (Koffi and Okabe, 2020); voltage multiplication was achieved with a multistage AC/DC voltage multiplier and a storage unit for storing the enhanced energy. Here, a 4-stage multiplier increased the voltage up to 17 ± 1 V within a period of 20 h; this voltage increased further to 35 ± 2 V while the stage of the multiplier was increased to eight. Finally, with 20 stages of AC/DC voltage multiplier circuits, the magnitude of voltage reached 99 ± 2 V with a maximum of 101.24 V. This circuit configuration could hold the boosted voltage with stability for a duration of 50 h, and it was equivalent to about 243-fold DC/DC voltage gain. However, the performance of the PMS is dependent on the characteristics of the MFC and it deteriorated with time. The efficiency related to energy harvesting obtained by this voltage booster and multiplier was about 82%. A special type of boost converter is a flyback converter, which is the simplest inductive step-up converter with galvanic isolation. While working with the low-power MFC circuits, simplicity of the boost converter is the most important factor to be considered. The flyback topology is constructed upon the use of coupled inductors. The use of coupled inductors effectively reduces the need for repeated variation in the duty cycle. However, exploitation of the additional winding in the flyback configuration reduces the need for input voltage for start-up and operation of the circuit (Damaschke, 1996). Moreover, a controlled operation of the flyback converter can extract power from MFC at the point of maximum power (MPP) (Degrenne et al., 2012b, 2012a). The flyback design configuration proposed by Degrenne et al. (2012) was operated at the MPP of the BFC, i.e., at 0.3 V with 62% conversion efficiency. In addition, this converter could be connected in series to achieve higher power. A recent work reported the use of a commercially available DC/DC boost converter built on semiconductor technology and using an integrated circuit named CE8301 (Prasad and Tripathi, 2021b). This IC CE8301 possesses

a CMOS (complementary metal-oxide-semiconductor), a PFM control (pulse frequency modulation control), an oscillator, a reference voltage source and a comparator. Besides these, a capacitor and an inductor were also connected to this IC during the conversion operation. The IC could provide a regulated voltage output up to a magnitude of 5.02 V to the load when an MFC could supply more than 0.288 V with the help of the PFM.

1.4.6.3 Maximum power point tracking (MPPT)

The maximum power point tracking (MPP or MPPT) defines a technique based on the principle of the maximum power transfer theorem for extracting power at maximum magnitude from an MFC. The theorem states that maximum power is only extractable from the cell when the resistance of the load is exactly equal to the internal resistance of the cell. An MPP based PMS utilizes a variable resistor which changes accordingly to match the magnitude of the MFC's internal resistance with the load resistance for extracting the maximum power from the MFC. Earlier reports presented that PMSs designed for MFCs characteristically exploited mostly DC/DC converters with applications of discrete components for accentuating efficiency (Adami et al., 2011), along with the MPPT method (Park and Ren, 2012). However, these implemented methods for MPP introduced some drawbacks, such as the DC/DC converters continuing to consume power even during the period of inactivity and the lack of dedicated schemes for matching impedance to run MFCs at MPP (Bautista et al., 2015b). Furthermore, during the application of the PMS with MFC, power conditions suffered from reduced overall efficiency due to defective MPP and severe current losses in the inductor (Bautista et al., 2014). Addressing all these drawbacks, Bautista et al. (2015) proposed a PMS that was composed of two unique characteristics. First, the PMS had an accurate maximum power extraction algorithm (MPEA), which was implemented to efficiently monitor the MFC's time constant. Second, the PMS had a zero current switching tracking (ZCST) loop, whose function was to effectively reduce the current losses in the inductor (Bautista et al., 2015b).

Several techniques can be exploited to achieve the MPP. In general, MFC is a source of voltage that is equivalent to an electrical component having internal resistance, storage of energy in terms of voltage, and capacitance all together. Moreover, it is well known that the MFC output is in DC mode. Hence, the internal capacitance and the (OCP) can be exploited to determine the MPP. Erbay et al. (2014) implemented the MPPT model by first measuring the OCP of the MFC, then calculating the voltage at MPP (VMPP), which was half of the

OCP magnitude (VMFC). The comparator unit constantly monitored the VMPP for matching the input impedance of the converter to that of the MFC's internal resistance. In another MPPT based PMS, the MPPT logic functioned considering 40% of the OCP as a reference voltage. Consideration of this constant voltage ratio was based on the pre-acquired maximum power condition of the MFC. The PMS extracted maximum power from the MFC by adjusting its voltage to the reference voltage. This process does not require any support from an external energy source since the PMS consumed a tiny amount of energy to complete this function. The process of energy conversion was accomplished with a commercially available integrated circuit (IC) (BQ25504, Texas Instruments, Dallas, TX, USA). Functionally, this IC requires 330–450 mV to start and possesses a voltage conversion range from below 1.0 V to 3.8 V. In the PMS the reference voltage can also be configured on requirement by introducing variations in the external resistance value into the circuit (Erbay et al., 2014).

In another instance, a DC/DC boost converter was programmed in such a way that during operation its input resistance varied and remained equal to 50% of the MFC's (OCP), thus validating that the MFCs deliver maximum power to the load only when the load and internal resistance of the MFC have similar magnitude (Bautista et al., 2015a). The algorithm also took effective measures to set conditions for minimal power losses that could be tolerated by internal resistances of all the components of the PMS (Reyes et al., 2018). Nguyen et al. (2019) designed an algorithm to produce optimal duty cycles for online monitoring of the MPP for a switched capacitor based PMS (Nguyen et al., 2019). Alaraj et al. (2017) proposed a boost converter in which the duty cycle was adjusted with a microcontroller in order to track the MPP of the MFC along with avoidance of voltage overshoot (Alaraj et al., 2017). Studies have also been made on the effectiveness of the MPP technique. MPP based PMS may not be best for systems that have a finite amount of initial energy, such as the MFCs. This is because at MPP the output voltage is equal to half of the OCP of the MFC or the internal thermodynamic voltage; also, this is the condition when the output resistance is equal to the internal resistance. At the MPP, though maximum power is achieved from the MFC, the conversion efficiency is only 50%, which also means that 50% of the MFC's internal energy is lost during the conversion process. Therefore, Park et al. (2018) formulated a multi-objective optimization problem in order to define an optimal operating point for the MFC. A multi-objective optimization problem in general is an objective function, which is defined in combination with more than one conflicting objective function. This function can be optimized simultaneously to define a globally feasible solution for each of the conflicting

objective so that none of the other objectives is dominated and the system constraint(s) is/are also fulfilled (Park et al., 2018). An MPP generally targets harvesting more energy from the initial energy in the MFC reactor; however, this optimal operating point could acquire comparable electricity generation efficiency from an MFC.

1.4.6.4 Elimination of voltage reversal with PMS

The best configuration for removal of voltage reversal could be by using a single PMS connected to one unit of MFC or several MFCs connected in parallel (Kim et al., 2019). Several such combinations of MFC and PMS may be connected in series to eliminate voltage reversal. Studies suggested several approaches that could protect against voltage reversal through stack operation and PMS. As discussed earlier, Kim et al. (2011) showed a possibility for boosting the voltage of MFC by utilizing programme controlled relay switches and supercapacitors. Another method introduced by Papaharalabos et al. (2017) involved the use of an autonomous switch-box circuitry for continuous reconfiguration of electrical connections among the MFCs in the stack to address the issue of reversal voltage. The MPPT techniques also introduced a method through which cell reversal could be eliminated (Wang et al., 2015). All these proposed arrays and techniques were effective for voltage reversal elimination but demanded for an external energy source to conduct their operations.

1.4.6.5 Ultra-low power PMS

Energy harvesting circuits built for MFCs mostly rely on components consuming more than 10 mW power for their respective operation. For example, Kim et al. (2014) proposed the system that coupled a customized small-scale (21.3 cm^2) ultra-low power-consuming PMS with a benthic MFC producing 5.4 μW. This ultra-low-power electronic unit included a programmable interface that enabled self-sustainability and was suitable for sensor applications. The circuit design included a customized chip (CTRL chip) that consumed ultra-low power for performing operations like harvesting energy from benthic MFCs and processor operations. Fabrication of this chip was conducted on a 180 nm CMOS technology, which was part of a 1.0 mm^3 die-stacked sensor node system (Kim et al., 2014; Lee et al., 2013). In another report, Winfield et al. (2014) presented a simple voltage converter circuit constructed with ultra-low power-consuming electronic components to work with the MFC designed by this group. The MFC could produce 110 mV under a load of 1 kΩ. Following these characteristics of the MFC, they proposed a PMS configuration that consisted of an inductor-based energy harvesting board, a bridge rectifier, a capacitor (6.3 mF) and a custom-

made comparator board with added hysteresis. The energy harvesting board had an internal resistance of 950 Ω, and it required 60 mV for its start-up. The energy harvester was an inductor-based DC-AC converter that converted the DC voltage of the MFC into an AC signal. The bridge rectifier that was present just next to the energy harvester rectified the AC signal into a DC voltage to charge a capacitor. The charge of the capacitor was again monitored with a voltage comparator board to set a threshold limit for voltage charge and discharge when connected to the load. With this PMS, the voltage of the MFC was increased by about 17 folds, which is recommendable for a PMS in conjunction with MFC. Here, since the energy harvester starts at 60 mV, the PMS has been termed as an ultra-low power consuming system (Winfield et al., 2014). However, the use of the diodes in the rectifier circuit may reduce the efficiency due to their barrier potentials. Later, Schievano et al. (2017) also showed an ultra-low voltage power management system that could be utilized to enhance the voltage of the floating MFCs to power appliances such as an LED or a buzzer and other sensors connected with a wireless data transmission unit (Schievano et al., 2017). Here the PMS consists of only a basic DC/DC boost converter based on linear technology LTC3108. The most advantageous feature of such a DC/DC converter is that they start up only at an input voltage of 20 mV. This device also consists of a feature that its output voltage can be set at different voltage levels, such as 2.35 V, 3.3 V, 4.1 V and 5 V (Kim et al., 2019; Thomas et al., 2013). Therefore, while powering the LED and the buzzer, the MFC was connected to the input end of the converter, and the LED or the buzzer was connected to the output end. However, the transmission of data from the sensors to the receiver was performed intermittently.

1.5 Research gap

Studies on aquatic plant-coupled SMFCs were reported by the scientific community from the late 2000s. However, the studies on aquatic plant-coupled SMFC increased after 2011, since the coupling of aquatic plants was proven to have prospects in improving contaminant removal and power performance of SMFCs. The future prospects of the plant-coupled SMFC technology attracted different research groups to come up with several ideas to understand plant and SMFC interaction for further improvement of this novel technology. Hence, there are research gaps in this field, and exploring them would help to improve the understanding of the plant and SMFC interaction for further improvement of the technology in terms of power production.

1. In plant-coupled SMFCs, it has been reported that the bottleneck of low oxygen availability for the air cathode can be solved with radial oxygen released by the plant (Nitisoravut and Regmi, 2017). However, the overall effect of the aquatic plant on the DO of the overlying water and the mechanism of regulating the DO are yet to be explored.
2. Studies explained the effect of pH and electrical conductivity of the overlying water on the overall power performance of the SMFC (Grattieri and Minteer, 2018; Guo et al., 2021; Alipanahi and Rahimnejad, 2018). However, the effect of aquatic plants on pH and conductivity and then the SMFC power performance is a less explored subject matter.
3. The catalytic effect of open-environment cathode biofilm was investigated with an isolated group of microorganisms with cyclic voltammetry analysis (Parot et al., 2011). An investigation of cathode biofilm and their correlation with aquatic plant rhizobia microbial community in plant-coupled SMFC is required.
4. In view of open-environment operating conditions, the microscale (Kim et al., 2015a) and macroscale (An et al., 2015c) approaches experience high costs, constructional challenges and regular maintenance. Hence, a robust, low-maintenance, sustainable strategy is required to eliminate voltage reversal in series-stacked SMFCs.
5. The MPPT topology can extract power from SMFCs with ~50% conversion efficiency, and most topologies require external power sources for operation (Bautista et al., 2015a). For commercialization of SMFCs, a self-powered and more efficient PMS is required to enable SMFC technology as a power source for modern-day electronics.

Moreover, in continuation of points, 1 and 3 mentioned above, floating aquatic plants hinder oxygen exchange at the gas-water interface, resulting in a lack of dissolved oxygen at the cathode. Again, floating aquatic plants release oxygen to maintain dissolved oxygen at the cathode (Yeruva et al., 2018). In addition, the roots of floating aquatic plants promote the growth of a wide variety of microorganisms, which enhance the biodegradation of organic matter by the release of root exudates (Kabutey et al., 2019b). The type of aquatic plant affects the root exudate composition and hence the microbial community structure of the plant rhizosphere (Kouzuma et al., 2014). The aquatic plant-coupled SMFC exploits the column height to maintain redox differences in the system. The aerobes of the rhizosphere dominate at the top, and the anaerobes dominate at the bottom. And the facultative microbes dominate the intermediate layer (Kataki et al., 2021; Sharma et al., 2021).

1.6 Objective of the study

In correlation with the above challenges and research gaps acknowledged through the review of the literature (presented in chapter 1), this study aims to portray the possibilities to enhance the bio-electrochemical activity of ecosystem based MFCs for real-world commercial applications. To accomplish this aim, a Water Lettuce (*Pistia stratiotes*) assisted SMFC is considered as the device to study the impact of the aquatic plant on the electrochemical activity and sustainability of the device. In addition, the series connection associated concern, the voltage reversal phenomenon, has been studied, and a design of a self-powered PMS has also been presented. Corresponding electrochemical (voltammetry, impedance) investigations, biological (metagenomics, growth study, biofilm density) investigations, LCMS, EDX microscopy, pH, conductivity, and dissolved oxygen measurements as described in the following sections were conducted to streamline the inferences of the study.

I. Installing a lab setup for SMFC using mud, water, and water lettuce from a designated pond.

II. Preliminary investigation of the installed SMFC for open circuit potential (OCP), current, and half-cell potentials.

III. Investigating the influence of parameters such as pH, conductivity, oxygen in different depth level, temperature, etc., on the performance of the WL-SMFC.

IV. Identification and characterization of microbial community in Water Lettuce rhizosphere responsible for cathodic potential enhancement.

V. Half-cell studies of the SMFC.

VI. Study the performance of the SMFC in series stacking.

VII. Designing a PMS to obtain a utilizable power from the SMFCs

1.7 Significance of the work

Aquatic plant assisted SMFCs can be beneficial for both aquatic pollutant remediation and electricity generation (Regmi et al., 2018). This concept of study carries both fundamental research and technology points of view. To gain the futuristic insights of plant impact on the SMFC electrochemical enhancement and sustainability, many investigations have been reported and are proceeding (Hubenova and Mitov, 2012; Zhang et al., 2024). Such studies

explore the plant-electrode interface for sustainable electricity generation. On the other hand, attempts to eliminate voltage reversal in the series stacking of MFC/SMFCs (Kim and Chang, 2018; Sugnaux et al., 2017) confront us with the possibility of eliminating the voltage reversal phenomenon in stacking operation. In addition, studies on ultra-low-powered PMS design introduce the scope to design a self-powered PMS for intelligent management of SMFC power. The study embodied in this thesis work aims to stitch the approaches to intensify the power output of SMFCs through the integration of the SMFC setup with aquatic plants to investigate mechanistic insights of plant-SMFC interaction for power enhancement. Which is then followed by the elimination of voltage reversal in the series stacking of WL-SMFC and its conjugation with a self-powered PMS for real-world application.

1.8 Structure of the thesis

The study incorporated in this thesis is categorized into the following chapters.

Chapter 1: Introduction and review of literature

This chapter aims to inform the readers regarding the theoretical basis of the concept of plant-assisted Sediment Microbial Fuel Cells for enhancement of the electrochemical activity of the cell and its sustainability. Further, it explains the phenomenon of voltage reversal in the conventional process of series stacking, its causes, and probable methods of elimination. Also, it emphasizes the necessity of a self-powered PMS for the practical utility of SMFCs. This chapter draws the conclusion by contextualizing the concept of utilizing plant-assisted SMFCs with a PMS and describing the state-of-the-art developments of this concept in this field of research.

Chapter 2: Improving power performance of sediment microbial fuel cell through Water lettuce (*Pistia stratiotes*) assisted boosting of cathodic activity

This chapter investigates the effect of an aquatic plant, Water lettuce (*Pistia stratiotes*) on the pH, electrical conductivity (EC), dissolved oxygen (DO), and oxygen reduction reaction (ORR) on the cathodic surface and, subsequently, on the overall power performance of a Water lettuce-assisted SMFC (WL-SMFC). In addition, this chapter elaborates the relationship between the Water lettuce rhizosphere microbial communities and the SMFC performance decisive factors (viz. pH, EC and cathodic ORR) to comprehend the mechanism involved in performance enhancement of the WL-SMFC. Finally, the self-sustaining ability of the WL-SMFC system is studied to assess its potential for long term operations.

Chapter 3: An approach to eliminate voltage reversal in series connected plant-assisted sediment microbial fuel cells through surface area tuning of the anode

This chapter lays down the effect of anode surface area on the removal of voltage reversal (VR) in series connected WL-SMFCs. This study proposes a concept of tuning anodic surface area to mitigate the occurrence of VR in series stacked plant-assisted-SMFCs. An effort has also been made to explain the underlying principle of the constructed design by deriving a mathematical expression to establish the relationship between the anodic surface area of the terminal anode and the voltage response of the series stacked WL-SMFCs. A detailed account of the findings has been presented in this chapter.

Chapter 4: Design and fabrication of a self-powered voltage booster for enabling real-time applications of Water lettuce-assisted sediment microbial fuel cell

In this chapter, an effort has been made to improve the power performance of the stacked WL-SMFCs by virtue of a power management system. This work emphasizes designing a self-powered power management system that exploited the voltage double configuration of a charge pump IC to multiply the voltage output of two series connected WL-SMFC. The detailed account of the design, fabrication, operation, and performance of the PMS has been presented in this chapter.

Chapter 5: Conclusion and scope for future work

This chapter lays down the key findings of the experiments. It highlights the prominence of these research outcomes for further improvements in the field of open environment bio-electrochemical systems and concisely discusses the future prospects of this technology in the context of practical applicability.

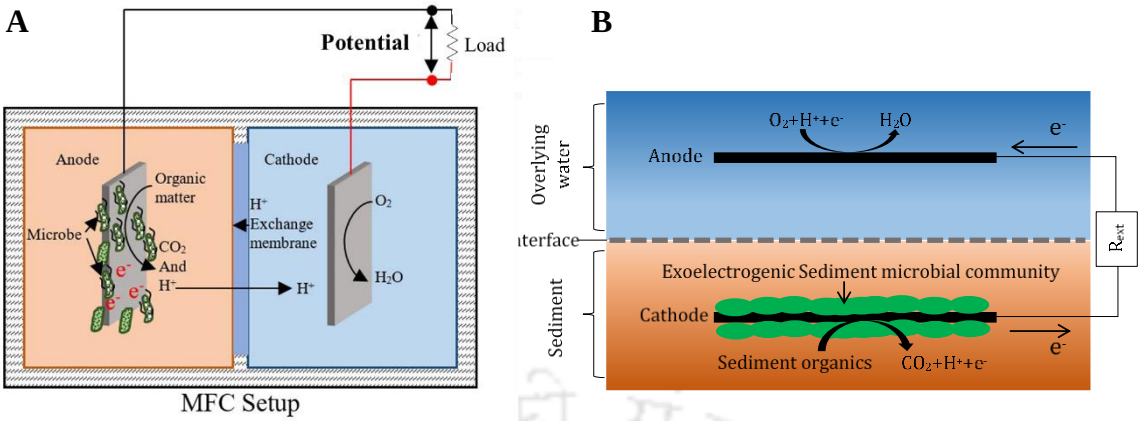

Figure 1.1: Typical (A) MFC and (B) SMFC configuration with main elements

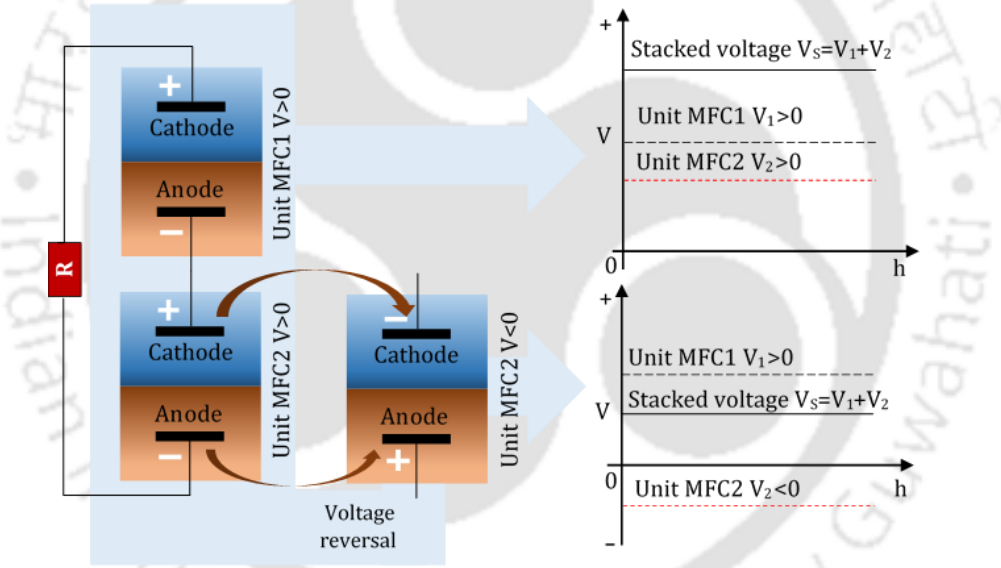

Figure 1.2: Voltage reversal (VR) occurrence in microbial fuel cells (MFCs) connected in series. Normally, when two galvanic cells are connected in series, the total voltage of the system is equal to the sum of the unit-cell voltages. During VR, the voltage across unit cells connected in series produces a negative voltage that significantly reduces the total voltage of the system (Kim et al., 2020)

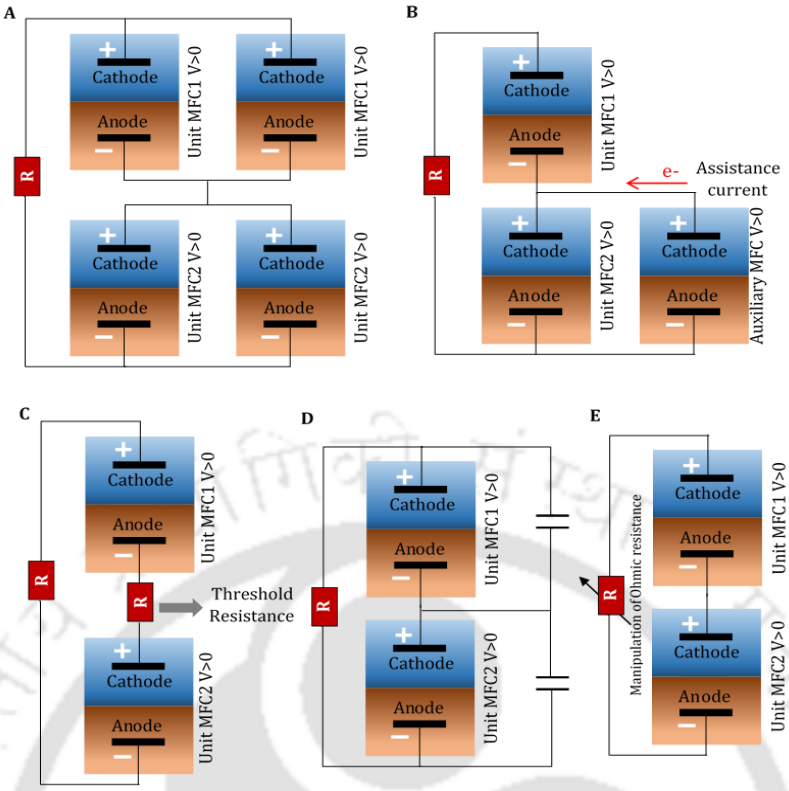

Figure 1.3: Different macro-scale strategies to eliminate VR in series stacking of MFC/SMFCs. VR control (A) by increasing current capacity, (B) with assistance current, (C) with resistor control, (D) with electronic circuit components, (E) with manipulation of internal resistance *(Kim et al., 2020)*

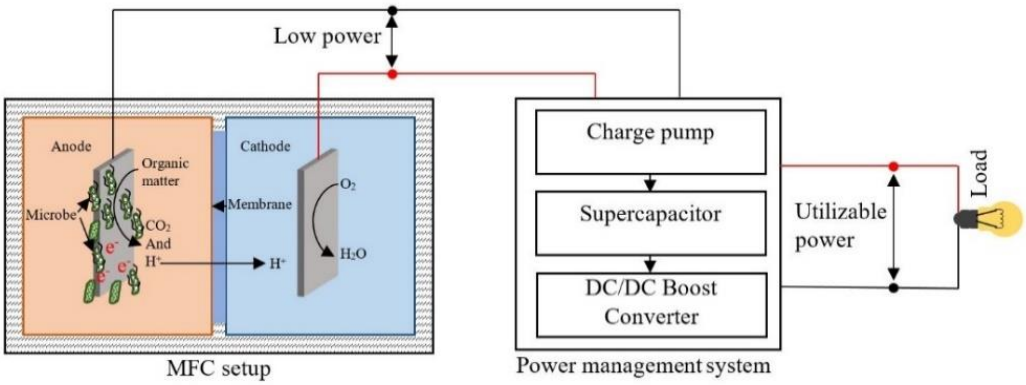

Figure 1.4: Basic configuration of a power management system (PMS) for scaling up the MFC/SMFC output power (Dutta et al., 2022a)

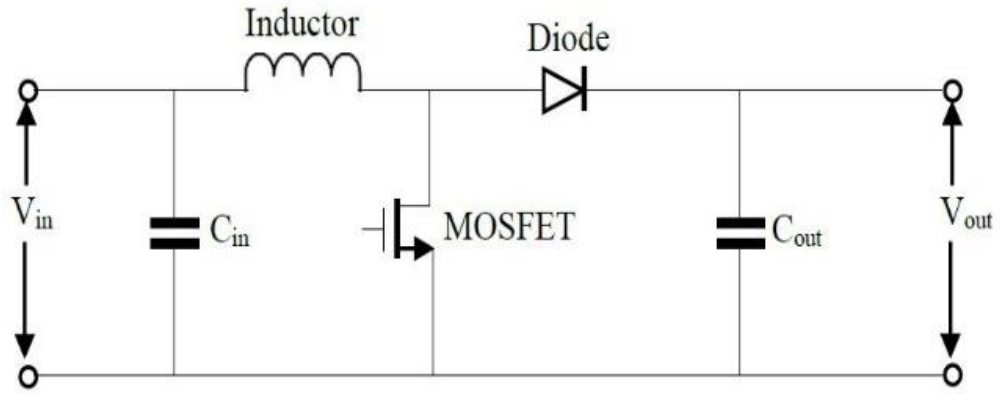

Figure 1.5: Simplified circuit diagram of a DC/DC boost converter (Dutta et al., 2022a)

CHAPTER 2

IMPROVING POWER PERFORMANCE OF SEDIMENT MICROBIAL FUEL CELL THROUGH WATER LETTUCE (*PISTIA STRATIOTES*) ASSISTED BOOSTING OF CATHODIC ACTIVITY

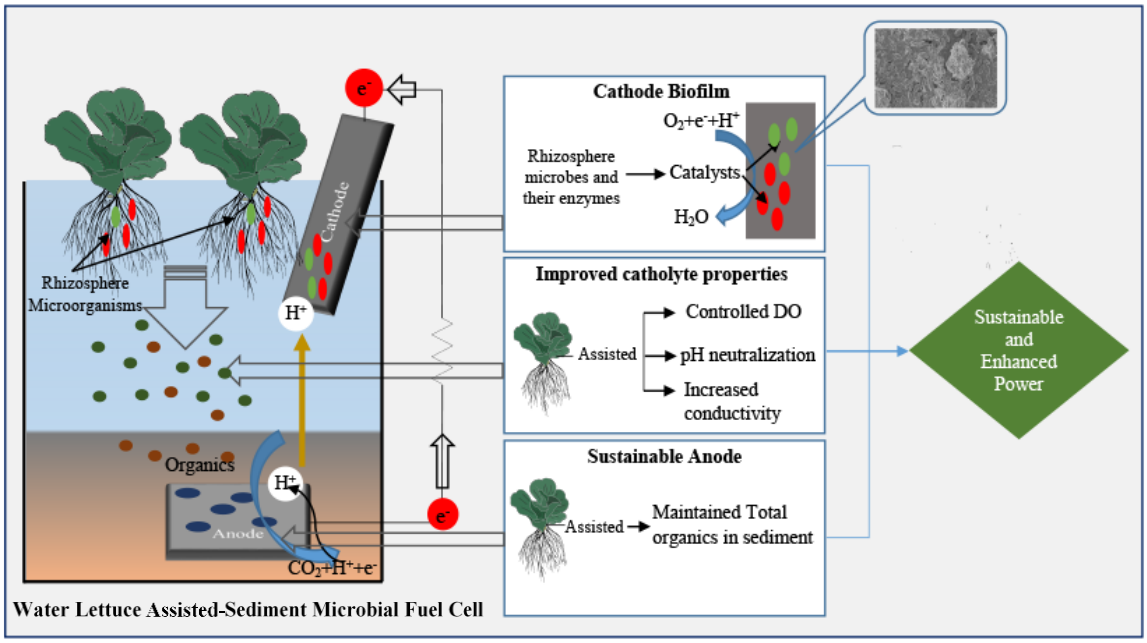

2.1 Introduction

Sediment microbial fuel cells (SMFCs) are evidential bio-electrochemical energy converters with simultaneous remediation capability for sediment pollutants (Sun et al., 2023). In an SMFC, electrochemically active microorganisms enable continuous energy recovery and waste utilization through the anaerobic oxidation process of the organic deposits (Yang and Chen, 2021). Studies have shown that they are sustainable in the context of energy recovery, cost effectiveness, and maintenance (Tommasi and Lombardelli, 2017). However, the power output of these devices is comparatively low, and contaminant removal is significantly sluggish, which poses limitations to their commercialization. (Ewing et al., 2017; Li et al., 2023; Tommasi and Lombardelli, 2017). The suboptimal factors, dissolved O_2 (DO), anode-cathode electrode displacement, ionic conductivity (EC), pH, microbial interference at the anode and cathode, and organic matter content are identified as the dominant factors limiting the power performance of the SMFCs (Domínguez-Garay et al., 2013; Parot et al., 2011; Rismani-Yazdi et al., 2008a; Song et al., 2019; Zhao et al., 2006). The suboptimal oxygen availability, higher anode-cathode displacement, and low ionic conductivity induce higher internal resistance in the SMFC setup. Precisely, the higher electrode displacement and low ionic conductivity contribute to higher ohmic losses; less oxygen availability at the cathode leads to higher mass transfer losses; and limited organic content results in inept exoelectrogenic microbial activity and higher activation losses (Logan et al., 2006a). The SMFCs are open-environment systems, and optimization of the electrolyte characteristics is a challenging task. In laboratory-scale setups, the optimization of the electrolyte parameters, EC, and organic content has been achieved with the addition of exogenous organic or inorganic salts (He et al., 2007; Najafgholi et al., 2015). This approach to SMFC optimization is limited to laboratory-scale setups and would be far-fetched for setups established in natural water bodies.

Suboptimal pH, in contrast to low EC, strongly influences oxygen reduction reaction (ORR) kinetics (Zhao et al., 2006). ORR over potential is also accountable for higher internal resistance in SMFCs. Efforts have been made to address the cathodic ORR limitations by introducing noble metal catalysts (Clauwaert et al., 2009), bacterial catalysts (Parot et al., 2011), metal-organic framework-derived electrocatalysts (You et al., 2016), and large cathode surface areas (Freguia et al., 2007b). In regards to the production of sustainable energy for SMFCs, bacterial enzyme-based catalysis of ORR is the most promising since the

technique requires less maintenance and cost (Milner et al., 2016). Studies have also conducted on coupling of plants in SMFC systems to enhance the power performance (Wang et al., 2023). Incorporating plants into SMFCs also supports efficient contaminant removal from the water bodies and fosters self-sustainability to this bioelectrochemical device. Plant root microbial interactions with the electrode surfaces can promote ORR through electroactive biofilm. The root exhudates are utilized as substrates for the electroactive biofilms on the anode and cathode, and they also release oxygen to support the ORR (Li et al., 2023; Nitisoravut and Regmi, 2017; Regmi et al., 2018). The effect of the plant on the pH, DO, and EC and their corresponding interactions with the SMFC system is however, a less explored subject matter. Moreover, the open environment cathodic biofilm and their catalytic response towards O_2 reduction are also not adequately studied.

The choice of plant in plant assisted SMFC is subject to their availability in the local environment. Macrophytes or hydrophytes are widely used in constructed wetland MFCs and offer simultaneous phytoremediation as an additional benefit (Regmi et al., 2018). In this study, the effect of an aquatic plant, Water lettuce (*Pistia stratiotes*) (WL) on the SMFC performance has been investigated. WL is a fresh water free-floating small aquatic plant belonging to the family of monocotyledon and is the sole species of its genus, *Pistia* (Buzgo, 1994; Schmid, 2000). These fast-growing plants usually float on the surface of the water and exist in colonies, forming a green and dense covering over the surface of the water bodies while their roots remain submerged and hang beneath the fronds. The WL flourishes in the temperature range of 22–30 °C and can withstand up to 35 °C and the pH range of 6.5–7.2 (Tamada et al., 2015). These morphological and growth characteristics are expected to facilitate technical issues for their applications in the SMFC. The microbial community that the WL rhizosphere houses is anticipated to be beneficial for the catalytic performance of the SMFC electrodes. Additionally, the rhizodeposits of the plant are likely to support the growth of catalytic bacteria on electrodes. Some preliminary studies indicated that the root exudates of plants are sequestered as substrates for the electroactive biofilms on the electrodes, and the plant releases oxygen to support the ORR in the cathode (Li et al., 2023; Nitisoravut and Regmi, 2017; Regmi et al., 2018). The effect of plants on the pH, DO, and EC of SMFCs is, however, yet to be adequately explored.

Herein, a laboratory-based WL (*Pistia stratiotes*)-assisted SMFC has been constructed to replicate a natural pond environment. The study investigates the effect of the aquatic plant on the pH, EC, DO, and ORR on the cathodic surface and, subsequently, on the overall power

performance of the SMFC. In addition, this investigation elaborates the relationship between the WL rhizosphere microbial communities and the SMFC performance decisive factors (viz. pH, EC and cathodic ORR) to comprehend the mechanism involved in performance enhancement of the WL-SMFC. Finally, the self-sustaining ability of the WL-SMFC system is studied to assess its potential for long term operations.

2.2 Materials and methods

2.2.1 Materials, chemicals and media solutions

Pond sediment, natural water, and WL for setting up of a laboratory-scale WL-SMFC were collected from a pond located within the campus of the Indian Institute of Technology Guwahati, India (26.1903° N, 91.6920° E). Iso-molded graphite plates, used as electrodes, were purchased from GraphiteStore.com (USA). Silver-conductive epoxy, used to connect the electrodes with peripheral devices, loads, copper wire, etc., was purchased from MG Chemicals (USA). Highly conductive copper wire with a PVC coating used as electrode terminals was purchased from M/S KEI wires and cables (India). The glassware used to construct the WL-SMFC was purchased from Borosil, India. MilliQ water with 18.2 MΩ.cm was used for preparing media and cleaning species.

$NaH_2PO_4.H_2O$, Na_2HPO_4, glutaraldehyde solution, and ethanol (99%), used in the experimentation, were of AR grade and purchased from Himedia, India; HPLC grade acetonitrile and LCMS grade formic acid were purchased from Merck, India. Hoagland's media, consisting of 1 ml/L $MgSO_4.H_2O$ (246 g/L stock), 2.3 ml/L $Ca(NO_3)_2.4H_2O$ (236 g/L stock), 0.5 ml KH_2PO_4 (136 g/L stock), 2.5 ml KNO_3 (101 g/L stock), 0.5 ml/L micronutrients, and 20 ml/L Fe.EDTA solution used as the microbial growth media was purchased from Himedia, India. The micronutrient stock solutions used in the experiment consisted of 2.86 g/L H_3BO_3, 1.82 g/L $MnCl_2.4H_2O$, 0.22 g/L $ZnSO_4.7H_2O$, 0.09 g/L $Na_2MoO_4.2H_2O$, and 0.09 g/L $CuSO_4.5H_2O$. The Fe.EDTA solution was prepared with $FeCl_3.6H_2O$ (0.48 g/L) and $Na_2EDTA.2H_2O$ (1.5 g/L)(Carvalho and Martin, 2001; Hoagland and Arnon, 1950).

2.2.2 Fabrication of WL-SMFC

A laboratory-scale WL-SMFC of 500 ml capacity was constructed using a glass beaker. 1/4 of the beaker height (about 3 cm) was covered by the pond sediment layer, and the water

height was maintained at 7 cm during the entire period of experimentation. Two iso-molded graphite plates with dimensions of 6 cm × 2 cm × 0.3 cm and 3 cm × 4 cm × 0.3 cm were used as the cathode and the anode, respectively. The electrodes were sonicated at ultrasonic power of 150 W for 30 minutes in ultrasonic water bath (Labman Instrument Pvt. Ltd., India) prior to the installation. The anode was placed centrally in a horizontal position within the sediment layer. The cathode was placed vertically near the surface, with one half exposed to air and the other half submerged in water. The total surface areas of the cuboid-shaped anode and cathode were 28.2 cm^2 and 28.8 cm^2, respectively. Silver-conductive epoxy was used to attach the wire to the electrode surface, while non-conductive epoxy glue was used as anti-corrosion to envelope the exposed surface of the copper wires. Finally, WL plantlet was seeded on the water surface to complete the setup.

2.2.3 Operational conditions for the WL-SMFC

The WL-SMFC system was operated at ambient conditions (25-31 ^{0}C, 68-82% humidity), which is reported to be the optimal for the vegetative growth of WL (Ahmed et al., 2020; Gadkari et al., 2020). A photoperiod of 10 and 14 hours light and dark respectively was maintained throughout the period of experimentation with artificial light of intensity 1120 LUX was provided with a digital LUX meter (Dr.Meter, LX1010B, China).

2.2.4 WL-SMFC performance analysis

Electrode potentials of SMFCs were measured using a digital multimeter (Fluke 87v, Fluke Corporation, USA) with respect to Ag/AgCl as the reference electrode (BASI Research Products, USA). Ohm's law: I= V/R, where I is the current, V is the voltage across the load, and R is the value of the load resistor, was applied to calculate the current produced in SMFCs under closed circuit conditions. In this study the SMFCs were operated for seventy-two days both in OC and CC conditions. Under CC mode of operation, a 10 kΩ resistor was connected to observe the SMFC potential variations. The polarization curves were obtained with different resistive loads in the range of 300 kΩ to 50 Ω and after seventy-two days of SMFC operation.

2.2.5 Physicochemical characterization of the electrolytes

The physicochemical properties of the aqueous electrolyte were analyzed with a DO metre (Eutech DO700) for DO, a pH metre (Eutech Instruments) for pH, and an EC metre (Metler Toledo USA) for EC. Oven-dried sediment samples (100 °C for 24 hours) from the SMFCs

were characterized for their organic content thermogravimetrically in an O_2 environment in the temperature range of 30-900 °C at a ramping of 10 °C per second with a thermogravimetric analyzer (TGA4000, PerkinElmer). The measure of the total organic content was predicted from the weight loss in the temperature range of 200-430 ^{0}C in the sediment samples (Pallasser et al., 2013).

2.2.6 Analyses of WL root exudates

The WL roots were cleaned with MiliiQ water before being cultured on nutrient media. Thereafter, the plants were transferred to MilliQ water for two days. The procedure was repeated multiple times to increase the concentration of root exudates in the collection medium. The objective of using the MilliQ water to collect the root exudates was to reduce the potential interference from salts in the growth media. Subsequently, the samples were lyophilized and analyzed using the LC-MS/MS (Liquid chromatography mass spectrometry) technique on an Agilent 6410 Tripple Quad MS-MS following a specific protocol. The sample was injected into a reverse phase C18 column at a flow rate of 200 nL/m. The mobile phases were H_2O, with 0.1% formic acid as phase A, and 80% acetonitrile with 0.1% formic acid as phase B. The HPLC gradient ranged from 5% to 80%. An MS database (Mass Hunter) was used to analyze the mass of the eluted samples from the column. The elemental analysis of the moisture free root exudates was conducted using Energy Dispersive X-ray spectroscopy (EDX) (Make: Zeiss, Model: Sigma 300) (Sable et al., 2020).

2.2.7 Analyses of biofilm and WL rhizosphere microbial community

2.2.7.1 Analysis of microbial biofilm

Biofilms developed over the cathode were examined using a field emission scanning electron microscope (FESEM) (Make: Zeiss, Model: Sigma 300). Electrode surfaces were prepared by following the standard protocol described previously (Bora et al., 2022). Briefly, the surface of the electrode was cleaned with 0.1 M sodium potassium phosphate buffer solution (NaPBS) of pH 7.2, followed by air drying. Before imaging, the biofilm-coated electrodes were fixed with a 2.5% glutaraldehyde solution for 12 hour of retention time and washed using a 0.2 M NaPBS, pH 7.2. Afterward, the electrodes were dehydrated using a 10–100% gradient alcohol series for 10 minutes for each stage with very gentle periodic agitation and then left overnight for air drying. The desiccated samples were mounted onto stubs, sputtered with gold, and then images were captured in the magnification range of 10 µm to 1 µm.

The biofilm was extracted from the cathodic surface into sterile water samples using sonication, and then the optical density (OD) was recorded instantaneously. The microbial density of the cathodic biofilm was determined by measuring the ratio between the OD at 600 nm of the extracted biofilm using a UV-Vis spectrophotometer (Make: Agilent, Model: Carry 100) and the total surface area of the cathode (Cobine et al., 2013; Mira et al., 2022).

2.2.7.2 Analyses of microbial metagenomics

The microbial diversity of the WL rhizosphere and cathodic biofilm were examined by metagenome analysis. The first step involved the extraction of the rhizosphere and the biofilm microbes into 1X NaPBS. The microbe extraction from the WL roots and biofilm on cathode surface was achieved through sonication at 20 kHz with a 150 W sonicator (Labman Instrument Pvt. Ltd., India) (Bjerkan et al., 2009). Thereafter, the sample was prepared for metagenome sequencing, which was done using the NGS technique on an Illumina platform (Vo and Jedlicka, 2014). Initially, the DNA was isolated, and its quality was checked using an Xcelgen DNA Isolation Kit. 1 µl of each sample was used to determine concentration using a Qubit 2.0 Fluorometer. After quality-checking of the isolated DNA, the paired-end sequencing libraries were prepared using a DNA library kit (Truseq Nano). The library preparation method involved the ligation of platform-specific adapters to both ends of the DNA to allow for PCR amplification and the binding of standard Illumina sequencing primers. The quantity and quality of the amplified library were analysed by a bio-analyzer (Bioanalyzer 2100, Agilent Technologies). After obtaining the concentration for the library and the mean peak size from the bio-analyzer profile, the library was loaded onto the Illumina platform for cluster generation and sequencing. The data generation and sequencing for the sample were performed on the Illumina Platform with a chemistry of 2 x 150 base pairs (bp) ("Principle and Workflow of Illumina Next-generation Sequencing | CD Genomics Blog," 2018). All the samples were then assembled using a standalone metagenome assembly program (SPADes Assembler). The assembled scaffolds for all the samples were then subjected to gene prediction using the metagenome gene prediction method using Prodigal (v2.6.3). These predicted genes were then taken further for taxonomic and functional analysis using a standalone metagenome classifier tool, Kaiju (Menzel et al., 2016).

2.2.8 Electrochemical characterization of the cathodic biofilm

Electrochemical characterization of the cathodic biofilms was done using a potentiostat (PGSTAT Metrohm, USA) in a three-electrode assembly setup with a glassy carbon electrode

(GCE) as the working electrode, Ag/AgCl as the reference electrode, and a platinum wire as the counter electrode. Differential Pulse Voltammetry (DPV) was employed to study the catalytic behaviour of the cathodic biofilm. The electrodes were first rinsed with sterile water for the removal of surface impurities, followed by immersion in growth media, which served as the electrolyte. Thereafter, they were subjected to sonication for 20 minutes for the detachment of the biofilms from the electrode and dissolute into the growth media for the DPV analysis.

2.2.9 Statistical analysis of the data

In this study, each data point in the graphs for potential, polarization, pH, DO, EC, electrical parameters and microbial growth is a means of triplicate data and error bar represents standard error of the mean. Matrix Laboratory (MATLAB) tool was used to analyze the statistical data.

2.3 Results and discussions

2.3.1 Electrical performance of the WL-SMFC

The SMFC setups as shown in Figure 2.1, were operated in OC and CC modes, along with controls (without WL), and their respective potential variations were monitored over a period of seventy-two days and has been shown in Figure 2.2. The startup time at which the potential gets stabilized for the WL-SMFC was five days as against fifteen days for the C-SMFC. In the initial phase of the OC operation mode, WL-SMFC exhibited significantly higher OCP than the control (Figure 2.2A). Beyond the day twenty, though the OCP difference between WL-SMFC and C-SMFC waned, the OCP for WL-SMFC was still higher (minimum 720 mV) than the control setup throughout the operation.

Under the CC operation mode, the potential of both C-SMFC and WL-SMFC were dropped as expected, followed a general trend of biofuel cells, and the reduction was a cumulative-downplaying effect of anodic and cathodic potentials as shown in Figure 2.2E and in Figure 2.2F respectively. Continuous negative potential on the anode of WL-SMFC was evidential for sustainable current generation. Irrespectively, shifting of polarity of the anode (positive to negative) of C-SMFC beyond day twenty signified full discharge of the anode and hence incoherence in current generation (Figure 2.2E).

A maximum of 22.45 mW/m^2 power density was recorded for WL-SMFC as shown in Figure 2.3A. Coupling of WL to the SMFC could significantly enhanced the current density from 77.89 µA/m^2 (C-SMFC) to 136.84 µA/m^2 as shown in Figure 2.3B, indicating improved redox mass transfer to the electrodes. This improved performance is a consequence of internal resistance reduction of the SMFC upon its coupling to WL. Based on the power transfer theorem, the internal resistance of 3 kΩ of the control was reduced to 2 kΩ upon coupling the cell with WL.

In the OC mode of operation a sacrificial dip in the potential value on day seven, thirty-four and sixty-five as shown in Figure 2.2A was caused by the adjustment of water levels in the setups that effected the physicochemical properties of the catholyte, particularly pH and ionic conductivity as shown in Figure 2.5E-F. This disturbance was mostly contributed by the cathodic potential, as the anodic potential was unaffected and stable during the period as shown in Figure 2.2C and Figure 2.2B correspondingly. This result infers that the cathode, which is located in the sub-surface of the setup, is sensitive to the physicochemical parameters (such as oxygen, pH and solution conductivity); whereas, the activity of the anode, which is submerged inside the mud in the bottom of the setup, is greatly immune to these environmental parameters in such a transient disturbance. The overall cathodic and anodic potentials of the WL-SMFC were higher than the C-SMFC under the OC condition as shown in Figure 2.2B-C. The results confirmed a positive role of the WL in improving the electrical potential of the SMFC (see Table 2.1).

Interestingly, the reduction of cathodic potential was much higher than the anodic potential under the CC conditions. The anodic potential of both the WL-SMFC and C-SMFC is stronger than their corresponding cathodic counterparts that resulted in negative over potential on the cathode under CC mode of operation. Beyond day twenty, the anode of C-SMFC shifted its polarity from negative to positive, whereas the anode of WL-SMFC had steady negative potential (-121.01±6.5 mV) since day ten and can be seen in Figure 2.2E. The variation in the positive potential in the anode of C-SMFC as shown in Figure 2.2E, had a similar trend to that of the corresponding cathode as show in Figure 2.2F, signifying the sharing of cathodic potential with the fully discharged anode. The complete discharge of the anodic potential was confirmed by recording instantaneous null potential after disconnecting the load of C-SMFC. Sustainability of the anodic reactions in the WL-SMFC setup is reliant on the availability of organics in the sediment. The content released from the WL root

exudates and dead parts of the plant settled on the anodic sediment sustained the anodic activity as revealed from the result discussed below in section 2.3.2.1.

In spite of the steady-state reduction of the potential, the WL-SMFC delivers current continuously, albeit at a low magnitude, indicating sustainability of the system. Further, the polarization studies have shown improved power generation and current generation in the WL-SMFC and the respective improvements can be seen in Figure 2.3A-B. An activation loss of 23 mV in the current density range of 0.89 to 3.7 mA/m^2 was observed for the C-SMFC, whereas the activation loss for WL-SMFC was limited to 8 mV and in the current density range of 0.90 to 1.78 mA/m^2. In the Ohmic loss region, the C-SMFC had voltage loss gradient of -8.4 whereas voltage loss gradient for the WL-SMFC was -5.9. Mass transfer loss was evidential for the C-SMFC beyond the current density of 87.72 mA/m^2 and interestingly negligible mass loss was observed for the WL-SMFC. The reduced internal resistance was due to the increased conductivity of the catholyte as shown in Figure 2.5F.

Table 2.1: Electrical potentials of SMFCs and half-cells with and without WL seeded setup recorded at peak operations hours (the presented values are average of the potential values of the SMFCs recorded at peak operation hours, number of replica for each system was 3).

Set-up	Type of potential	C-SMFC(mV) (A)	WL-SMFC(mV) (B)	Difference (mV) (B-A)
SMFC	OC	683.61	793.75	110.14
	CC	162.89	165.07	2.18
Anode	OC	-443.23	-451.05	-7.82
	CC	-184.78	-235.71	-50.93
Cathode	OC	239.47	342.08	102.61
	CC	-22.11	-71.04	-48.93

2.3.2 Effect of WL on the SMFC parameters

2.3.2.1 Sequestration of organic mass

The organic content accumulated in the anodic sediment of WL-SMFC over a period of seventy-two days operations under CC condition was analyzed. The organic content in the setup was 5.82% as against 3.01% in the control setup as shown in Figure 2.4, indicating an additional organic content of 2.81% accumulated in the WL-SMFC sediment over the

operation time. Notably, the average biomass growth of the WL species in the WL-SMFC setup was 6.7±0.0023 mg/day.

2.3.2.2 Effect of WL on DO and cathodic potential

Figure 2.5A shows that the overlaying column of water in the SMFC setups was vertically divided into six layers with each level height of 1 cm. The DO level at each layer was then recorded to evaluate the effect of WL on the DO gradient across the column. The WL inclusion reduced DO concentration steadily and more intensely than the control setup from the top to bottom of the column (Figure 2.5B). The DO at level 1 (near the cathode area) was reduced from 5.84 mg/L (in control) to 4.91 mg/L. Whereas, in the level 6 (over the anodic sediment), it was reduced from 3.18 mg/L (in control) to 2.3 mg/L. The average rate of oxygen reduction across the column for the control (0.56±0.03 mg/L/cm) and WL-SMFC (0.49±0.02 mg/L/cm) was though, not much different (0.07±0.5 mg/L/cm), the overall reduction of the DO in WL-SMFC setup was higher than the control by an average of 0.7±0.08 mg/L.

Next, the relationship between the DO and cathodic potential was examined under OC and CC conditions in the setup (Figure 2.5C-D). Under the OC mode, an optimum DO concentration of 2.07 mg/L was identified. However, under the CC operation, the DO concentration of 1.12 mg/L was identified as the critical value for the cathodic ORR. Interestingly, an inverse relationship between catholyte conductivity and DO was observed in Figure 2.5C.

It is known that the concentration of DO in the water overlying the sediment directly affects the air-breathing cathode potential (equation 2.1) (Renslow et al., 2011). However, in spite of the reduction of DO concentration in WL-SMFC, it generated a better cathodic potential than the control. Thus, to analyze the critical level of DO for ORR in the cathode, an experiment was conducted wherein the cathode potential of the SMFC was monitored under OC and CC modes against different DO concentrations adjusted by purging Ar gas through the electrolyte. The setup was covered with a lid bearing all the necessary electrodes and probes (Ag/AgCl reference electrode, DO probe, conductivity probe etc.) to prevent the interference from the atmospheric O_2.

$$E = \frac{T}{T_0}E^0 - \frac{\Delta H_r^0}{\Delta H_{sol}}\frac{RT}{nF}ln\left(\frac{CK_H^0}{p}\right) \quad (2.1)$$

Under the OC mode, an optimum DO concentration of 2.07 mg/L was identified. Whereas, according to Figure 2.5D under the CC mode, when the DO was squeezed from 4.2 mg/L to 1.12 mg/L, the cathodic potential increased at an average rate of 4.5±0.12 mV/mg/L. This increment could be attributed due to the increased ionic conductivity as shown in Figure 2.5C. Remarkably, below 1.12 mg/L the cathode rapidly accumulated negative potential at a rate of 20.75±7.9 mV/mg/L and eventually stabilized at an average of -46±1.2 mV when the DO concentration was further reduced below 0.69 mg/L to 0 mg/L. This indicates sharing of anode potential due to absence of any cathodic activity. This fact was confirmed from the generation of null potential on the cathode at a DO concentration of 0 mg/L by removal of the load connecting the anode and cathode. Based on the above findings, it may be comprehending that the magnitude of DO concentration (0.7±0.08 mg/L) reduced by WL inclusion does not affect the ORR in the air-breathing cathode (working area of 28.2 cm^2) as under the inclusion conditions, the level of DO in the SMFC was much higher than the critical level across all the depth levels shown in Figure 2.5B. Whereas, this WL–led reduction of DO in the sediment surface level might reduce oxygen diffusion to the anode, supporting anoxic environment in its periphery and thus minimizing the waste electron scavenging reactions. Notably, for anodic reactions the DO level should be less than 1 mg/L at the periphery of the electrode (Elmaadawy et al., 2022; U.S. Geological Survey, 2006).

2.3.2.3 Effect of WL on the pH

The catholyte pH value was increased in both C-SMFC and WL-SMFC in the initial phase upto 24 hour of operations under CC mode of operation and the variation of pH with respect to time can be seen in Figure 2.5E. Following the increase, the pH was leveled off at pH~ 8.0 in case of C-SMFC. Whereas in case of WL-SMFC the pH value was leveled off within 7.2-7.6, indicating a metabolic role of the plant to bring the pH value closer to pH 6.5–7.2 for its optimal growth. The troughs in the graph are caused by the adjustment of water level during the operation period.

The WL in the SMFC setups induces pH neutrality of the catholyte and this activity in turn reduces the ORR overpotential in the cathode (Zhao et al., 2006). The metagenomics study of the bacterial species present in the rhizosphere of WL planted in the SMFC helped us to understand their role on pH hemostasis. A sizeable number of bacterial species shown in Table 2.2, identified through the study have been previously reported to produce various metabolites and enzymes contributing to the pH neutralization of the growth medium for its

sustainability (Foster, 2004; Krulwich et al., 2011; Lund et al., 2014). Such root-induced pH changes involving the plant roots and their microbes are subject to the release of charges (H^+ or OH^-). Rhizosphere microbes release protons in response to an alkaline pH through the process of ATP consumption (Russell, 2007). When the pH is acidic, some microbes consume protons through the process of decarboxylation reactions as a response to a low or acidic pH, such as the decarboxylation of amino acids such as glutamate, arginine, or lysine (Krulwich et al., 2011; Lund et al., 2014, 2020). Also, microbial cells can deploy reactions that produce basic compounds to help neutralize the pH, such as the production of ammonia from urea or amine-containing amino acids such as arginine or glutamine to counteract acidity (Krulwich et al., 2011; Pennacchietti et al., 2018).

Table 2.2: Species of WL rhizosphere and their metabolites and enzymes responsible for pH neutralization ("National Center for Biotechnology Information," n.d.; Schober et al., 2025).

Metabolite	Species
Glutamate	*Pannonibacter phragmitetus, Clostridium tagluense, Lachnotalea glycerine*
Arginine	*Halomonas hydrothermalis, Pannonibacter phragmitetus, Clostridium tagluense, Lachnotalea glycerine*
Lysine	*Pannonibacter phragmitetus, Clostridium tagluense, Lachnotalea glycerine*
Enzyme	Species
Urease	*Pseudomonas linyingensis, Rhizobiales bacterium, Pannonibacter phragmitetus*

2.3.2.4 Effect of WL on the Conductivity

Figure 2.5F shows the variation in the conductivity of the catholyte in CC mode of operation of the SMFCs. The conductivity of the catholyte in the WL-SMFCs increased with time, the maximum being 492.1 µS/cm, while a decreasing trend was observed in case of that of the C-SMFCs, the maximum being 354.8 µS/cm.

The ionic conductivity of the catholyte significantly impacts the power generation capacity of the SMFC. An increase in the ionic conductivity lowers the internal resistance and consequently improves the power production (Najafgholi et al., 2015). Figure 2.5C represents the inverse relationship between the DO and conductivity values. Reduction of DO lowers the partial O_2 pressure in the water, which subsequently increases the solubility of partially dissolved solids and thereby leads to an increase in the conductivity of the solution (Koralay

et al., 2018). The diffusion of atmospheric O_2 into the catholyte was reduced due to the canopy of the WL on its surface, and hence an increase in conductivity was observed along with reduction of the internal resistance by 1 kΩ. Moreover, some of the plant metabolites might have also contributed to the conductivity enhancement (Ma et al., 2023).

LCMS and EDX analyses were conducted to identify the metabolites of the WL plant contributing to the conductivity of the WL-SMFC, and the data are presented in Figure 2.6 and Table 2.3. The WL plant root exudates consisted of complex compounds $C_{14}H_{51}Ca_2Fe_3N_7$, $C_{17}H_{53}Fe_4N_6$, $C_{18}H_{53}Fe_4N_4O$, $C_{19}H_{57}Fe_4N_4$, $C_{21}H_{58}Fe_4P$, $C_{26}H_{64}Fe_3KN$, $CH_{49}ClFe_{14}N_5$, $C_3H_{53}ClFe_{14}N_3$, $C_{10}H_{47}Fe_4N_{14}$, $C_{12}H_{51}Fe_4N_{12}$, $C_{25}H_{63}Fe_4$, $C_{24}H_{59}Fe_4O$, $C_{22}H_{59}CaFe_4$, $C_{23}H_{55}Fe_4O_2$, $C_{22}H_{60}Fe_4K$ etc. The compounds identified as the WL rhizosphere exudates are mostly organic compounds and are iron (Fe)-based. Notably, the root exudates of aquatic plants contain various organic compounds like amino acids, organic acids, phenolics, sugars, polysaccharides, proteins, and enzymes that serve as carbon and nitrogen sources for rhizosphere microbial growth (Fan et al., 2023). The aquatic plant roots are also susceptible to the formation of iron plaques due to various Fe-oxidising bacteria and Fe-reducing bacteria, etc. (Xiao et al., 2023). These iron plaques can be mobilized by the root exudates due to ligand exchange and chelation; also, the root exudates contain Fe solubilizing agents (Aggarwal et al., 1999; Sardans et al., 2023) which result in the formation of such Fe-based-organometallic compounds as the final exudates from the roots. These compounds in their dissolved state could be responsible for the increase in the ionic conductivity of the catholyte. These soluble Fe containing compounds may facilitated charge transfer thereby improving the cathode performance (Ucar et al., 2017). The aquatic plant root microbe and root exudates interactions may be interesting to know to address the phenomenon. The exudates here have been collected from roots inhabited by microbes. Hence, the compounds represented here are the products released mostly by the rhizopshere microbes. In the process of converting the root exudates into the complex organic compounds the microbes also utilized the O_2 released by the aquatic plant roots (Srivastava et al., 2017). Other than the Fe oxidation or reduction, the microbes exhibited two more symbiotic approaches with plants: endophytic (such as N_2 fixing) and ectophytic (such as ammonia oxidation). In the ectophytic microbe interaction, several biochemical reactions occur at the interactive surface that influence the elemental cycles in the aquatic ecosystem (Laanbroek, 2010). In these processes, O_2 is utilized in the aerobic decomposition of organic matter present as plant exudates by heterotrophic bacteria (Bodelier, 2003). This oxygen consumption likely to be

one of the reasons for reduction of DO concentrations in the catholyte of WL-SMFCs as discussed above.

Table 2.3: EDX analysis of the WL-root exudates

Elements	Weight %
Carbon (C)	23.60
Nitrogen (N)	9.60
Phosphorus (P)	3.50
Sulfur (S)	4.35
Chlorine (Cl)	0.70
Potasium (K)	6.03
Calcium (Ca)	9.03
Magnesium (Mg)	3.33
Oxygen (O)	57.18
Iron (Fe)	0.33

2.3.3 WL rhizospherale bacterial community improve cathodic reactions

The influence of WL on DO, pH and catholyte conductivity to enhance the cathodic potential has been presented above. In this step, the possible sequestration of bacterial community from the WL rhizobia to the cathodic surface for forming a biofilm, and the characteristics of the biofilm in terms of electrogenicity and metabolic function for supporting cathodic activity have been explored. Figure 2.7 shows the surface morphology of the cathode after seventy-two days of operation under CC and OC modes for both WL-SMFCs and C-SMFCs, indicating the formation of biofilms on their surfaces. The CC operation induced higher bacterial population on the cathode surface of WL assisted cells than the corresponding OC operational modes and the difference can be visualized in Figure 2.7B(1-2) and Figure 2.7C. However, the population for WL-SMFC was far higher than the corresponding control experiment and the difference can be seen in Figure 2.7B-E. The impact of operating conditions (OC and CC) on the cathodic biofilm was further investigated by determining the bacterial density present per unit area of the cathode. The corresponding biofilm density for WL-SMFC and C-SMFC under CC operations were 0.28±0.11 AU/cm^2 (0.16±0.03 AU/cm^2) and 0.05±0.03 AU/cm^2 (0.05±0.01 AU/cm^2), and the respective density values under OC operation are shown in brackets. It is thus, confirmed that a highest biofilm growth occurred

on the cathodic surface of WL-SMFC under the CC operational mode. The catalytic nature of these biofilm microbes has been demonstrated by the DPV studies (Figure 2.8). A positive shift in the reduction potential by 156 mV and 80 mV, respectively, from the reduction peaks of the blank and the C-SMFC was observed for the WL SMFC biofilm in the potential range of -0.2 to -0.6 V.

2.3.4 Rhizospherale bacterial community linked to cathodic biofilm

The metagenomic analysis was performed through NGS for the bacterial samples isolated from the rhizosphere root of the WL. The rhizosphere of the WL is the habitat of a wide range of microbial communities. The analysis of the rhizosphere microbial community includes mostly bacteria (identified 53.6% at species level and 17.3% at genus level), viruses (0.03%), and some unclassified microbial species (29.07%) (Figure 2.9A). The bacterial community of the WL rhizosphere was dominated by the species of alpha, beta and gamma subclasses of *Protreobacteria* (38.63%), *Firmicutes* (24.12%), *Bacterodetes* (9.79%), *Actinobacteria* (3.23%), *Planctomycetes* (1.16%), *Verrucomicrobia* (1.12%), *chloroflexi* (0.77%), *Acidobacteria* (0.37%), *Cyanobacteria* (0.28%), *Spirochaetes* (0.17%), *Bacillariophyta* (0.14%), *Euryarchaeota* (0.10%) *etc* as shown in Figure 2.10A1 (Genome accession- SAMN39410320). The microbial species identified on the cathodic biofilm were representatives of alpha, beta, and gamma subclasses of *Proteobacteria* (93.1%), *Actinobacteria* (5.36%), *Planctomycetes* (1.06%), *Cyanobacteria* (0.94%), and a few eukaryotic cells from the *Strepophyta* (0.51%) group (Figure 2.10B1) (Genome accession- SAMN40275077). Figure 2.9A and Figure 2.9B show the whole microbial diversity present in the WL rhizosphere and cathode biofilm, respectively. In this study, the characteristics of the top 100 species of these phyla and their active participation in the WL-SMFC power enhancement were analyzed. The top 30 species from rhizosphere and the biofilm are shown in Figure 2.10A3 and Figure 2.10B3, respectively. Many bacterial species (Table 2.2), which are also present in the WL rhizosphere of the current study, are widely known to possess metabolites such as glutamate, arginine, lysine and enzyme such as urease. These metabolites and enzyme are likely to influence the pH of the catholytes in the WL-SMFC as discussed in "effect of WL on pH" subsection. While, the cumulative deposits of plant and rhizosphere microbes may influence the conductivity of the catholytes as presented under "effect of WL on the conductivity" subsection.

An analysis revealed that the bacterial species identified in the cathodic biofilm of WL-SMFC was mostly aerobic in nature. Upon mapping the microbial community, it was observed that the aerobic microbial species belonging to the *Proteobacteria, Actinobacteria, Planctomycetes*, *Cyanobacteria*, and *Strepophyta* that were present in WL rhizosphere colonized on the cathode surface to form biofilms. The catalytic behavior of these aerobic microbes is revealed from the cathodic ORR shown in Figure 2.8.

The biofilm formed in aerobic conditions has been reported to possess the ability to catalyze the electrochemical reduction of oxygen and other redox-active compounds released by the microbes on the cathode surface (Parot et al., 2011). Studies have also shown that the growth of biofilm on the cathodic surface can enhance ORR with the association of some enzyme catalysts or O_2-reducing compounds produced by the microbes (Erable et al., 2010; Faimali et al., 2008; Parot et al., 2011; Scotto et al., 1985). The DPV result indicates catalytic participation of the biofilm microbes in the ORR that diminishes the O_2 reduction overpotential on the cathode and its linked contribution to the SMFC's power generation (Faimali et al., 2008; Scotto et al., 1985).

The metagenome analysis of the cathodic biofilms was performed to understand the type and role of the bacterial cohorts that contributed to the cathodic performance. From the analysis, *Ferrovibrio terrae, Comamonas aquatic, Achromobacter xylosoxidans, Hydrogenophaga taeniospiralis, Phreatobacter stygius, Sphingobium xenophagum, Cupriavidus pauculus, Sphingomonas panacis, Delftia acidovorans, Comamonas thiooxydans, Acidovorax citrulli* were found to be catalase-positive bacteria whose abundance was among the top hundreds of the microbial population in the cathodic biofilm of the WL-SMFC (CC). Notably, these microbes have link with the rhizosphere microbial community of the WL. The similarity between the bacterial profiles of the WL rhizosphere and the cathodic biofilm is evidential to understand the participation of WL rhizosphere microbes in the cathodic activity and formation of biofilm. The higher microbial density on the cathode of WL-SMFC operated with a load (CC mode) is a consequential of the electrical stress on the electrotrophs which elicit faster biofilm growth as a response towards the energy draining metabolic reactions occurring at the cathode (Li et al., 2020).

It is known that many of the bacterial species of the cathodic biofilm are reported to secrete catalase to protect them from toxic by-products of O_2 metabolism, which simultaneously aids the ORR in microbial fuel cells (Ammam and Fransaer, 2013; Chelikani et al., 2004; Parot et

al., 2011; Plumeré et al., 2012). Catalase breaks H_2O_2 and produces O_2 molecules, which act as the electron acceptor at the cathode (Heck et al., 2010). The conversion of H_2O_2 to water and O_2 by catalase is a two-step process. At the first step, the catalase heme Fe^{+3} reduces a singular molecule of H_2O_2 to water by producing a covalent $Fe^{+4}O$ oxyferryl species referred to as compound I and a porphyrin cation radical. This compound then oxidizes a second H_2O_2 molecule, forming molecular oxygen and another molecule of water (George, 1948; Jones and Dunford, 1977; Kirkman and Gaetani, 2007).

The metagenomic analysis of the cathodic biofilms confirmed *Pannonibacter phragmitetus*, a bacterium of the *alphaproteobacteria* class that possesses a heme metabolism pathway. Heme groups absorbed onto the surface of the carbon electrode can bind and activate the O_2 molecule, causing its reduction to H_2O_2, and hence symbiotically supplying H_2O_2 to the catalase-positive bacteria, where it is oxidized to O_2 and water (Heck et al., 2010). In situations where the level of H_2O_2 is insufficient, the peroxidative activity of catalase is reported to result from the ability of compound I to oxidize alcohols to aldehydes and water (Keilin and Hartree, 1955; Kremer, 1970; Zámocký and Koller, 1999). Each catalase monomer is a constituent of a single heme subunit, and the tetrameric holoenzyme binds NADPH (Heck et al., 2010).

In addition to the metagenome analysis, the presence of catalase-active bacteria in the biofilm was investigated with the standard catalase test protocol (Reiner, 2010). Presence of catalase active bacteria was evident only in the broths containing biofilms from WL-SMFCs operated in CC and OC modes.

Many of the catalase-positive bacteria, such as the species of the genus *Pseudomonas*, are also reported to be oxidase-positive (Dodd, 2014). The enzyme oxidase belongs to the oxidoreductase class and is capable of catalyzing oxidation-reduction reactions using dioxygen as an electron acceptor, leading to the formation of water or H_2O_2 as a by-product (Phale et al., 2019). Less abundant bacterial species of the genus *Streptococcus* (*S.pyogenes*, *S.mutans*, and *S.pneumoniae*), *Lctobacillus* (*L.johnsonii*, *L.crispatus*, *L.jensenii*, and *L.gasseri*), and the heme-containing peroxidase-active bacteria *Thermobifida fusca* were also identified in the cathodic biofilm, producing H_2O_2. The reduction of current peaks obtained by DPV analysis was due to DO reduction and was confirmed by DPV analysis in deoxygenated (with Ar purging) and oxygenated conditions for both control and experimental solutions as shown in Figure 2.8B. The nonexistence of the reduction peak in the potential

range of 0.4–0.2 V for the WL-SMFC biofilms in the deoxygenated DPV analysis signified that the compound formation could not be established due to the absence of O_2. The presence of multiple reduction peaks in the DPV for the WL-SMFCs could be beneficial in the context of power generation in the WL-SMFC; however, identification of the compound with oxidation potential value is challenging due to the presence of numerous microbes in the biofilm, leading to the formation of various compound formation probabilities. In the OC mode of operation, reduction reactions are not expected to occur on the cathode surface; the enhancement in potential in this mode signifies the presence of more positive ions, most likely H^+, on the cathode (Surhone et al., 2010). The increase in the conductivity value of the catholyte with the assistance of WL reduced the DO in the water in a controlled manner and created a higher DO concentration gradient between the top and bottom of the water column. This higher concentration gradient imposed an improved proton movement from the anodic to the cathodic region (Kornyshev et al., 2003).

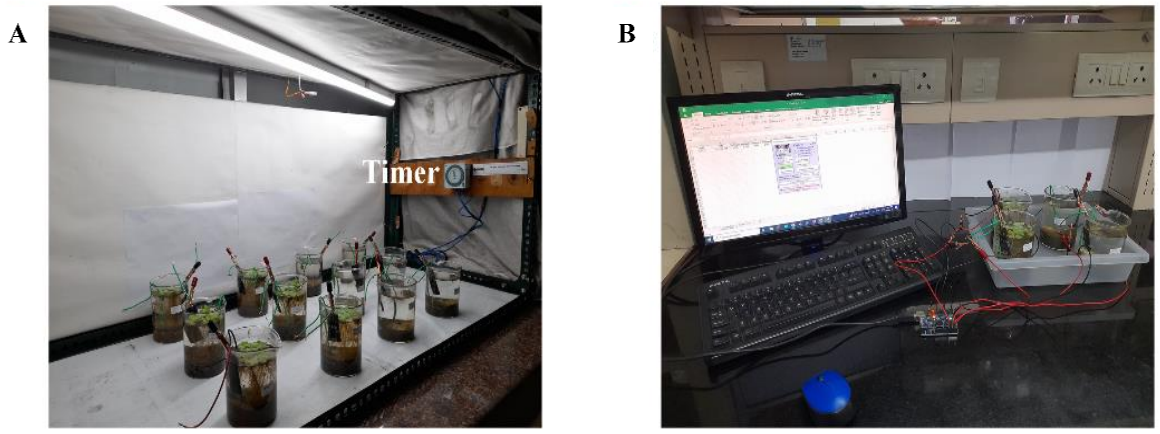

Figure 2.1: (A) Photoperiodic chamber with timer containing laboratory-based WL-SMFC and Control-SMFCs setups. B. Electrical data collection from the SMFCs using a data logger

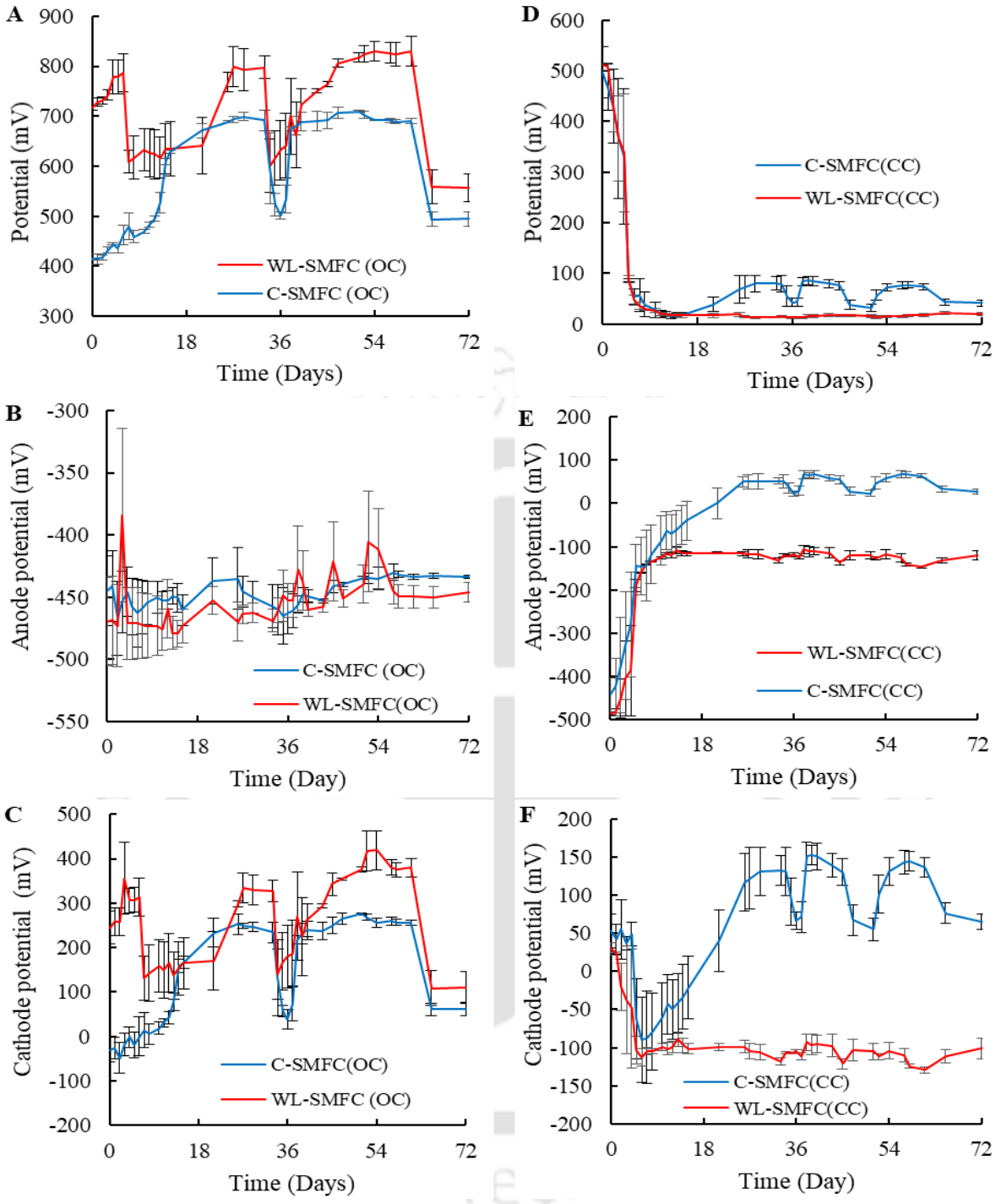

Figure 2.2: Comparison of the (A) OCP, (B) Anode potential in OC mode, (C) Cathode potential in OC mode of the WL- SMFC and Control-SMFC setups and comparison of (D) CC potential, (E) Anode potential in CC mode, (F) Cathode potential in CC mode of the WL-SMFC and C-SMFC

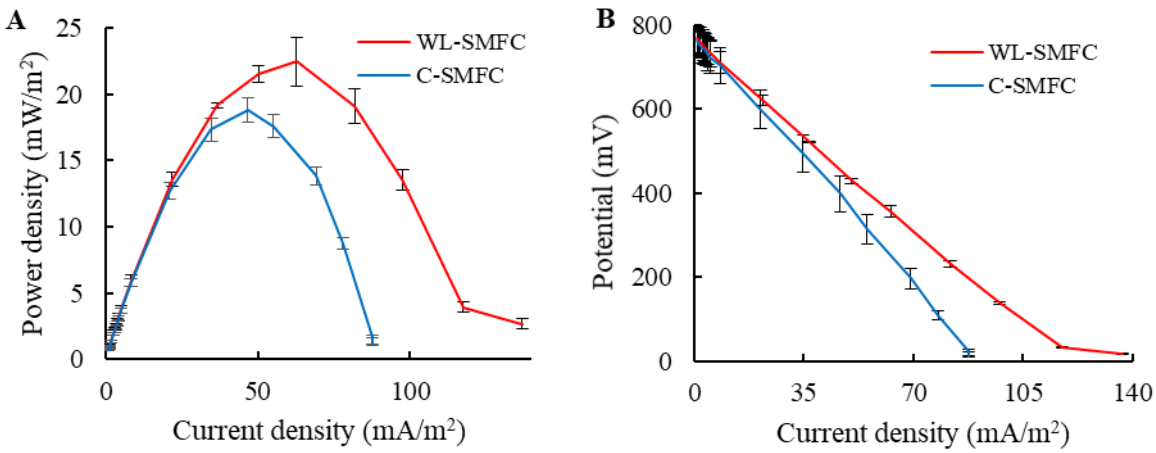

Figure 2.3: The polarization study showing the (A) Power density and (B) Current density profiles of the C-SMFC and WL-SMFC

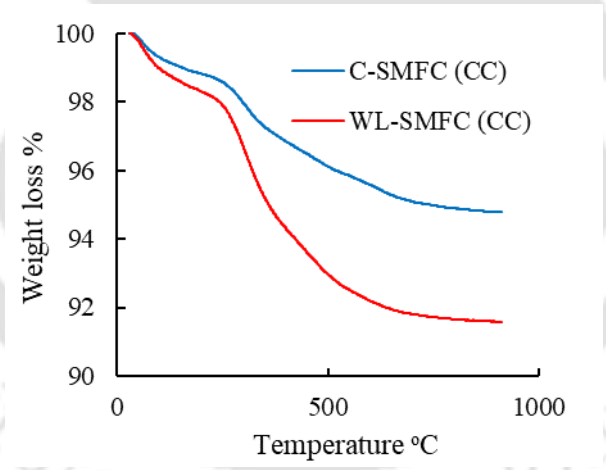

Figure 2.4: TGA analysis of the sediment of the SMFCs to investigate the total organic content available in the sediment

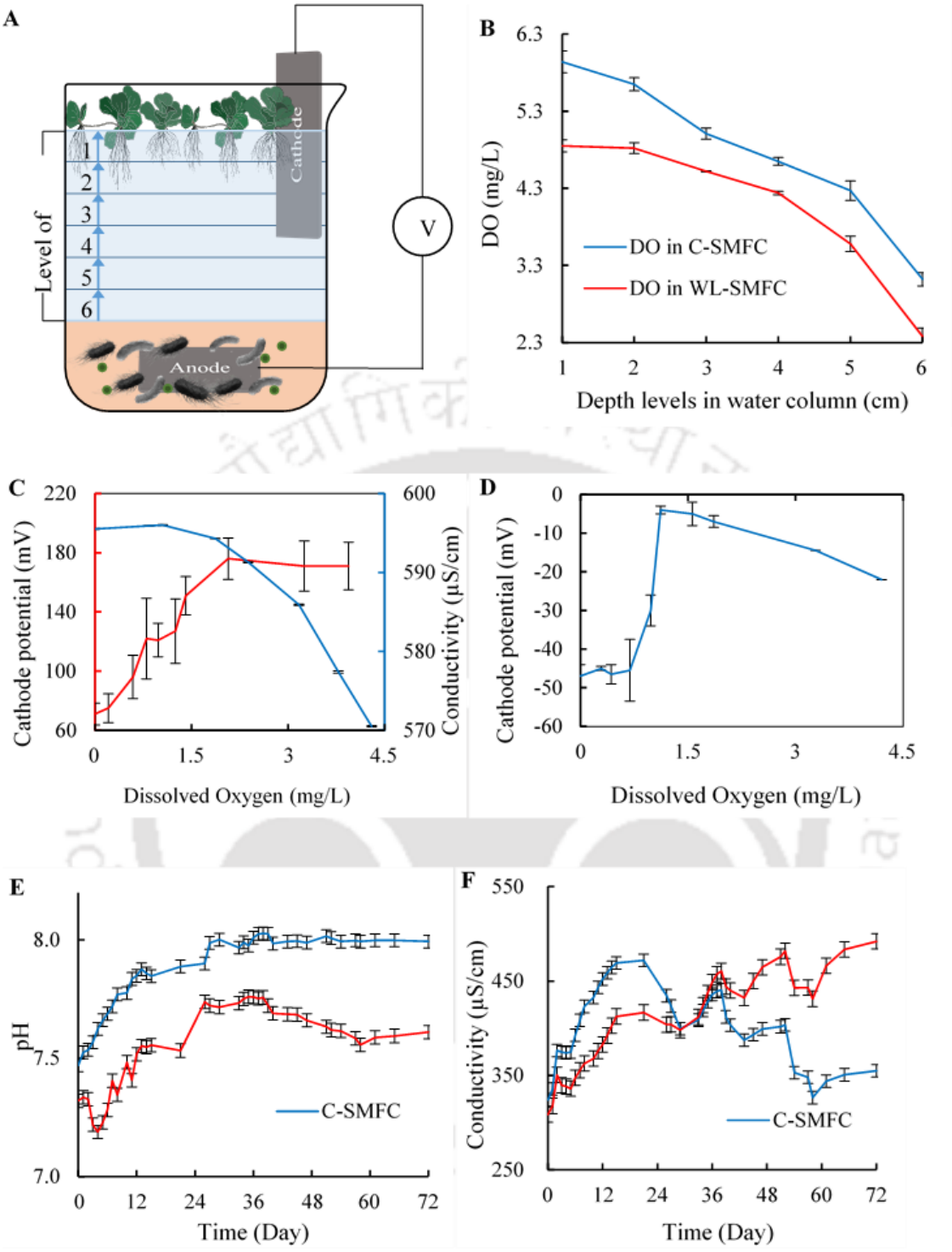

Figure 2.5: (A) WL-SMFC setup showing height level-grading of the water column and (B) DO concentrations versus depth levels of the water column, (C) DO concentration vs cathode potential under OC mode and vs ionic conductivity in the catholyte in the WL-SMFC setup, (D) DO concentration vs cathodic potential under CC mode at a load of 22 kΩ.s. The presented DO value indicates the DO concentration at the interface of level 1 and 2. Operation time versus (E) pH and (F) conductivity of the catholyte in SMFCs

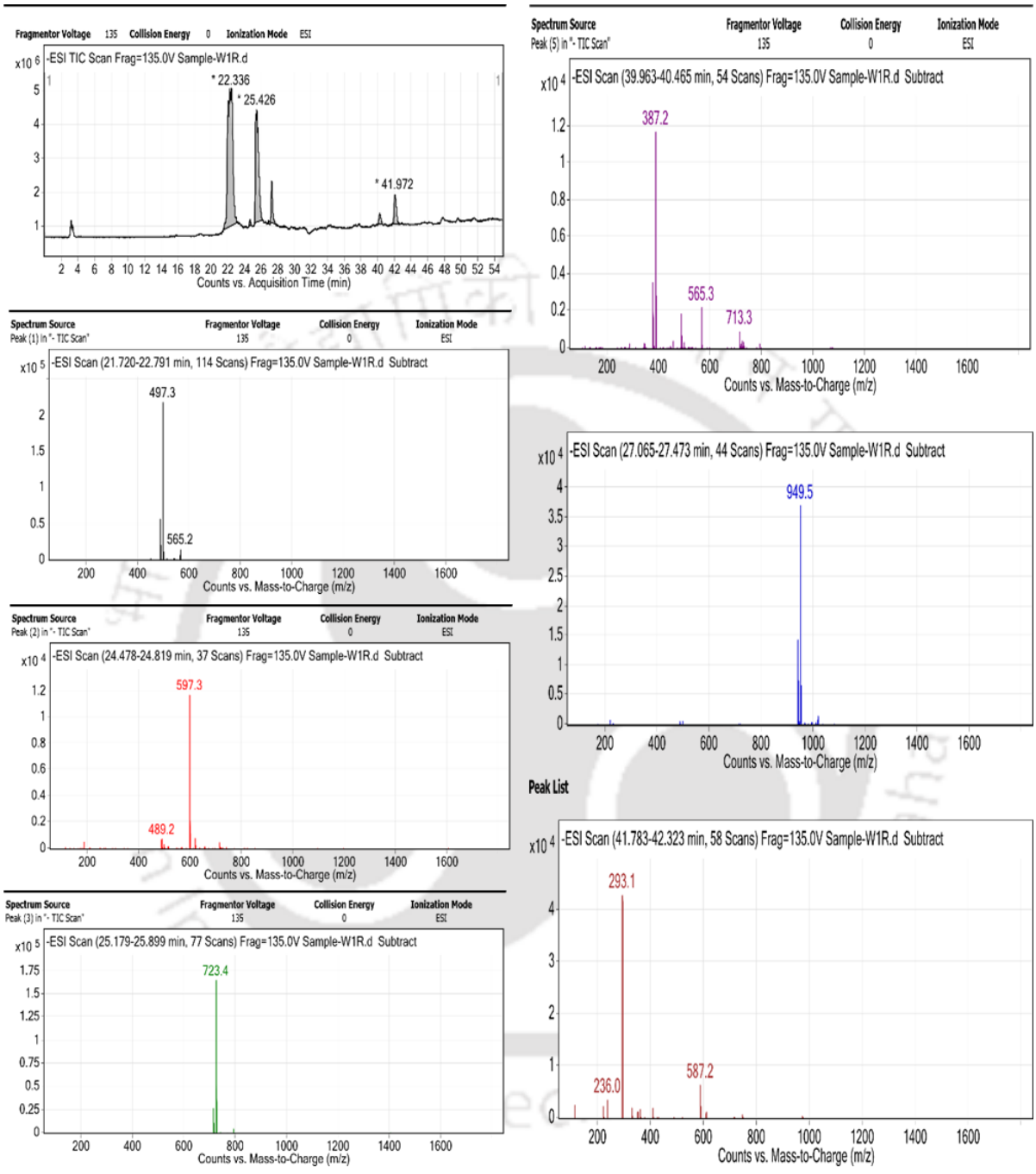

Figure 2.6: LCMS analysis of the WL plant metabolites present in the catholyte

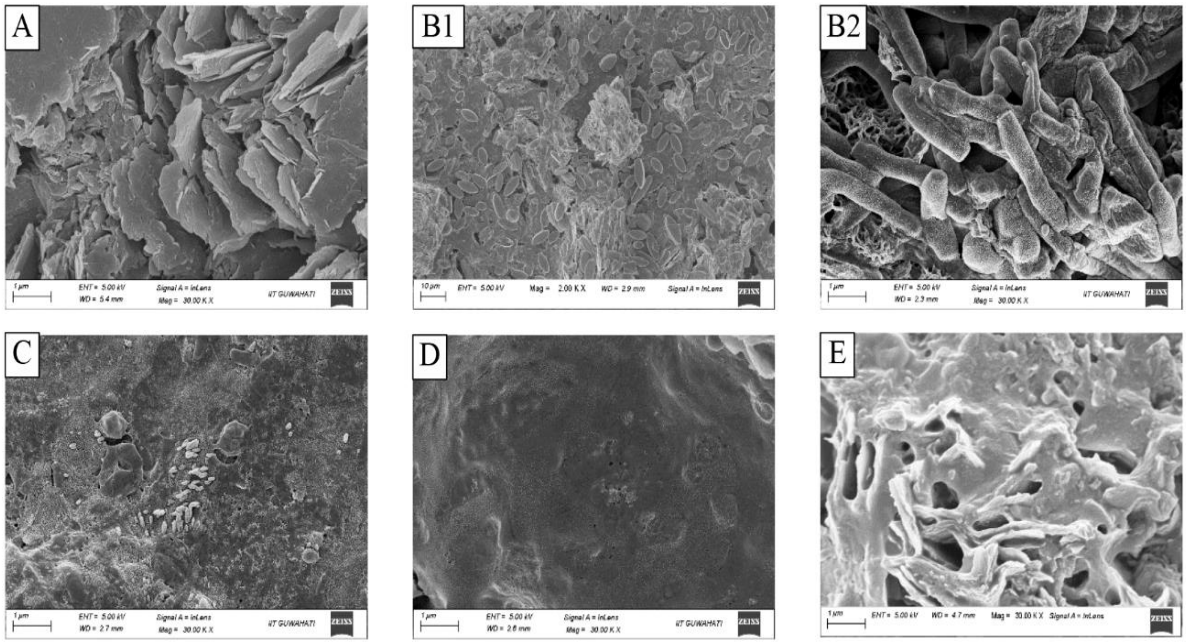

Figure 2.7: FESEM images of biofilm on the surface of the cathodes of (A) Bare graphite cathode, (B1-2) WL-SMFC operated in CC mode, (C) WL- SMFC operated in OC mode, (D) C-SMFC operated in CC mode and, (E) C-SMFC operated in OC mode

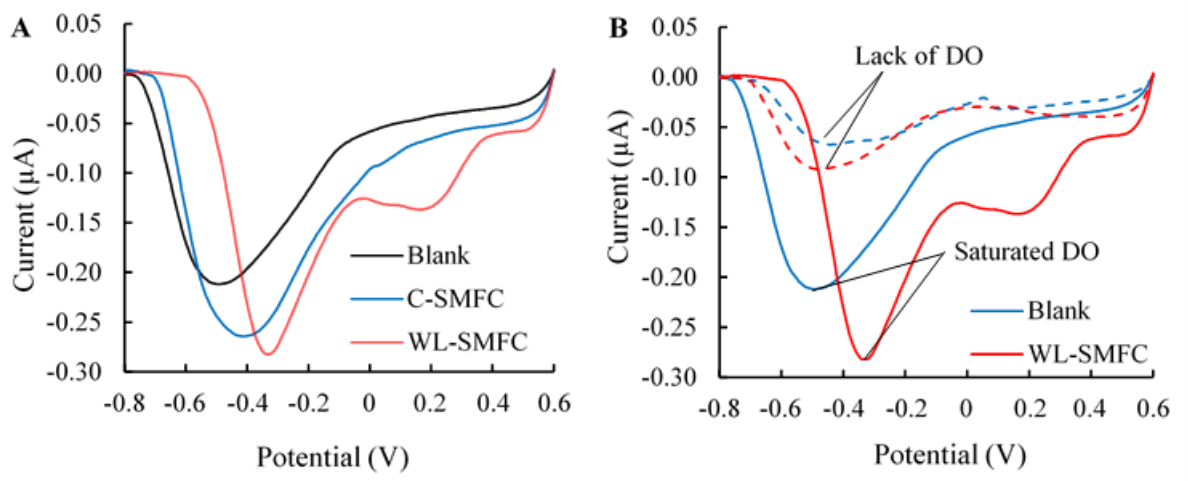

Figure 2.8: DPV performed on (A) biofilm extracted from the cathode of different SMFC setups and (B) biofilms of cathode in oxic and anoxic (using Ar purging) conditions

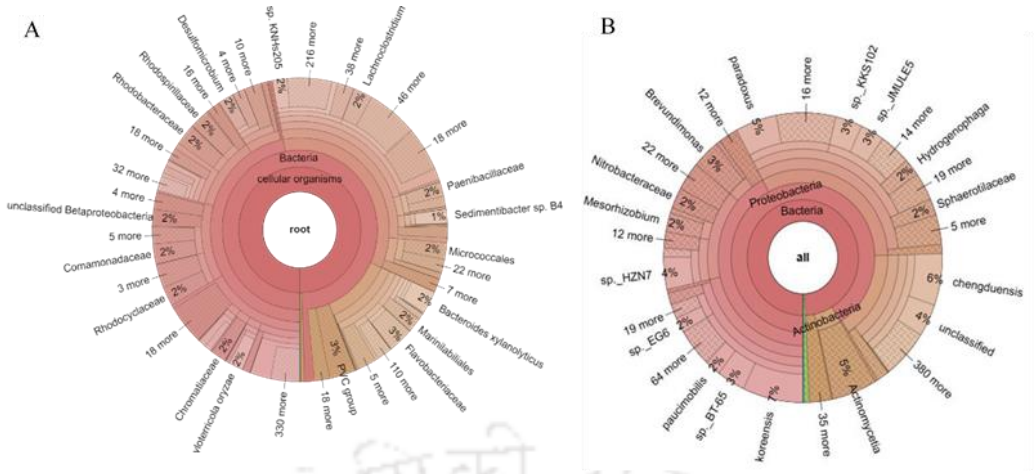

Figure 2.9: Krona plots on the taxonomic distribution of (A) WL rhizosphere and (B) Cathodic biofilm microorganisms

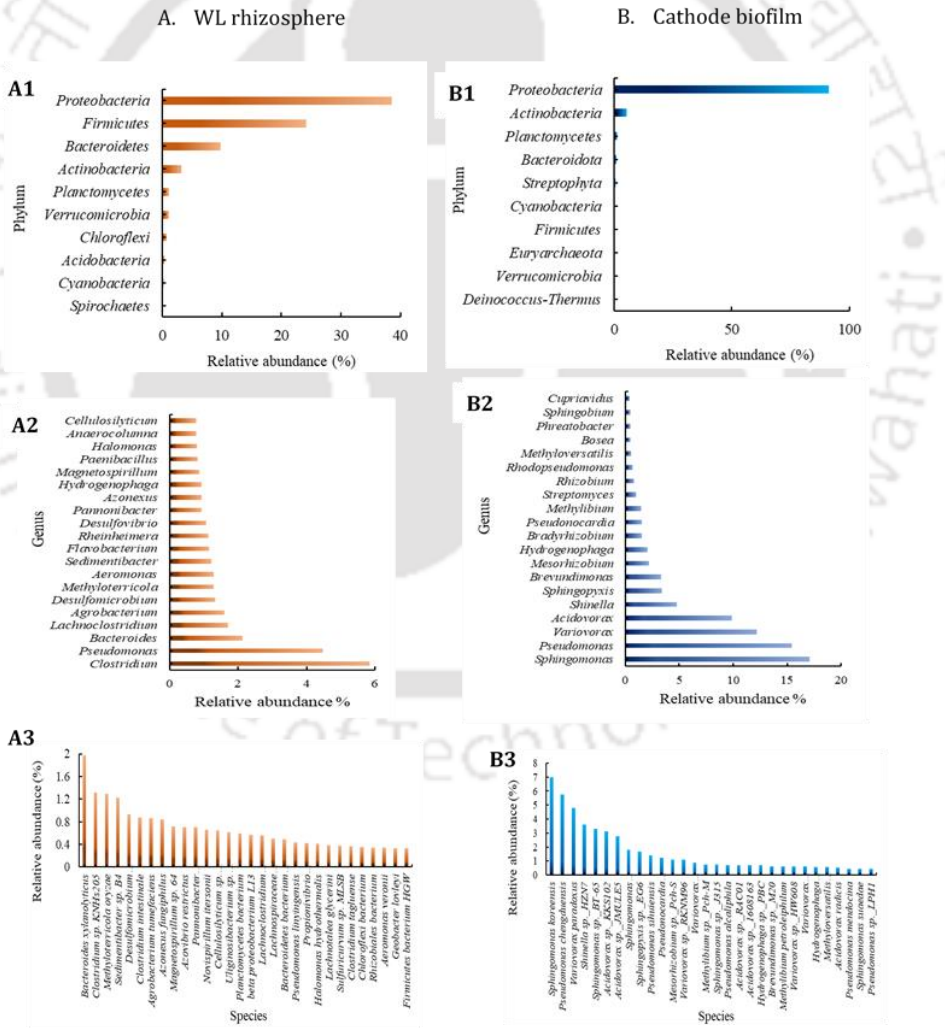

Figure 2.10: Abundances of predominant microbes at (A1) phylum, (A2) genus, (A3) species levels in WL rhizosphere and abundances of predominant microbes at (B1) phylum, (B2) genus, (B3) species levels in cathodic biofilm

CHAPTER 3

AN APPROACH TO ELIMINATE VOLTAGE REVERSAL IN SERIES CONNECTED PLANT-ASSISTED SEDIMENT MICROBIAL FUEL CELLS THROUGH SURFACE AREA TUNING OF THE ANODE

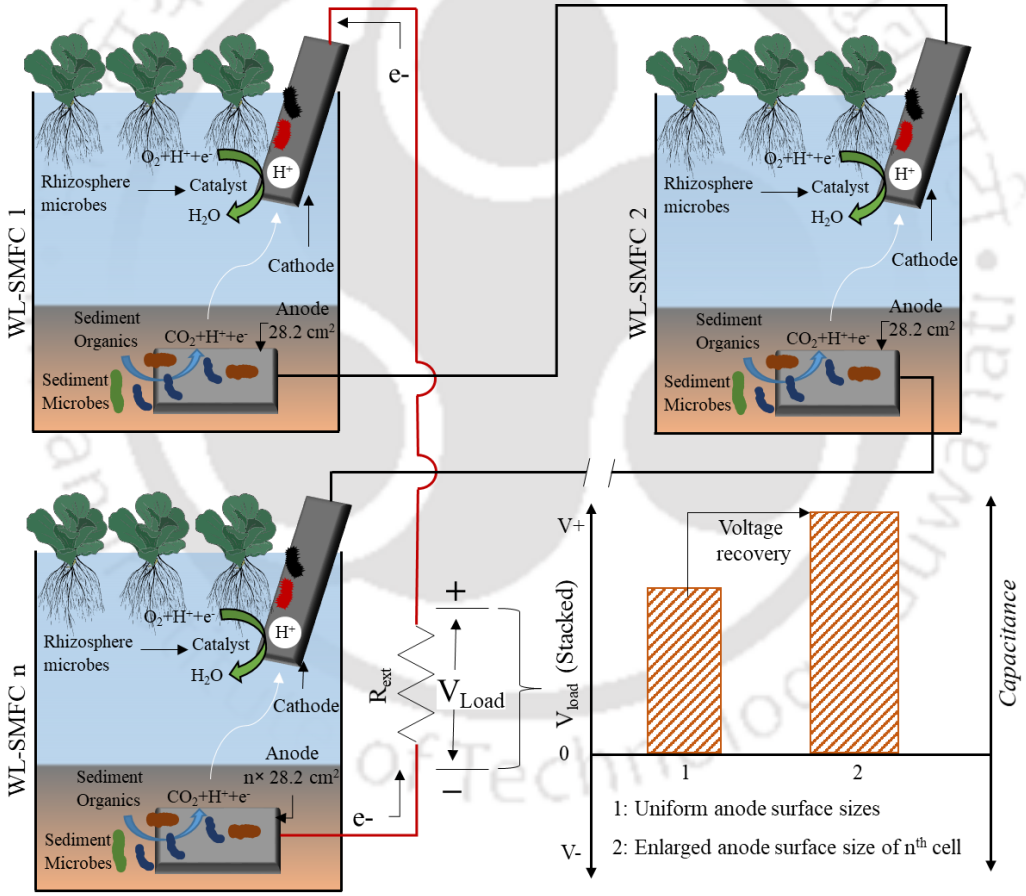

3.1 Introduction

Microbial fuel cells (MFCs) and their variants, such as sediment microbial fuel cells (SMFCs) and plant-assisted SMFCs, are emerging as self-powered, low-cost, sustainable, and environmentally friendly bioelectrochemical devices with promising applications in bioremediation and biosensors. However, the theoretical maximum potential of an individual MFC is only ~1.1 V (Dutta et al., 2022a), which is insufficient for powering most consumer electronics and other targeted applications. To overcome this limitation, multiple units can be connected in series or parallel to form stacks capable of delivering higher voltages. Yet, stacked MFCs often suffer from voltage reversal (VR), a phenomenon that disrupts their ability to maintain a stable output voltage at the desired level.

Voltage reversal (VR) is a more critical issue in MFCs than in chemical fuel cells because the microbial catalytic communities on the electrodes are highly susceptible to damage when exposed to reversed voltages, which can significantly reduce long-term performance. Eliminating VR in stacked MFC units is therefore essential for practical applications.

One primary cause of VR in series-stacked MFCs is the disruption of bioelectrochemical activity in one or more units due to fuel starvation (Oh and Logan, 2007). Additional contributing factors include mismatches between anodic and cathodic reaction kinetics and kinetic imbalances among the units (An et al., 2016, 2015c). Enhancing anodic reaction kinetics—such as by supplying exogenous fuel substrates or promoting electrogenic biofilm growth—can reduce VR and improve overall stack performance (Gurung and Oh, 2012; Hemdan et al., 2023). However, such micro-scale interventions require continuous monitoring of each MFC unit to ensure uniform anodic activity. This is challenging due to inconsistent fuel distribution, varying microbial metabolic rates, and fluctuating physicochemical parameters (e.g., pH, oxygen, electrolyte concentration) during operation.

There are several macro-scale level approaches, which mostly deal with external electronic circuits and components, have been proposed (Kim et al., 2020; Kim and Chang, 2018; Papaharalabos et al., 2017), but they face operational limitations. Some prominent macro-level approaches and their downsides in eliminating VR are as follows. 1. Connecting a threshold resistance at the cathode-anode junction of the series connection (An et al., 2015c): The threshold resistor would increase the internal resistance, and eventually, the overall power generation may be affected. 2. Resistor control (Kim and Chang, 2018): This strategy requires continuous monitoring of the cells. Additionally, connecting multiple resistors in the

circuit makes the system complicated from an operational standpoint. 3. Connecting an auxiliary cell to assist current in the cell experiencing VR (Kim et al., 2015): In this strategy, identification of the cell in the stack experiencing VR is necessary to provide the assistance current that requires continuous monitoring of every cell of the stack. 4. Manipulation of internal resistance (Sugnaux et al., 2017): This strategy requires a dedicated system for the internal resistance manipulation process. 5. External electronics (Dutta et al., 2022; Prasad and Tripathi, 2022): Required voltage can be achieved with this strategy. However, the electronic components of the circuits are passive in nature and require external energy for operation, affecting the overall system's efficiency. 6. Combination of series and parallel connections to increase current capacity (An et al., 2016; Wu et al., 2016): This strategy results in a bulky system, and a large number of cells in parallel can introduce inner current losses.

Herein, we propose a new approach to mitigate voltage reversal (VR) in plant-assisted sediment microbial fuel cells (SMFCs). SMFCs are a promising green energy technology with significant potential for wastewater treatment coupled with renewable electricity generation (Donovan et al., 2011, 2008). Their performance can be enhanced by integrating suitable plant species, forming plant-assisted SMFCs (Regmi et al., 2018). Incorporating plants not only supports efficient contaminant removal from water bodies but also promotes the self-sustainability of these bioelectrochemical devices.

Plant-assisted SMFCs operate in open environments and are therefore subject to natural variations in physicochemical parameters such as temperature, pH, conductivity, and dissolved oxygen (DO) (Dutta et al., 2025). Under these fluctuating conditions, implementing strategies such as resistor control, internal resistance manipulation, or regulation of bacterial biocatalyst populations is complex and requires continuous system monitoring. Similarly, approaches involving exogenous carbon supplementation, auxiliary units, or series/parallel combinations are often impractical in the large-scale and variable conditions of natural ecosystems where SMFCs are typically deployed (Donovan et al., 2008; Meehan et al., 2009). Consequently, most conventional macro- and micro-scale VR mitigation methods are challenging to apply effectively in plant-assisted SMFCs.

This study introduces a novel concept of tuning the anodic surface area to mitigate voltage reversal (VR) in series-stacked, plant-assisted SMFCs. A mathematical framework was first developed to describe the relationship between the anodic surface area of the terminal cell

and key electrical parameters, including the voltage response of series-connected water lettuce-assisted SMFCs (WL-SMFCs). The concept was then experimentally validated using WL-SMFCs, in which the aquatic plant Water lettuce (*Pistia stratiotes*), the sole species of its genus, was grown on the electrolyte surface. *P. stratiotes* is a small, free-floating freshwater plant with submerged roots extending beneath its fronds (Thakuria et al., 2023). Its rapid growth, manageable size, and morphology make it well suited for SMFC integration.

Previous studies have shown that root exudates from *P. stratiotes* serve as substrates for electroactive biofilms on the anode while also supporting oxygen reduction reactions at the cathode (Dutta et al., 2025). The plant's presence has also been reported to positively influence SMFC parameters such as pH, dissolved oxygen, and electrolyte conductivity. In this work, multiple WL-SMFC units were connected in series to construct stacks, whose electrical performance was monitored under extended closed-circuit operation. The results revealed that the anodic surface area of the terminal cell plays a pivotal role in controlling VR in the stack. A detailed account of the experimental validation, analysis, and implications of these findings is presented in this chapter.

3.2 Materials and methods

3.2.1 Materials

The WL-SMFC construction materials, such as the sediment, natural water, and WL, were collected from a pond within the campus of the Indian Institute of Technology Guwahati, India (26.1903° N, 91.6920° E). Electrodes of the cells were prepared with Iso-molded graphite plates purchased from GraphiteStore.com (USA). The copper wire with PVC coating used as the electrode terminals was purchased from M/S KEI Wires and Cables, India. The electrode and copper wire connection was established with silver-conductive epoxy (MG Chemicals, USA). The glassware used for the construction of WL-SMFC was purchased from Borosil, India.

3.2.2 WL-SMFC configuration

The WL-SMFC configuration used in this study has been mentioned in the previous chapter (Dutta et al., 2025). Briefly, the laboratory-scale WL-SMFC has a reactor volume of 500 ml, where 1/4 of the reactor height (about 3 cm) contains the pond sediment layer. Above the sediment layer, the reactor was filled with water, maintaining a height of 7 cm during the entire period of operation. The anode and cathode electrodes in the setup were prepared with

iso-molded graphite plates. Copper wires were used to connect the electrode terminals with silver-conductive epoxy. Non-conductive epoxy glue was pasted at the node to envelop the exposed surface of the wires. The anode was fixed horizontally within the sediment layer, and the cathode was positioned vertically at the surface, with one half exposed to air and the other half submerged in water. Finally, the setup was completed by planting WL at the water surface. For the standard setups, the total surface areas of the cuboid-shaped anode and cathode were 28.2 cm^2 and 28.8 cm^2, respectively.

3.2.3 WL-SMFCs stacking and operation

The potential (voltage) behavior of WL-SMFC stacks was investigated separately in open circuit (OC) and close circuit (CC) modes. Figure 3.1 shows the equivalent block diagram of the stack containing unit cells connected in a series configuration. The units of WL-SMFCs were termed WL-SMFC1, WL-SMFC2, etc., according to their position in the stack. In any stack configuration, the stacking potential was the potential difference between the terminal cell's anode and the cathode of the unit cell located at the top. When a load was connected across these terminals, electrons from the anode of the terminal cell flow through the load to the cell's cathode at the top of the stack, facilitating the extraction of current at a potential of ΔVs (Figure 3.1).

The WL-SMFC stacks were operated inside a photoperiodic chamber under an ambient condition (25-31 ^{0}C, 68-82% humidity), which is optimal for the vegetative growth of WL (Ahmed et al., 2020). The stacks were exposed to an artificial light intensity of 1120 LUX (measured with Dr.Meter, LX1010B, China) for 10 hours per day throughout the experimentation. Under these environmental conditions, the stacks were operated in OC and CC modes. 10 kΩ load was applied during the CC mode of operation.

3.2.4 Analyses of the electrical parameters

The potential variation in the individual WL-SMFC unit and stacked unit, as well as individual electrodes in the units and stacks, was monitored with a digital multimeter (Fluke 87v, Fluke Corporation, USA). The electrode potentials were recorded against an Ag/AgCl reference electrode (BASI Research Products, USA). All the CC modes of operations were conducted with a 10 kΩ resistor as the load across the terminals. The load was connected to the stack after five days of OC operation. The polarization study was performed by scanning the potential response across differential resistive loads in the range of 300 kΩ to 50 Ω.

3.2.5 Anode surface capacitance measurement

Electrochemical impedance spectroscopy (EIS) was performed for anodes of various electrode sizes in a three-electrode setup connected to an electrochemical workstation (PGSTAT Metrohm, Netherlands). A platinum electrode and an Ag/AgCl electrode (BASI Research Products, USA) were used as counter and reference electrodes in the setup. The EIS scan was performed at the maximum potential obtained for the anode and within the frequency range of 0.1 Hz to 1 MHz. The Randles equivalent circuit (RC) was fitted to the Nyquist plot obtained from the EIS with Nova 1.1 software (Metrohm, Netherlands). The fitted RC produced the surface capacitance value for all the anode electrodes. The effect of anode surface area on the capacitance and the total charge (q) stored in the electrode was investigated. The total charge storage was calculated with equation 3.1, where V is the electrode potential, and C is the electrode surface capacitance discerned from the EIS analysis and the corresponding RC fitting.

$$q = CV \tag{3.1}$$

3.2.6 Statistical analysis

All experiments were repeated three times to understand effectiveness and reproducibility of the proposed strategy. The data presented in all the graphical images represents the average result out of the three experiments.

3.3 Results and discussions

3.3.1 Detection of voltage reversal in stacked WL-SMFCs

Two units of WL-SMFCs were connected in a series, and their potential behavior was recorded over five days of operation under both OC and CC conditions. The occurrence of VR under the OC operation was negligible (Figure 3.2A), whereas, under the CC operation, the polarity of the unit 2 (WL-SMFC2) was altered on day two (Figure 3.2B). Analysis of the individual electrode potentials revealed that the cathode of WL-SMFC2 was more negative than the anode, resulting in overall negative potential of the cells under the CC mode. The cathode potential gradually reduced, and simultaneously, the anode became more positive, leading to higher VR over time. A similar potential output trend was observed when the number of cells in the series stack increased to three and four units (Figure 3.3A-B). The VR was observed in the 2nd unit (WL-SMFC2) for the three-unit stack and the third and fourth units (WL-SMFC3 and WL-SMFC4) for the four-unit stack on the second day of CC

operation. The VR was negligible under a very high load (> 350 kΩ) connected to the stack when the current flow in the circuit was close to zero. These studies confirmed that the VR occurs in series stack operation of WL-SMFCs in CC condition only and as a consequence of mainly anodic potential loss, which was obviously due to poor anodic activity. A previous study (Dutta et al., 2025) had shown that WL maintains the organic substrate level in the sediment, and hence, substrate limitation may not be the causative factor for this poor activity. Thus, the kinetic imbalance-linked charge imbalance among the anodes is the probable reason causing the VR in the stacked cells (An et al., 2015b; An and Lee, 2014). To mitigate the VR in series stacked WL-SMFCs during the prolonged operation, optimization of the anodic surface area was explored, which is discussed in the following sections.

3.3.2 Theoretical foundation on the relation between the anodic surface area and electrical parameters

If *V1* and *V2* stand for the potential of WL-SMFC1 and WL-SMFC2, respectively, and *Vs* denotes the potential across the load connected to the stack that can be expressed as equation 3.2:

$$Vs = V1 + V2 \tag{3.2}$$

Again, *V1* and *V2* are the difference between the individual electrode potential of WL-SMFC1 and WL-SMFC2. Hence, this indicates that,

$$V1 = V1_{Cathode} - V1_{anode} \tag{3.3}$$

$$V2 = V2_{Cathode} - V2_{Anode} \tag{3.4}$$

If equation 3.2 is iterated with equation 3.3 and 3.4 the following relationship is obtained,

$$Vs = (V1_{Cathode} - V1_{anode}) + (V2_{Cathode} - V2_{Anode}) \tag{3.5}$$

Since this investigation is structured under CC condition, the load voltage is subject to change with respect to time and hence the individual potential of the cells in the stack. So, the equation 3.7 can be rewritten as

$$\frac{dVs}{dt} = \frac{d(V1_{Cathode} - V1_{anode})}{dt} + \frac{d(V2_{Cathode} - V2_{Anode})}{dt} \tag{3.6}$$

Or,

$$\frac{dVs}{dt} = \frac{dV1_{Cathode}}{dt} - \frac{dV1_{anode}}{dt} + \frac{dV2_{Cathode}}{dt} - \frac{dV2_{Anode}}{dt} \tag{3.7}$$

The operation of fuel cells can be related to supercapacitors (Houghton et al., 2016; Santoro et al., 2018; Walter et al., 2020), and hence the following relationships of voltage, charge, capacitance and current shall also be true in WL-SMFC operations.

$$q=CV \tag{3.8}$$

And

$$I=\frac{dq}{dt} \tag{3.9}$$

Also,

$$C=\frac{\varepsilon A}{\delta} \tag{3.10}$$

Here, q is the charge in coulombs available on the electrode surface, C is the double layer capacitance in farad, V is the potential of the electrode in volts, and I is the magnitude of current in ampere, ε is the permittivity of the electrolyte in farad per meter and δ is the distance between the centre of the capacitance layer and the surface of the electrode in meters.

Iterating the relationships shown in equation 3.10 and 3.11 in equation 3.9, the following relationship can be obtained,

$$\frac{dVs}{dt}=\frac{1}{C1_{Cathode}}I_1-\frac{1}{C1_{Anode}}I_1+\frac{1}{C2_{Cathode}}I_2-\frac{1}{C2_{Anode}}I_2 \tag{3.11}$$

Since

$$\frac{dV1_{Cathode}}{dt}=\frac{d}{dt}\left(\frac{q1_{Cathode}}{C1_{Cathode}}\right)=\frac{1}{C1_{Cathode}}\frac{dq1_{Cathode}}{dt}=\frac{1}{C1_{Cathode}}I_1 \tag{3.12}$$

Similarly,

$$\frac{dV2_{Cathode}}{dt}=\frac{1}{C2_{Cathode}}I_2,\ \frac{dV1_{Anode}}{dt}=\frac{1}{C1_{Anode}}I_1 \text{and}\ \frac{dV2_{Anode}}{dt}=\frac{1}{C2_{Anode}}I_2 \tag{3.13}$$

Now, if the equivalent electrical circuit (Figure 3.11) is followed, only one current *Is* is flowing in the circuit. So, we can write

$$I_1=I_2=I_S \tag{3.14}$$

And can rewrite equation 3.11 as

$$\frac{dVs}{dt}=\frac{1}{C1_{Cathode}}I_S-\frac{1}{C1_{Anode}}I_S+\frac{1}{C2_{Cathode}}I_S-\frac{1}{C2_{Anode}}I_S \tag{3.15}$$

Or,

$$\frac{dVs}{dt} = \left[\left(\frac{1}{C1_{Cathode}} - \frac{1}{C1_{Anode}}\right) + \left(\frac{1}{C2_{Cathode}} - \frac{1}{C2_{Anode}}\right)\right] I_S \quad (3.16)$$

The boundary condition for non-occurrence of VR in the WL-SMFCs is

$$\frac{1}{C1_{Cathode}} > \frac{1}{C1_{Anode}} \quad \text{(i) and} \quad \frac{1}{C2_{Cathode}} > \frac{1}{C2_{Anode}} \quad \text{(ii)}$$

Since the conditions such as the electrolyte parameters (pH, conductivity, DO), surface area, material and operating conditions for the cathodes are constant in both the WL-SMFCs and hence, considering ideal cathode capacitance, we get

$$C1_{Cathode} = C2_{Cathode} \quad (3.17)$$

So, from equation i and ii, it can be concluded that

$$\frac{1}{C2_{Anode}} > \frac{1}{C1_{Anode}} \quad \text{or} \quad \frac{1}{C1_{Anode}} > \frac{1}{C2_{Anode}} \quad (3.18)$$

Substituting equation 3.12 in the above condition, the following conclusion can be achieved:

$$A2_{Anode} > A1_{Anode} \text{ or } A1_{Anode} > A2_{Anode} \quad (3.19)$$

Here, equation 3.19 shows increasing the anodic surface area of either of the WL-SMFCs can be effective for mitigating the occurrence of VR during the stack. The effectiveness of this strategy has been validated with experimental results in the subsequent sections of this study.

3.3.3 Effect of anodic surface area enhancement on VR

In a stack of two unit cells, the VR was reduced when the surface area of the WL-SMFC2 anode was increased up to 56.4 cm^2, which is two times the standard anode (28.2 cm^2) (Figure 3.4A-B). The VR was also reduced in the reverse condition, where the anodic surface area of WL-SMFC1 increased to 56.4 cm^2 while maintaining the standard anodic surface area of WL-SMFC2 (Figure 3.5A). However, on a comparative note, the reduction of VR was higher in the previous configuration, where the anodic surface area of the terminal cell unit (WL-SMFC2) was double the anode surface area of WL-SMFC1 (Figure 3.4A**,** Figure 3.5A). When the anodic surface of the WL-SMFC2 unit was larger, the rates of voltage discharge for WL-SMFC1 and WL-SMFC2 in CC conditions were 1.3±0.4 mV/day and 5.1±0.48 mV/day, respectively. In the reverse configuration, i.e., when the anode with the standard surface size in SMFC2 and its double size in WL-SMFC1 was installed, the discharge rate obtained were -19±4.2 mV/day, and 33.5±8.9 mV/day, respectively, indicating the larger anode is

complementing the smaller anode in CC operation. However, when the SMFC2 had a larger anode, the rate of discharge in both the units of WL-SMFCs was less, subsequently better performance delivered with respect to time (Figure 3.4A and Figure 3.5A). Nevertheless, increasing the anode surface area equally (1:1 ratio) up to 56.4 cm^2 for each of the WL-SMFC units was not effective in the VR reduction (Figure 3.6). When the WL-SMFC units were connected in series with a load, the anode of the terminal unit (WL-SMFCn, Figure 3.1) performed as the major functional anode of the stack; hence, its improvement boosted the overall stack's activity. The modality was further examined with stacks of three (Figure 3.4C) and four (Figure 3.4D) unit cells separately and found to be effective. Interestingly, on the initial two days of operation of the four-unit stack, recovery of VR was seen in units 1 and 2. Considering the potential values of all the stacks on the fifth day of operation and comparing them with the stacks with standard anodes, a maximum of 70%, 57%, and 54% potential recovery was observed when corresponding two, three, and four units of WL-SMFCs were stacked (Figure 3.7). From these observations, the following standard formula can be adopted to design the anodes in series stacked WL-SMFC units to eliminate VR:

$$A_{SMFC_n} = n \times A_{SMFC} \tag{3.20}$$

Here, A_{SMFCn} is the surface area of the anode of the terminal WL-SMFC unit in a stack as shown in Figure 3.1, n is the number of WL-SMFC units in the stack; A_{SMFC} is the standard surface area (no modification) of the anode of a unit. Hence, to eliminate VR in a stack of cell units 1 to n, the anodic surface area for individual cell units from unit 1 to n-1 will be A_{SMFC} and for the n^{th} unit (WL-SMFCn), the surface area should be A_{SMFCn}.

3.3.4 Effect of enhanced anode surface area on the electrical parameters

The EIS was performed to investigate the effect of the increased surface area of the terminal anodes on its charge storage capacity in 2, 3, and 4-unit stacked WL-SMFC configurations. Four different anodes with a surface area of 28.2 cm^2 (standard), 56.4 cm^2, 84.3 cm^2 and 113.7 cm^2 were used in the terminal unit in the respective 2, 3, and 4 unit stacks (Figure 3.8). The Randles equivalent circuit fitting to the Nyquist plot provided the surface capacitance of the anode, which was further used for the analysis of total charge storage, overall cell capacitance, and the cell's specific capacitance. The charge storage capacity was measured using the electrode capacitance (equation 3.1). Table 3.1 shows that with the increasing anode surface area, the surface capacitance and total charge storage increased, but not beyond the size of the anode three times the standard anode surface area. Notably, the charge collected

on the anode under the CC operation is directly related to the kinetics of the electro-catalytic oxidation reaction occurring at the anode. The reactions, in turn, are controlled by the bacterial catalysts density and substrate concentrations available in the sediment of the WL-SMFCs (Dutta et al., 2025). Thus, the substrate concentration and abundance of catalytic bacterial populations in the anodic sediment are the limiting factors for generating charge in a particular anodic surface area. Hence, for the given volume of the WL-SMFC unit and the sediment microbial population and substrate concentration, the optimum anode surface area for the highest capacitance and total charge was 84.3 cm^2, about three times the standard anode size. The higher surface area of an anode may store more charge on it, although increasing the surface area of all anodes in a stack was not beneficial in addressing the issue of VR. The VR can be mitigated if the ratio of the anodic surface area is maintained as per the strategy stated in section 3.3.2. The anode with a higher accumulated charge in the terminal cell complemented the charge of the rest of the anodes facing charge limitation in the WL-SMFC stack. For instance, when the WL-SMFC1 and WL-SMFC2 experienced voltage loss, the WL-SMFC3 unit with higher anodic surface area shared its charge with these two cells to prevent the VR (Figure 3.4C). Likewise, in a four-units stack configuration (Figure 3.4D), the shared charges could significantly avert the charge limitation in unit 1and the rest of the units channelized from the unit 4. Beyond day 3, a stable discharge pattern could be observed in all SMFC units where the WL-SMFC4 had the highest potential amongst the cells.

Table 3.1: The effect of increased anodic surface area of the terminal units of stacked WL-SMFCs on various electrical parameters.

Anode area (cm^2) (units in stack)	Capacitance (pF)	Cathode capacitance (pF)[a]	Total anode charge (C)	Overall WL-SMFC capacitance[b] (pF)	WL-SMFC Specific capacitance[c] (pF/g)	Internal resistance (kΩ)	Max Power (mW) $\times 10^{-3}$	Max Current (mA) $\times 10^{-3}$
28.2 (1)	523±55	309±106	240.58±25.65	191.57±50	1.22	5	17	71
56.4 (2)	670±26		318.25±12.35	207.17±53	1.32	10	18	53
84.3 (3)	964±26		453.08±12.12	229.65±63	1.46	10	16	60
113.7 (4)	872±19		422.92±9.39	223.55±60	1.42	10	17	60

[a]For surface area of 28.8 cm2. [b]Ability of the unit to store electric charge. [c]The capacitance of the unit normalized to anode surface area and mass of sediment

The impact of the increased anodic surface area of the terminal cell on power performance was evaluated on the individual and the stack of 2 units, and these were compared with that of the standard setups (Figure 3.9). Maximum power on an average of $17x10^{-3}$ mW was generated in all the units (Table 3.1). However, the internal resistance value increased to 10 kΩ upon increasing the anode surface area from the standard size of 28.2 cm^2. Moreover, a mass transfer limitation was observed for all the enlarged anodes beyond an average value of 0.041 mA (at 10 kΩ) for the terminal WL-SMFCs (Figure 3.9A). In the unit with the standard anode, the mass transfer loss started beyond 0.058 mA (at 5 kΩ) (Figure 3.9A). Likewise, a significant difference in mass transfer limiting current was detected between the stacks of 2 standard units (0.077 mA) and of 2 units (0.57 mA) with an anode surface area ratio 1:2, as presented in the brackets for 5 kΩ and 10 kΩ loads, respectively. Thus, it can be inferred that the internal resistance of the WL-SMFC has a significant role in the mass transfer limitation. The loss is also evident when the external resistance is below the internal resistance value of the unit cell. The polarization curve shows that the mass transfer limitation occurs when the surface area is increased to 2, 3, and 4 times the standard (Figure 3.9A) at load < 10 kΩ. Notably, the mass transfer limitation started in every situation when the load resistance was reduced below the internal resistance value. For the WL-SMFC with a larger anode surface area, the internal resistance was 10 kΩ; the mass transfer started for these WL-SMFCs when the load connected was below 10 kΩ. Similarly, for the WL-SMFC with the standard anode size, the internal resistance was 5 kΩ, and the mass transfer limitation started when the load connected was below 5 kΩ. Thus, the increased surface area increases the internal resistance; the cell's mass transfer limitation started when the load resistance was below the internal resistance. Hence, the operation of the stacks fabricated with the given strategy at the maximum operating point by connecting a load matching the internal resistance can eliminate VR in the stack.

The increased surface area allows the attachment of more electroactive bacterial cells, resulting in enhanced reactions and charge accumulation on the enlarged anodes, which is validated by the improved charge storage and its linked higher discharge time under a close circuit operation (Figure 3.8 and Table 3.1). Nevertheless, the magnitude of current generated under a load also depends on the oxidation rate of organic species by the electroactive microbes. However, the reaction rate remains constant under a constant load, nutrients, and catalytic environment. Hence, this parameter has been excluded from formulating an ideal mathematical expression to elucidate the relation among the electrical parameters of the stack

we designed. Here, we investigate the effect of anodic surface area on the overall capacitance and specific capacitance of the WL-SMFC by comparing the system with a supercapacitor (Dutta et al., 2022b; Houghton et al., 2016; Santoro et al., 2018; Walter et al., 2020). The increased overall capacitance implies the increased charge storage ability and discharging time of the system. Thus, the specific capacitance value is suitable for evaluating the charge storage on the enlarged surface of the anode due to the higher conversion of sediment organics in the anodic compartment. It is inconsistent that when the anode area was 113.7 cm^2, the corresponding anode capacitance was reduced by ~92 pF; however, the effect of this reduction on the overall capacitance (by ~6.1 pF) and specific capacitance (0.04 pF) is less significant. The overall capacitance is calculated as:

$$C_{overall} = \frac{C_{anode} \times C_{cathode}}{C_{anode} + C_{cathode}} \tag{3.21}$$

Hence, it can be concluded that for the given reactor size and sediment content, the maximum anode surface area would be between 84.3 cm^2 and 113.7 cm^2. Moreover, considering the boundary condition to mitigate VR in series stacking of WL-SMFC units, the manipulation of anode surface area has been validated with the base equation 3.7 when two WL-SMFC are in series.

In section 3.3.2, it was demonstrated that increasing the surface area of the anode of WL-SMFC1 to two times the surface area of the anode of WL-SMFC2 could reduce VR; however, this strategy was not very effective in the context of performance over the operation time. Hence, the condition $A2_{Anode} > A1_{Anode}$ has been considered for the fabrication strategy. Moreover, if the number of WL-SMFC units is more than two in the stack, the condition would be $An_{Anode} > A1 \rightarrow (n\text{-}1)_{Anode}$.

Next, the rate of discharge of the WL-SMFC was tested by calculating the discharge current under the CC mode of operation to investigate the effect of surface area on the current production in WL-SMFC. The discharge current of the WL-SMFC can be calculated using Ohm's law (equation 3.20) and the potential drop across the external resistor.

$$I_{dis} = \frac{V_{OC} - \eta_{act} - \eta_{con}}{R_{ext} + R_{int}} \tag{3.21}$$

Here, I_{dis} is the WL-SMFC discharge current, η_{act} and η_{con} are activation and concentration over potentials, respectively. R_{ext} and R_{int} are external and internal resistances, respectively, and V_{oc} is the OCP for the WL-SMFC setup. The numerator terms of equation 3.21 is the

voltage drop across the external resistor, and the measured value during the CC operation is considered here for the discharge current calculation. The current discharge behavior of the WL-SMFCs under different conditions was studied (Figure 3.10). With the increase in anode surface area, the discharge rate reduces (Figure 3.10A), allowing the external resistor to dissipate power for longer. In operating a two-unit stack, the unit with a similar anode size offered a discharge rate faster than the stack, where the anode surface area in the terminal unit was twice the anode surface area of unit 1 (Figure 3.10B).

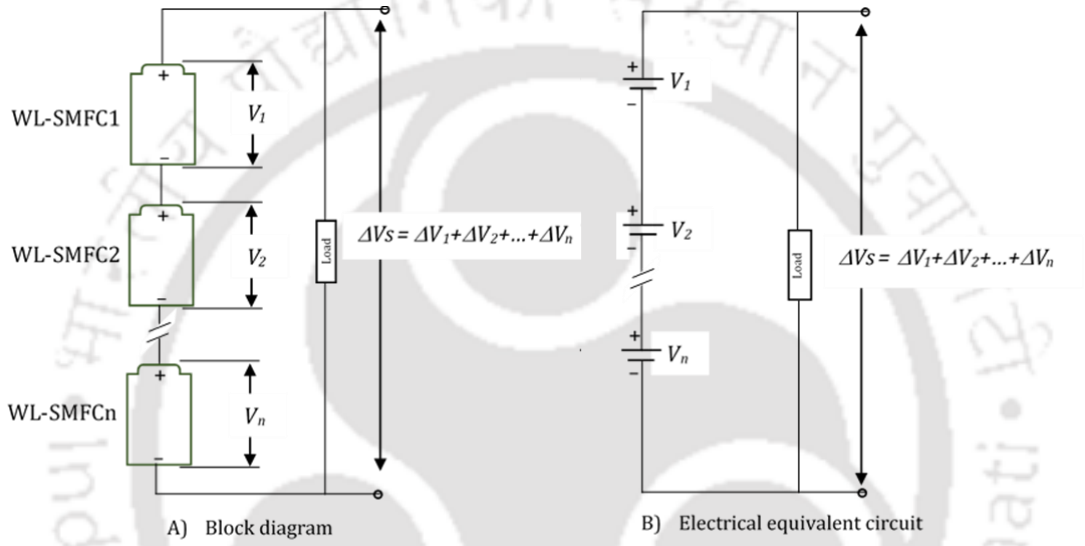

Figure 3.1: (A) Equivalent block diagram and (B) the equivalent circuit diagram of the series stacked WL-SMFCs

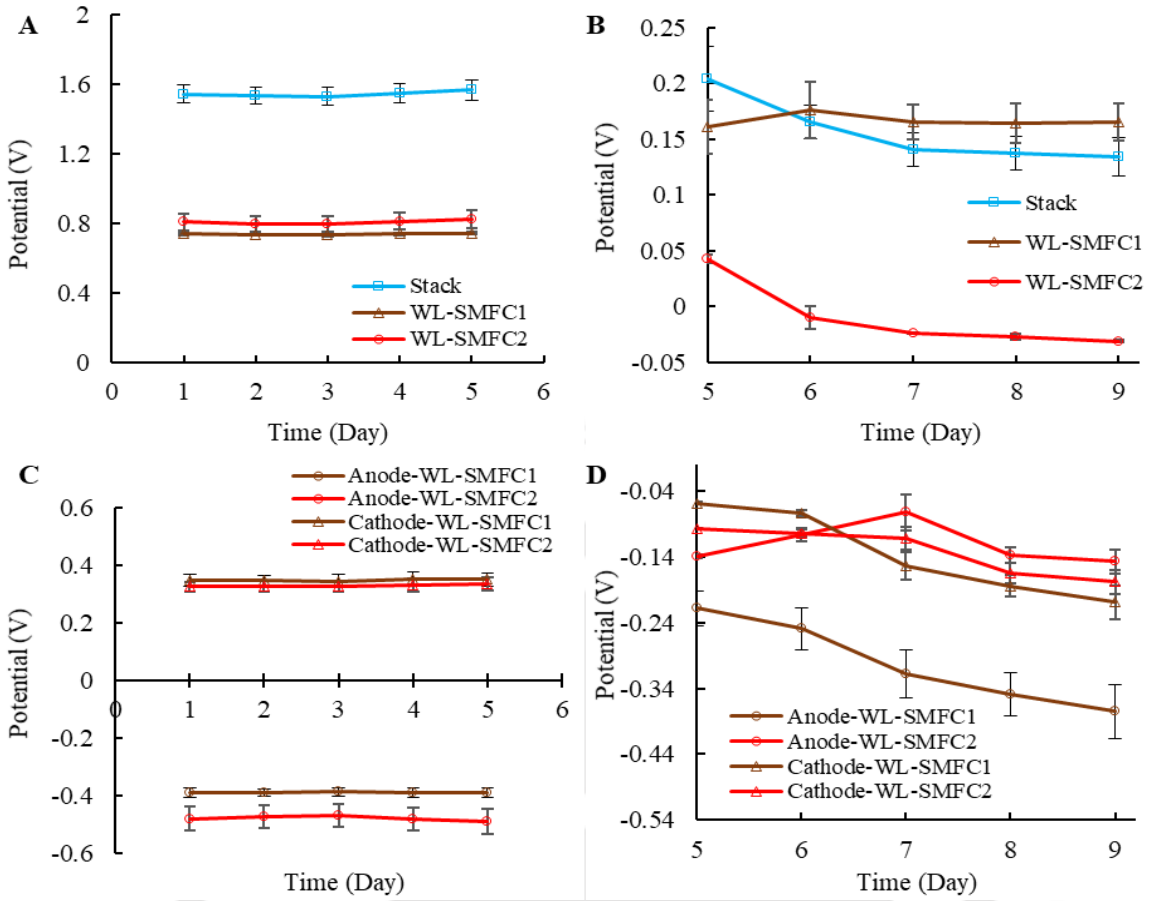

Figure 3.2: Potential variation in series stacks of two WL-SMFC units in (A) OC and (B) CC mode of operation. The potential variations in the individual electrodes of the cells in (C) OC and (D) CC modes of operations. The operation at CC mode was performed at a load of 10 kΩ

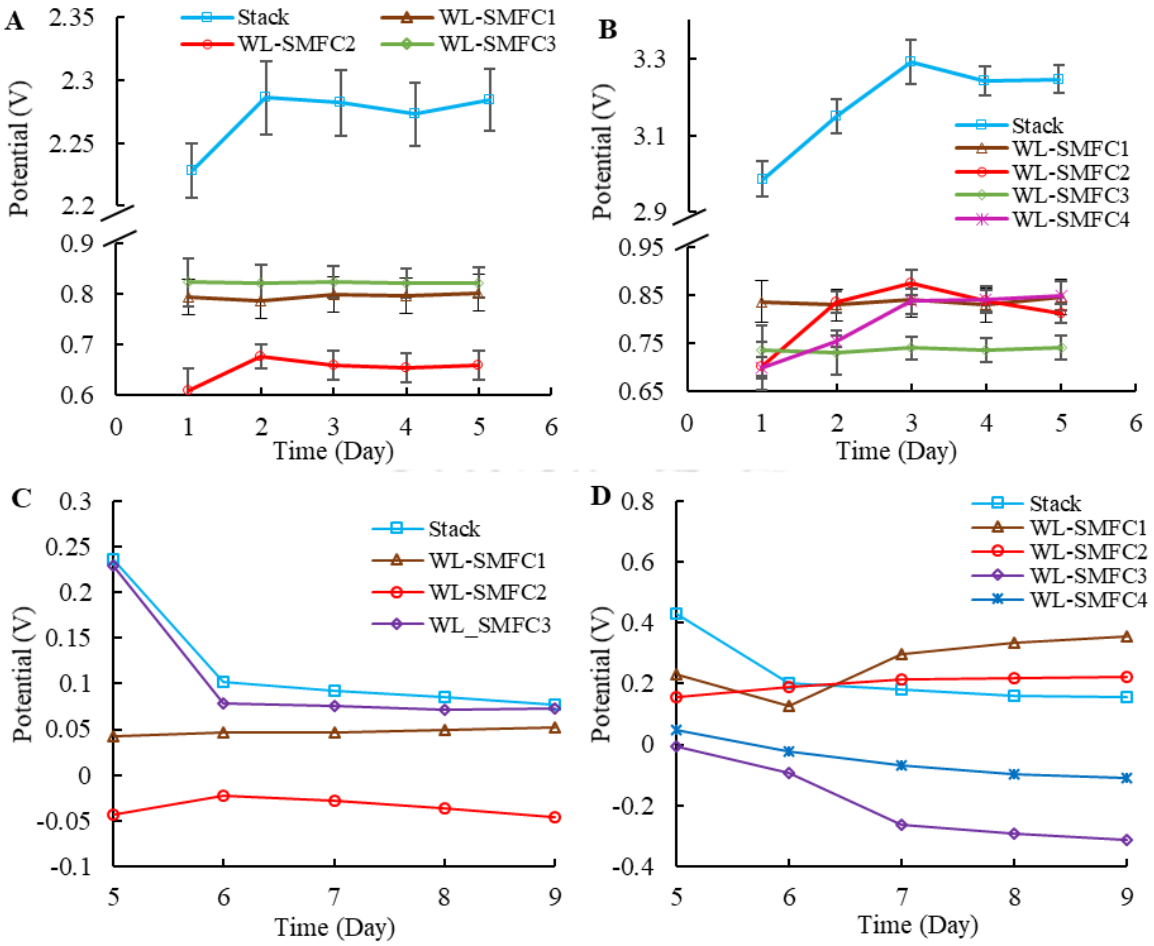

Figure 3.3: Potential variation in OC mode in a stack of (A) three unit cells, and (B) four unit cells. Potential variation in CC modes in a stack of (A) three unit cells, (B) four unit cells

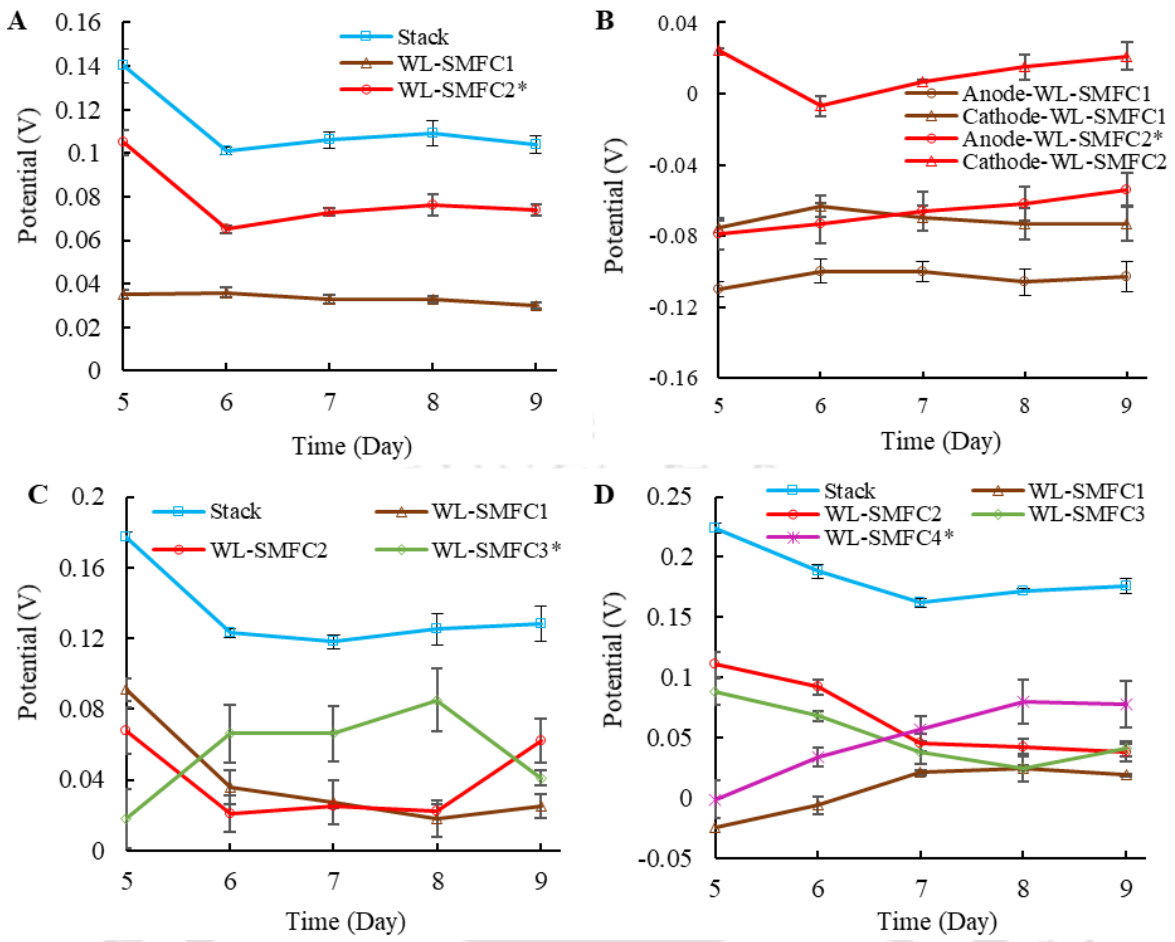

Figure 3.4: CC potential variation over operation time for (A) stack of two unit cells, and individual units, (B) individual electrodes of the two unit stacked cells, where the anode surface area ratio for unit one and two is 1:2, (C) stack of three unit cells and individual units, where the anode surface area ratio for unit 1, 2, and 3 is 1:1:3 and (D) stack of four unit cells and individual units, where the anode surface area ratio for unit 1, 2,3, and 4 is 1:1:1:4. Unit/electrodes with increased anode surface are marked with *

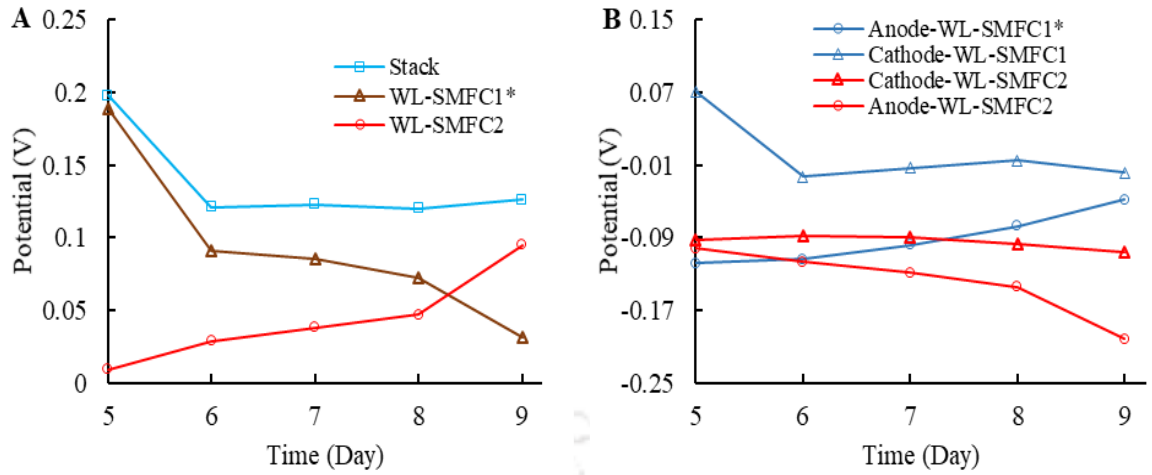

Figure 3.5: Close circuit potential variation of (A) the stack and individual WL-SMFC in a stack of two WL-SMFCs and (B) half-cell potential of the WL-SMFC in the stack where the anode surface area ratio for SMFC1 and SMFC2 is 2:1

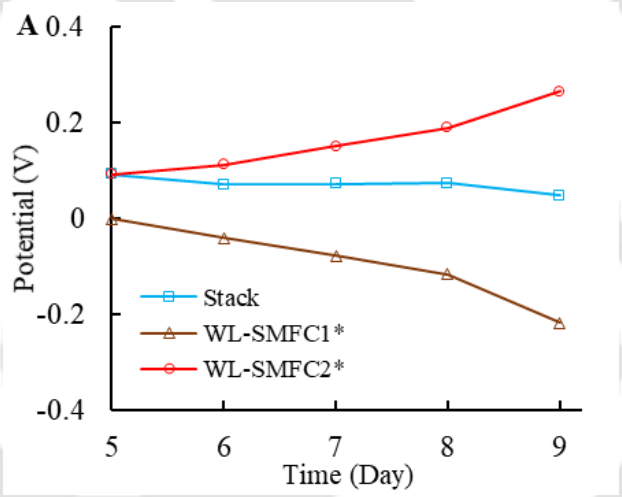

Figure 3.6: Close circuit potential variation of the stack and individual WL-SMFC in a stack of two WL-SMFCs if the anode surface area is increased to two times of the standard maintaining a ratio 1:1

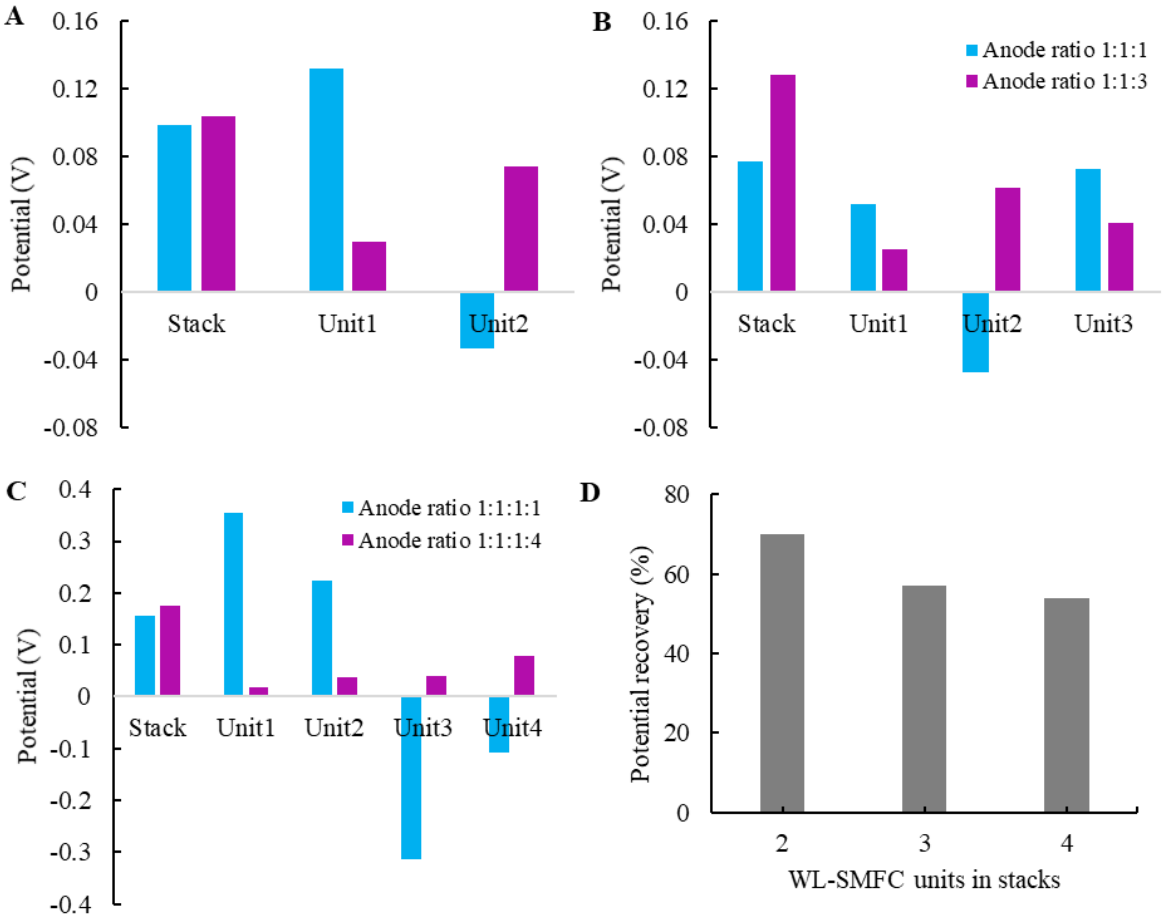

Figure 3.7: A-C: Voltage profiles in stack's individual units and in a stack of (A) two (B) three and (C) 4 units stacks with standard [ ] and enlarged [ ] anodic surface in the terminal units. The ratio of anodic surface area for standard to increased surface are 1:2 for two, 1:1:3 for three, and 1:1:1:4 for four units stacks. (D) Percentage recovery through terminal anodic surface enlargement from the losses caused by the VR in the different stacks. The respective surface area ratio of standard to enlarged terminal anode in the stack of 2, 3, and 4 units is 1:2, 1:1:3, and 1:1:1:4. The potential values of the units/stacks were measured on the fifth day of operation

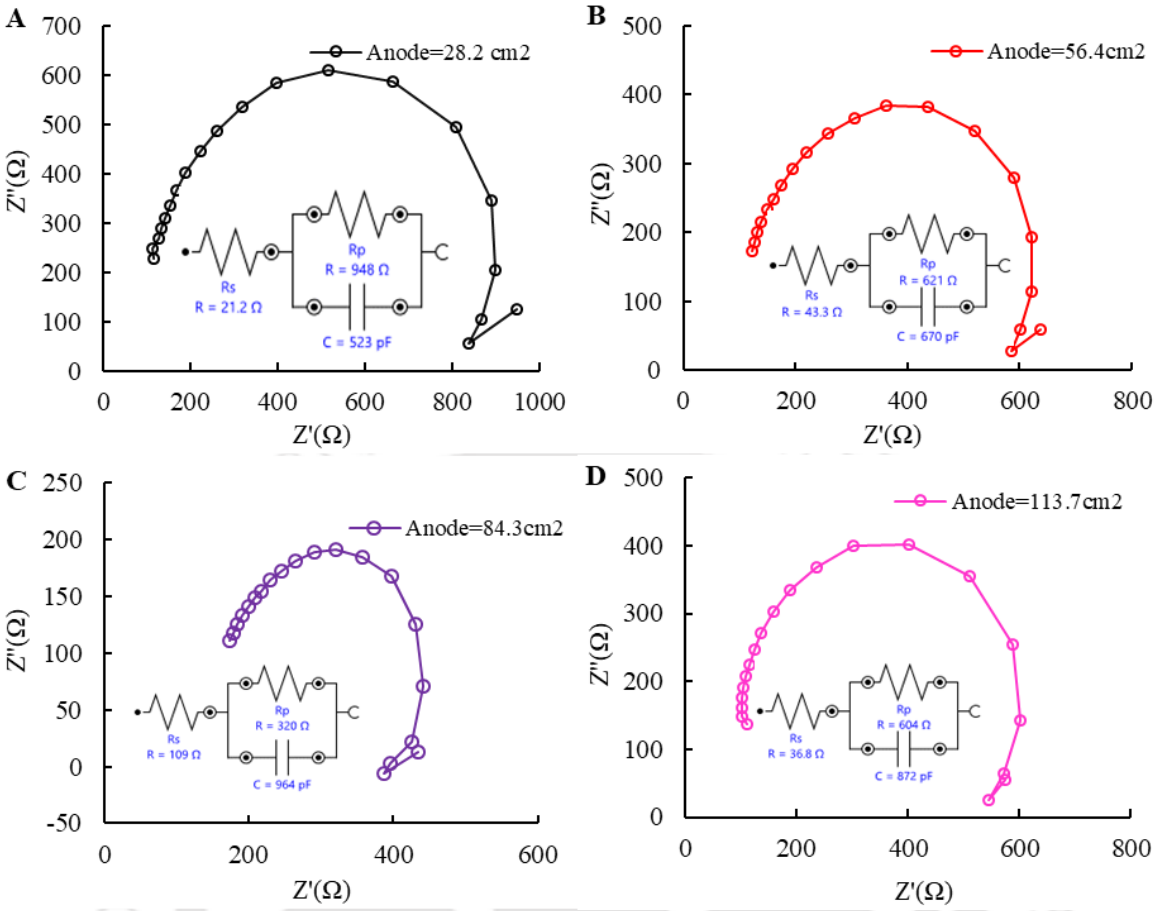

Figure 3.8: EIS analysis of the terminal anodes in WL-SMFCs: (A) the standard anode in an unit, (B) anode with enlarged surface in a stack of 2 unit, and (C) anode with enlarged surface in a stack of 3 unit and (D) anode with enlarged surface in a stack of 4 unit. The inset equivalent Randles' circuits shows the corresponding resistance and surface capacitance values

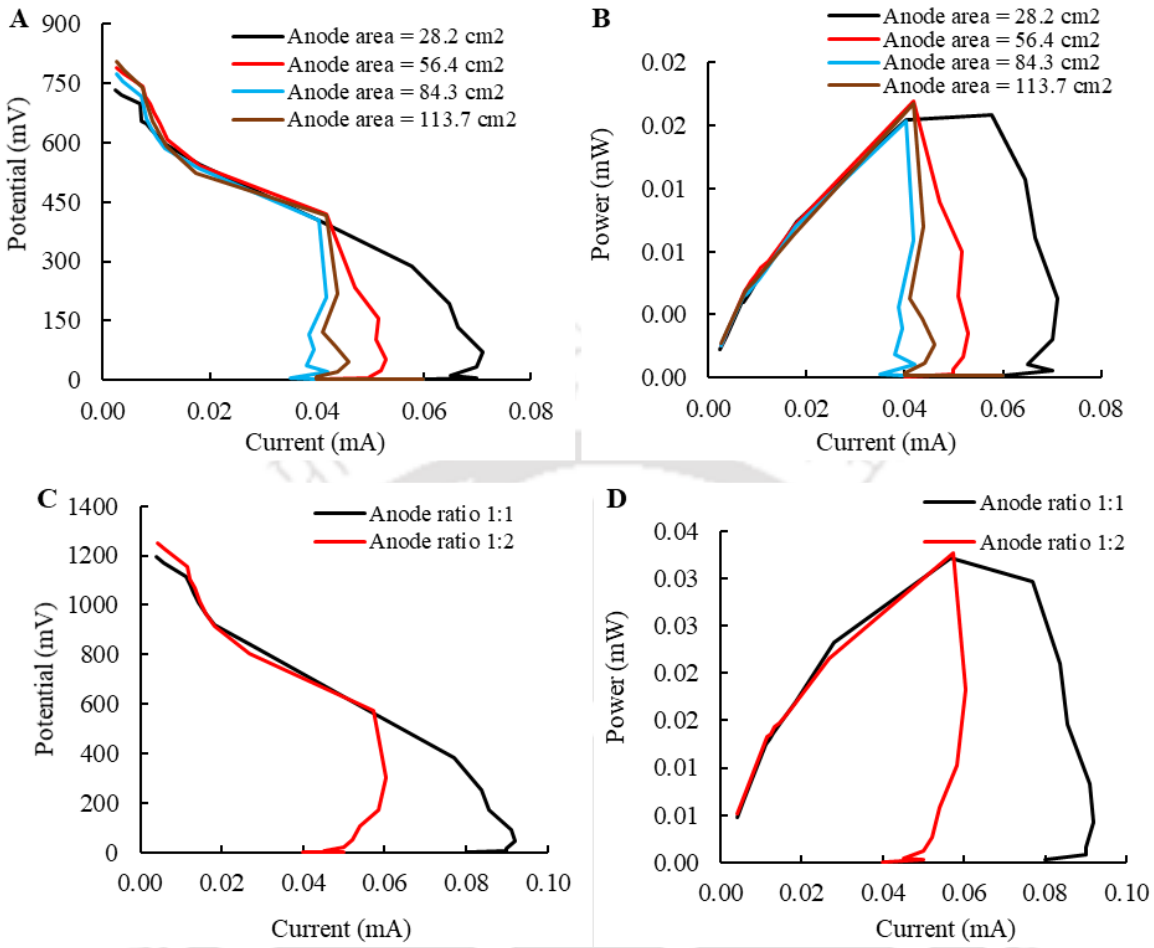

Figure 3.9: (A) and (B) Shows the polarization curves of individual WL-SMFC when the anode surface area was increased (C) and (D) Indicates the polarization curves of stack of two WL-SMFCs with anode surface area ratio of the two WL-SMFCs 1:1 and 1:2. The load value was changed from 300kΩ-50Ω during the polarization scan

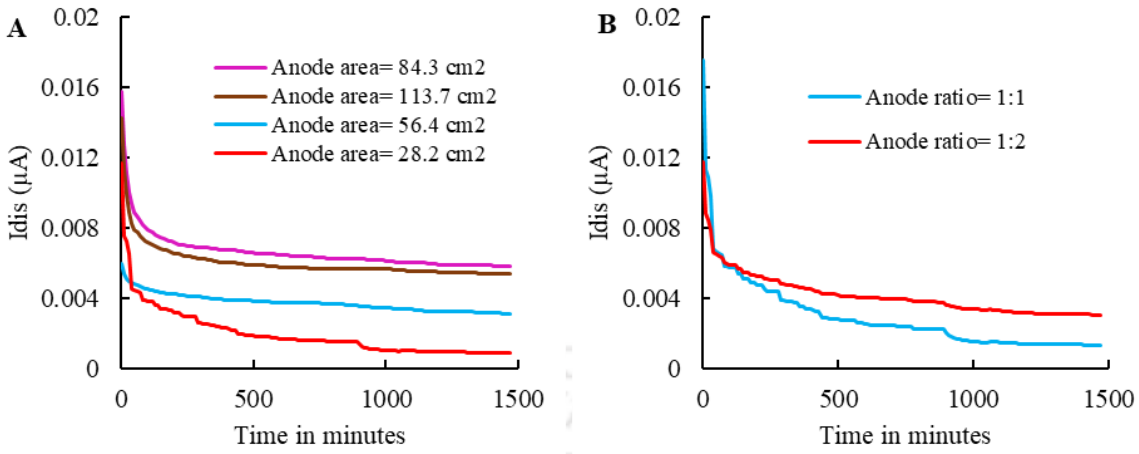

Figure 3.10: Discharge current of WL-SMFC at 10 kΩ load (A) with increased anode surface area and (B) in stack operation with two unit cells

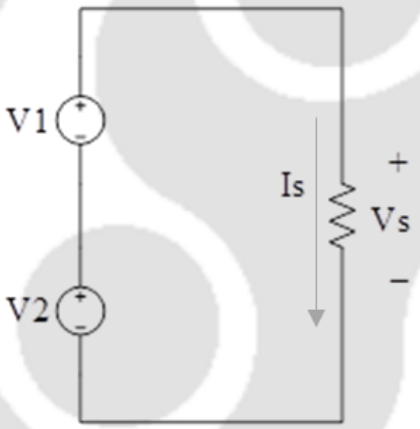

Figure 3.11: Electrical equivalent circuit of the WL-SMFC stack when connected to a load

CHAPTER 4

DESIGN AND FABRICATION OF A SELF-POWERED VOLTAGE BOOSTER FOR ENABLING REAL-TIME APPLICATIONS OF WATER LETTUCE-ASSISTED SEDIMENT MICROBIAL FUEL CELL

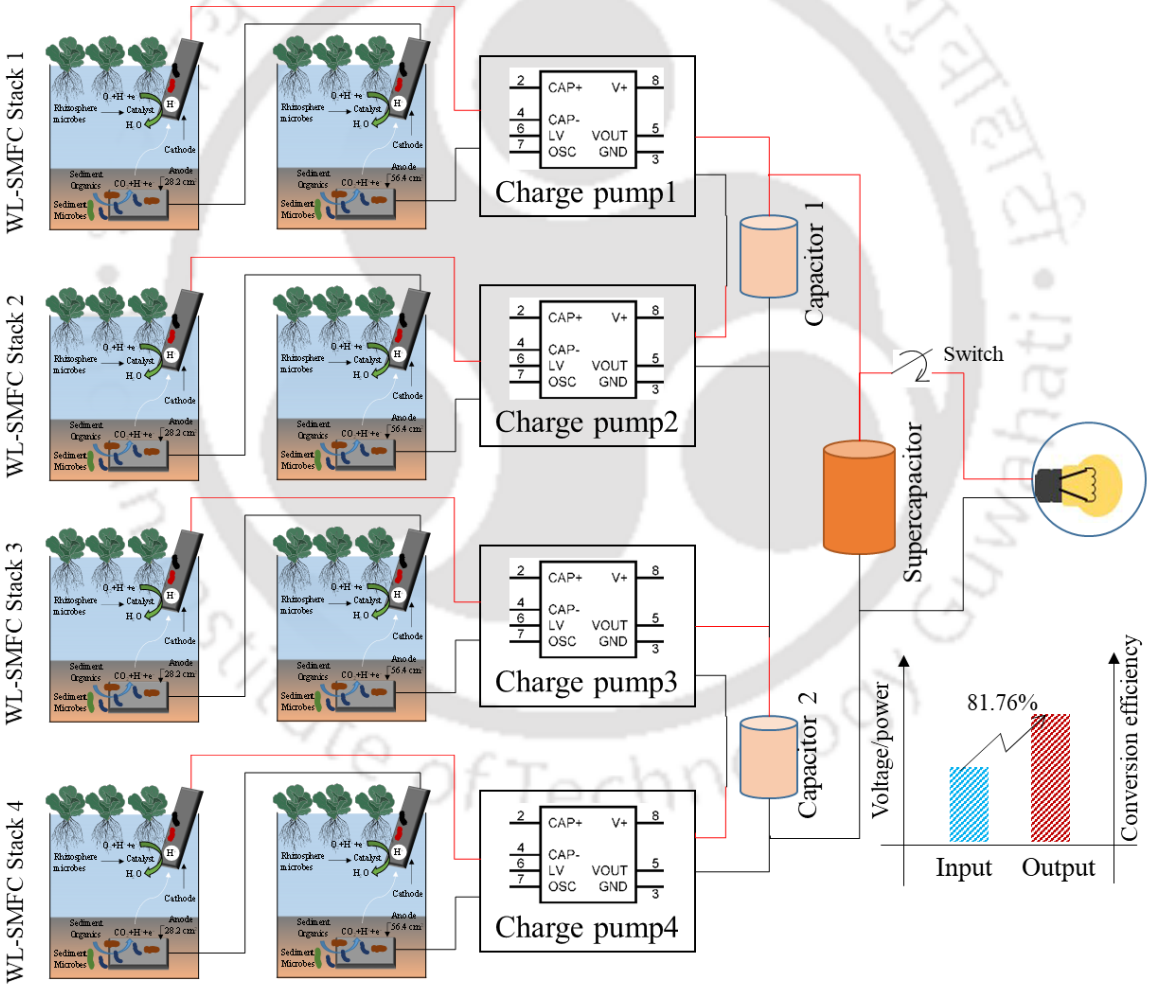

4.1 Introduction

Microbial fuel cells (MFCs) have been captivating attention in bioremediation of wastewater treatment and sensors for environmental monitoring due to their advantages for qualifying the conditions of self-sustainability and cost-effectiveness (Tommasi and Lombardelli, 2017). However, this bio-based green energy technology is still a myth for its commercial applications due to poor power performance constrained by the low theatrical potential value, delivering mainly in a single-digit range (Abbas et al., 2017). An effective approach to improve the working potential values of MFC is the stacking of several unit cells through either series or parallel connection networks. However, the real-time application even with the improved voltage is hampered by another challenge posed by the fast voltage discharge linked to the poor bioelectrode reaction kinetics (An and Lee, 2014; Shi et al., 2025). A viable approach to counter this challenge is to introduce a suitable power management system to improve the overall power output of the stacked MFCs (Dutta et al., 2022b).

A power management system (PMS) is a device that consists of some electronic components functioning together to convert a low electrical input into an utilizable power output. The basic configuration of a PMS mainly entails a charge pump, a supercapacitor (SC), and a boost converter (Dutta et al., 2022b). This basic configuration of the PMS may be modified to develop improved PMS topologies for efficient enhancement of MFC performance. MPPT, flyback boost converter, ultra-low power PMS are some of the modified and improved topologies of PMSs. The MPPT defines a technique based on the maximum power transfer theorem for extracting power at maximum magnitude from an MFC. In MPPT-based PMS an algorithm or circuit configuration is implemented to track the MPP of the fuel cell, which require dedicated power for its operation. The conversion efficiency of MPPT-based PMS is mostly reported around 50%. The flyback converter design configuration proposed by Degrenne et al., was operated at the MPP of the BFC i.e., at 0.3 V with 62% conversion efficiency. Energy harvesting circuits built for MFCs that mostly consume not more than 10 mW power for their operation are termed as ultra-low power PMS. Kim et al. (2014), proposed the system that coupled a customized small-scale (21.3 cm^2) ultra-low power consuming PMS with a benthic MFC producing 5.4 μW. This ultra-low power electronic unit included programmable interface that enabled self-sustainability and was suitable for sensor applications. The circuit design included a customized chip (CTRL chip) that consumed ultra-low power for performing operations like harvesting energy from benthic MFCs and

processor operations. Fabrication of this chip was conducted on a 180 nm CMOS technology, which was part of a 1.0 mm^3 die-stacked sensor node system (Kim et al., 2014; Lee et al., 2013). To meet the demand of energy sustainability, designing a PMS that consumes only a small part of the MFC's power for their operation and simultaneously converting the total MFC power for practical application is yet a broad area to be explored. Designing a self-powered PMS with high conversion efficiency for powering real-life applications is a subject matter of high significance.

Herein, an effort has been made to improve the power performance of the stacked WL-SMFCs, the design and fabrication of which have already been discussed in the previous sections. It may be mentioned that the PMS topologies built with too many passive components would increase the power requirement for their operation, and the excess power consumption would deteriorate the conversion efficiency. Additionally most of the PMSs designed with charge pump or switched mode capacitor topology reported to date primarily rely on external power sources for their functioning. Keeping the above critical issues in mind, this work designed a PMS with a limited number of components comprising a charge pump and capacitors of two different strengths. The charge pump ICs (ICL7660) was used to boost the SMFCs' output voltage. The voltage doubling setup of the integrated circuit was utilized to enhance the voltage output from two connected WL-SMFCs in series, and several of these configurations were linked together to increase the voltage level through the process of voltage addition. The boosted voltage was then stored in a SC finally. The approach of combining the output voltage from the voltage doubling configurations to generate usable power discussed in this study is an innovative strategy. A detailed account of the design, fabrication, operation, and performance of the PMS has been presented in this work.

4.2 Materials and methods

4.2.1 Materials

WL-SMFC fabrication materials: The WL-SMFC fabrication materials such as pond sediment, natural water, and WL were collected from a pond located within the campus of the Indian Institute of Technology Guwahati, India (26.1903° N, 91.6920° E) as mentioned in the Chapter 1 and 2. Iso-molded graphite plates used to prepare the electrodes for the system were purchased from GraphiteStore.com (USA). Conductive copper wire (1.21×10^{-2} Ωm^{-1} at 20 ^{0}C) with a PVC (polyvinyl chloride) coating used as electrode terminals were purchased

from M/S KEI wires and cables, India. The electrode and copper wire connection was established with silver-conductive epoxy purchased from M/S MG Chemicals (USA). The glassware used to fabricate the WL-SMFC reactor was purchased from Borosil, India.

PMS materials: The charge pump IC ICL7660 was purchased from Maxim integrated (USA), Schotky diodes (1N5817) were purchased from Multicomp PRO (UK), capacitors and SCs was purchased from AVX corporation (USA), and a 1W LED was purchased from electroncomponents.com (India). The data of the PMS input and output was recorded with a Data acquisition system (Agilent 34972A LXI data acquisition system, Agilent USA)

4.2.2 Fabrication of WL-SMFC series stacks

The unit WL-SMFC was fabricated following the procedure described in Chapter 2. Briefly, eight units of such cells were constructed by using glass beakers; each with a volume of 500 ml was used in this study. A total 1/4 of the beaker height (about 3 cm) was covered by the pond sediment layer, and the water height was maintained at 7 cm for the entire period of experimentation. Iso-molded graphite plates were used as both the cathode and anode material. The cathodes of dimensions of 6 cm×2 cm×0.3 cm (28.4 cm^2) were planted vertically by submerging 50% in water at the air/water interface. The anodes were placed horizontally at half depth of the sediment layer. The anode of four WL-SMFCs has dimensions of 3 cm×4 cm×0.3 cm (28.2 cm^2). Whereas, the anodes of the rest of the WL-SMFCs had dimension of 6 cm×4 cm×0.3 cm (56.4 cm^2). Silver-conductive epoxy was used to attach the wire to the electrode surface, while non-conductive epoxy glue was used as an anti-corrosion material to envelop the exposed surface of the copper wires.

The stacking of WL-SMFCs was performed by connecting two WL-SMFC units in series in a single stack. In the stacks, the unit at the top position whose cathode was open for load connection had the smaller anode (28.2 cm^2) and the terminal unit whose anode was open for load connection had the larger anode (56.4 cm^2) (Figure 4.1).

4.2.3 The charge pump based PMS

The charge pump IC ICL7660 is a monolithic, CMOS switched-capacitor voltage converters that is capable of inverting, doubling, dividing, or multiplying a positive input voltage. This charge pump IC can operate from an input voltage of 1.5 V to 10 V with no external diode over the full temperature range and can deliver output current 10 mA with a 0.5 V output

drop. The ICL7660 provides low quiescent current and high efficiency. The oscillation control circuitry and four power MOSFET switches were included on-chip. The voltage conversion was performed by first accumulating charge in a bucket capacitor and then transferring it into a reservoir capacitor. The design configuration of ICL7660 provide a simple, compact, low-cost solution while negative or doubled supply voltages are needed for a few low-power components. In this study the PMS was designed with voltage double circuit configuration of the ICL7660 (see Figure 4.2). The stack of two units WL-SMFC were connected to the input of the voltage double configuration of ICL7660. The output voltage of the IC was stored in the reservoir capacitor C2 (Figure 4.2). The loss of voltage at the output was attributed to the barrier potential (V_B) of the two diodes in the configuration. Hence, if V+ is the input voltage then the reservoir capacitor stores $2(V+)-2V_B$ across its terminals at the end of the voltage double operation of the IC. To minimize voltage drop, two Schottky diodes (1N5817) with a low P-N junction barrier potential range of 0.2-0.45 V at room temperature (25 °C) are used in the circuit, provided that the forward current remains below 1 A, while other diodes exhibit a barrier potential of 0.7 V under the same operating conditions. Herein, four stacks of WL-SMFCs were individually connected to voltage double configuration of ICL7660 and the output of the charge pump ICs were connected in pairs (in series) to charge a 3300 µF capacitor. The capacitors were then connected in series to charge the 0.5 F SC.

4.2.4 The performance analyses of the PMS

The performance of the PMS relates to the voltage conversion efficiency of the PMS circuit. The conversion efficiency of the PMS was estimated by calculating the input and output power characteristics of the PMS. The input power (P_{in}) was calculated by the equation 4.1.

$$P_{in} = V_{in} \times I_{in} \tag{4.1}$$

V_{in} and I_{in} are the voltage and current values of the WL-SMFC stacks when connected to the charge pump IC. The total input power P_{total} of the PMS was calculated by the sum of the input power of all charge pump ICs and by the equation 4.2.

$$P_{total} = P_{in1} + P_{in2} + P_{in3} + P_{in4} \tag{4.2}$$

Here, P_{IN1} to P_{IN4} designates the individual input power of the charge pump ICs in the PMS. When the output of the charge pumps is used to charge the SC from a charging voltage V_C to

a discharging voltage V_D, the energy stored in the SC of capacitance C is given by equation 4.3 (Li et al., 2022).

$$E_{SC} = \frac{1}{2} C (V_D^2 - V_C^2) \quad (4.3)$$

With the E_{SC} value, the power stored in the SC (P_{SC}) can be calculated with the SC discharging voltage V_D and discharging time T_C and by the following equation 4.4.

$$P_{SC} = \frac{C(V_D^2 - V_C^2)}{2T_C} \quad (4.4)$$

If the power output (P_{out}) at the load is obtained, the power efficiency of the PMS can be calculated with the given equation 4.5:

$$\eta_P = \frac{\int_0^{T_D} P_{out} dt}{\int_0^{T_C} P_{SC} dt} \quad (4.5)$$

4.3 Results and discussions

4.3.1 Power performance analysis of the WL-SMFC stacks

The OCP of the WL-SMFC stacks containing the standard anodic surface (28.2 cm^2) and the larger anodic surface (56.4 cm^2) were 791±0.02 mV and 818±0.03 mV, respectively. The OCP of the four stacks in a cluster were 1.546±0.01 V, 1.692±0.06 V, 1.594±0.05 V and 1.561±0.09 V, respectively. The OCPs were recorded when the SMFC's voltage reached saturation period, which was identified after 5 days of operation. The minor OCP variation among the stacks were impelled by the fluctuations of their half-cell potential caused by the open environment factors even though the cell materials were similar across the cells. The long-term potential behavior of the WL-SMFC, along with the influence of environmental factors on its electrical parameters, has been explored in Chapter 2 and (Dutta et al., 2025). The electrical performance of the four stacks were investigated with the polarization curves as shown in Figure 4.3A. The maximum power densities (mW) of the stack 1, stack 2, stack 3 and stack 4 were 0.033, 0.034, 0.033 and 0.029, respectively at an external resistance of 10 kΩ (Figure 4.3B). When maximum power was derived from the stacks the respective current values (mA) were 0.057, 0.058, 0.058 and 0.054 for stack 1, stack 2, stack 3 and stack 4 (Figure 4.3B).

4.3.2 The voltage double operation

The input voltage range for consumer electronics is between 3.3 and 12 V (Alipanahi et al., 2019b; Mamun et al., 2023). Therefore, the voltage rating and power output of the WL-SMFC stacks are inadequate for practical use, indicating a necessity for further improvements in voltage and overall power ratings. As mentioned in chapter 3, the highest voltage recovery was achieved with a stack of two WL-SMFCs, generating an open circuit voltage exceeding 1.5 V, which is sufficient for the operation of ICL7660 charge pump ICs. The voltage doubling functionality of the ICL7660 facilitates a voltage boost operation with minimal voltage loss. Figure 4.4 shows the input and output of the ICL7660 charge pump IC in the voltage double configuration when connected to a series stack of two WL-SMFCs. The default switching frequency of the charge pump ICL7660 was specified at a maximum of 10 kHz. The choice of the capacitor pair for the voltage double configuration of the charge pump IC was dependent on the output requirements. Moreover, the high-value capacitors can reduce the output impedance. Figure 4.4A show the input and output voltages of the charge pump IC configured with 1000 µF capacitor pairs during voltage double operation. The selection of these high-capacity capacitors, specifically 1000 µF, aims to lower the output impedance of the integrated circuit, resulting in a shorter charging duration for the terminal SC. The voltage conversion efficiency was 97.15±0.01% when the output voltage at capacitor C2 reached the saturation voltage level (Figure 4.4B). At this voltage saturation stage, a voltage drop of 0.286±0.003 V was observed at the input at a constant current of 0.4 µA. Here, the BOOST pin of the IC was also connected to the stack to increase the oscillator frequency, which reduces the output impedance. Connecting the BOOST pin with the stack voltage is also beneficial for protecting the WL-SMFC stack if the stack undergoes higher voltage losses. The reduced stack voltage reduces the switching frequency and hence allows the stack more time to restore the voltage loss.

4.3.3 Cascading the charge pumps

The voltage double configuration of the ICL7660 was cascaded in series in pair of two and the output was connected to a 3300 µF capacitor (Figure 4.5). In the PMS two cascades of the voltage double configurations were used to charge the 0.5 F SC. The output of the cascades can be coupled in series or parallel configuration as per requirement and in this study the output of the cascaded charge pumps was connected in series to charge the SC. The low

power input of the WL-SMFC stacks thrust higher charging time for the SC. When the SC was charged to 3.5 V (61.5% of the limited value) after 35 hours of charging operation (Figure 4.6A), a 10 kΩ and 1 kΩ load were connected to the SC to investigate the power outputs. The unit stack of WL-SMFC produced maximum power when a 10 kΩ resistor was connected directly to the stacks, and the summation of maximum power produced by all the stacks was 129 µW. However, with the PMS, the SC delivered an average output power of 3.95 mW to the load with a total input power of 4.22 µW (Figure 4.6B). Moreover, when a 1 kΩ resistor was connected, an average output power of 8.87 mW was consumed by the load with an average total power input of 4.13 µW from the four stacks (Figure 4.6C). The SC discharged at a rate of 0.4 µW/s and 20 µW/s, respectively when 10 kΩ and 1 kΩ loads were connected. The choice of SC depends on the power requirements by the load and the duration of operation. Here, considering the discharging voltage V_D and charging voltage V_C and the average power obtained for 10 kΩ and 1 kΩ loads, the choice of SCs has been determined with increasing discharging time (Figure 4.6D). It is evident that increasing the SC value would result in increased discharge time; however higher SC value would also induce higher charging time for PMS to charge the SC. The charging time can be reduced with combined parallel and series cascade of the charge pump output.

4.3.4 PMS efficiency analysis

The charge pumps in voltage double configuration converted the input voltage from the WL-SMFC stack with 97.15±0.01% efficiency. The output of the cascaded charge pump was supplied to the SC, and the SC is discharged through the external load. The input and output power values govern the overall efficiency of the PMS. The power efficiency of the PMS was obtained as 24.59%, 81.76% and 74.05% for the loads of 10 kΩ, 1 kΩ and 100 Ω, respectively (Figure 4.7). The power efficiency of the PMS is dependent on the charging time and discharging time of the SC. Shorter charging time and longer discharging time improves the power efficiency of the system. Optimization of the switching frequency of the charge pump would improve the charging time of the SC. However, this optimization is a challenging task considering the frequent electrical parametric changes of the WL-SMFC. Additionally, incorporation of a control circuitry for the switching frequency optimization process using WL-SMFC or external power source for its operation would deteriorate the power efficiency and the sustainability of the WL-SMFC system. Finally, an application of

the PMS was shown by lighting a 1 W LED as shown in Figure 4.8B and Figure 4.8A shows the fabricated circuit of the PMS.

Previous studies on PMS based on charge pump topology have shown the use of SCs in switching mode to boost MFCs power output with a conversion efficiency of 67%. However, the switching operation was performed through external energy sources (Kim et al., 2011). In some studies DC/DC boost converters were used to enhance the output voltage of the charge pump or switching mode capacitors to meet the energy requirement (Alipanahi et al., 2019a; Gao et al., 2011). However, the energy conversion efficiencies of the boost converters are usually not up to the mark. A PMS designed with a DC/DC boost converter can consume even up to 40% of the input energy for its operation (Donovan et al., 2011b). The PMS designed by (Gao et al., 2011) incorporated a charge pump, switching mode capacitors and a boost converter; which however, converted the MFC output with 79% efficiency. The present PMS design, however, could generate the WL-SMFC output with 81.76% efficiency when the SC was charged upto ~61.5% of the desired value. Furthermore, the design of the circuit is straightforward, using only a small amount of power from the WL-SMFC, and allows for the selection of capacitor size according to the load needs and mode of operation.

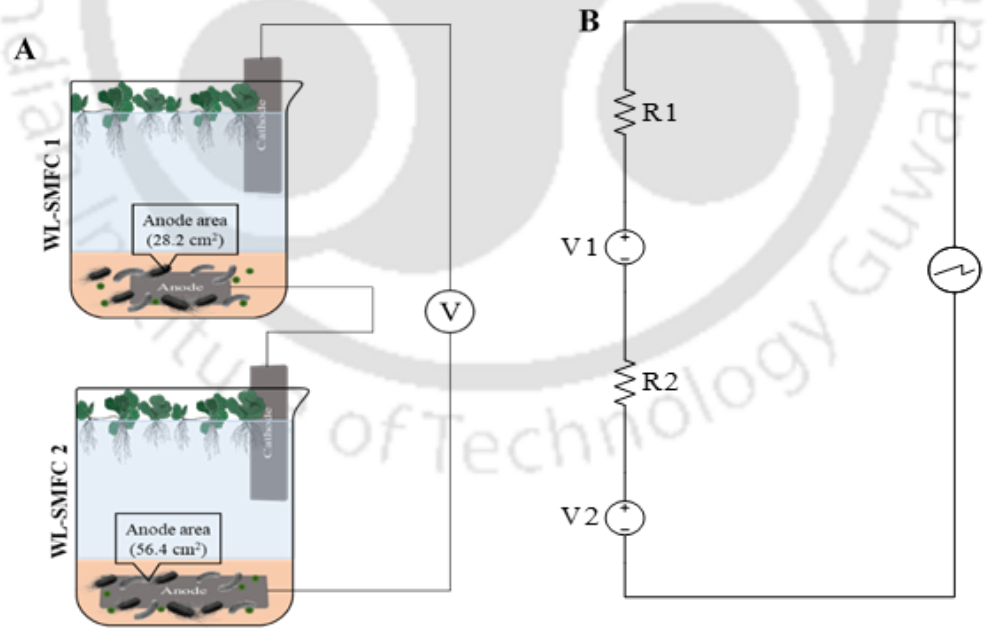

Figure 4.1: (A) Schematic diagram of the WL-SMFC and the stacking strategy, (B) equivalent electrical diagram of the stack system

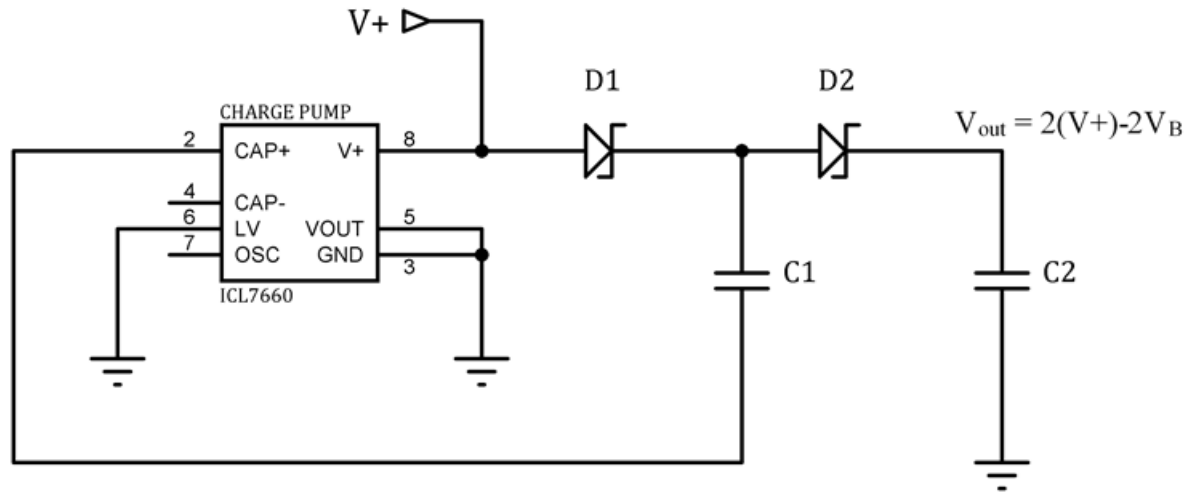

Figure 4.2: Voltage double configuration of ICL7660 with two Schotky diodes (D1 and D2), two capacitors (C1 and C2), V+ is the input voltage and V_D is the barrier potential of the diode

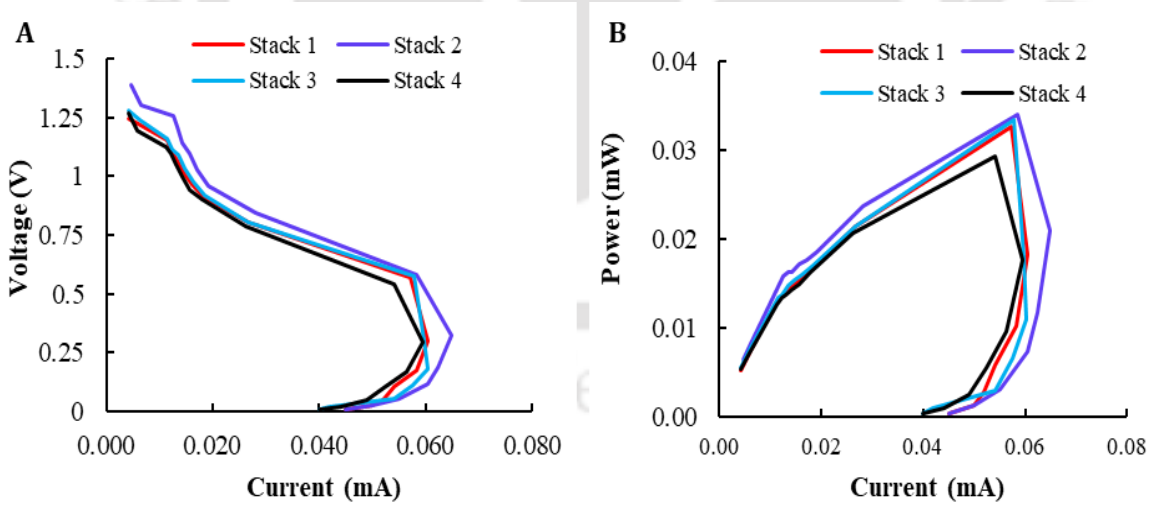

Figure 4.3: (A) Polarization and (B) power curves of the WL-SMFC stacks

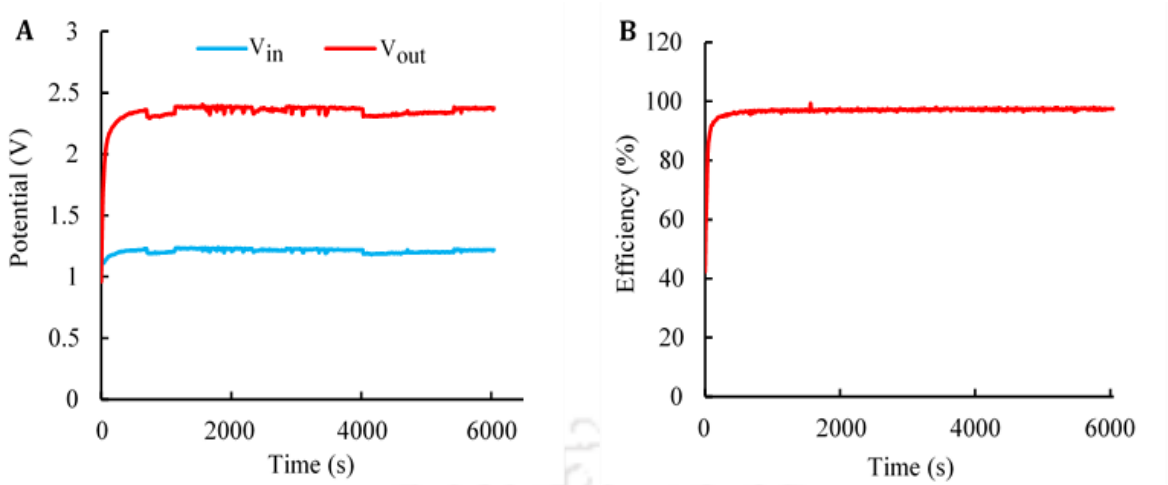

Figure 4.4: (A) Voltage boosting performance of ICL7660 in voltage double configuration with 1000 µF capacitor pair as bucket and reservoir capacitor and (B) voltage conversion efficiency with time for the voltage double configuration of ICL7660

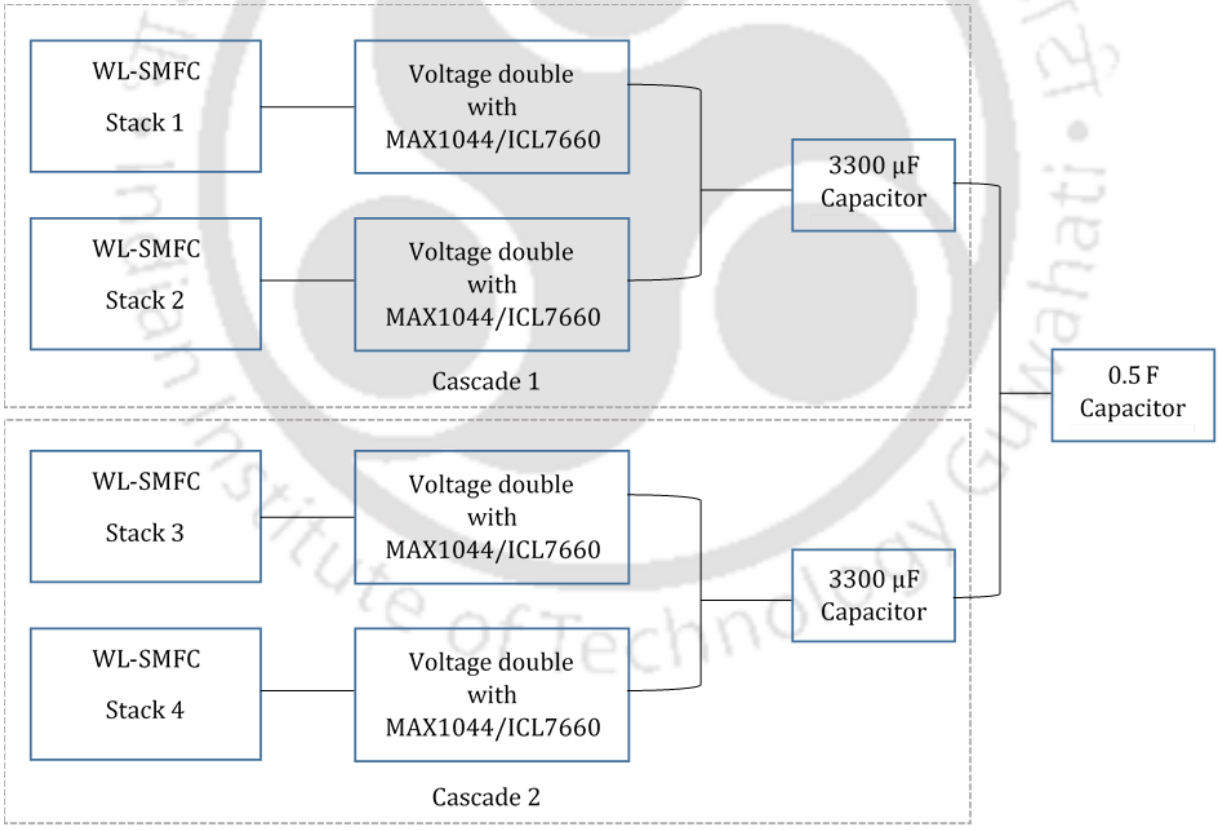

Figure 4.5: Cascading the output of the charge pumps for voltage boosting and the charging the SC

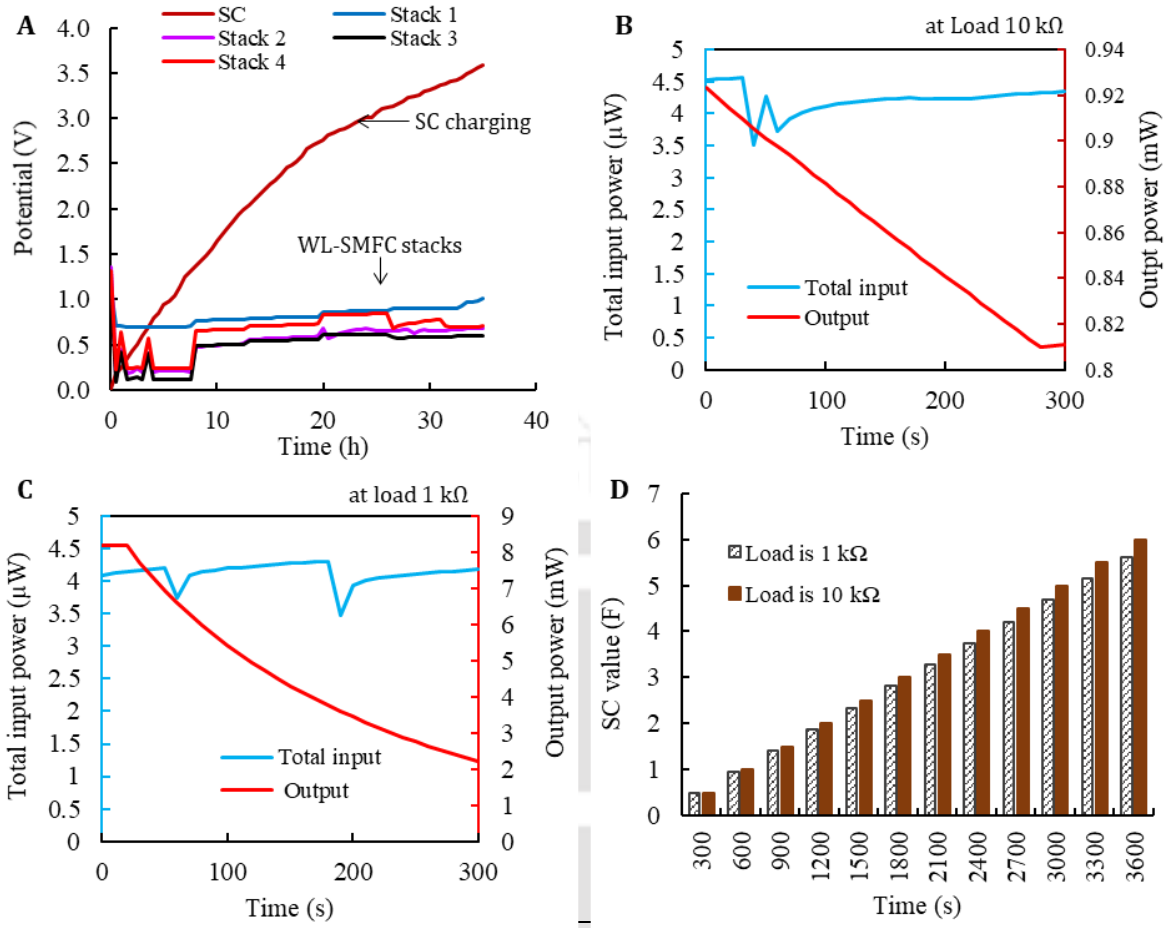

Figure 4.6: (A) the charging operation of the SC with the cascaded charge pumps, input and output power variation with time when the SC is discharged through a (B) 10 kΩ and a (C) 1 kΩ resistor, (D) estimation of SC value for increasing the discharge time

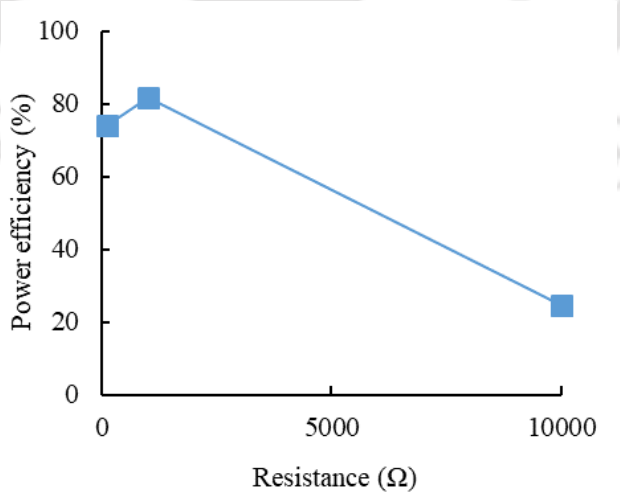

Figure 4.7: Power efficiency of the PMS at different loads

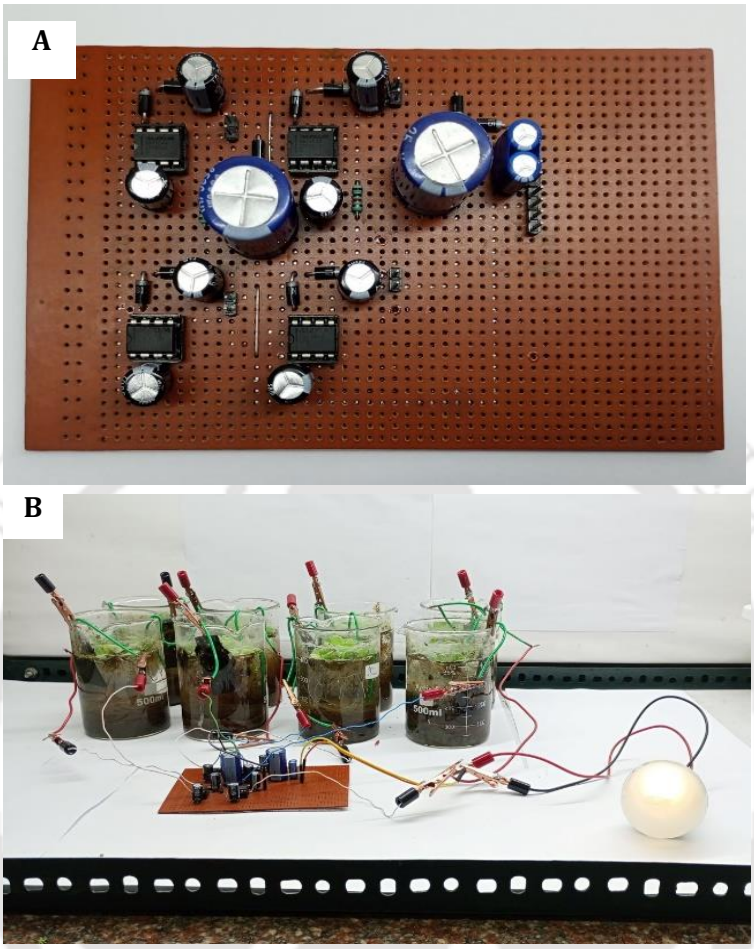

Figure 4.8: (A) The circuit of the PMS and (B) an application of the PMS shown by lighting a 1 W LED

CHAPTER 5

CONCLUSIONS AND SCOPE FOR FUTURE WORK

5.1 Conclusions

The work presented here unequivocally demonstrated the positive role of WL in boosting the electrical performance of SMFC. The significant impact of WL is visible in improving the cathodic performance by ~1.86 fold of the control (that void WL). The effect on critical parameters namely catholyte conductivity, pH, DO, and biocatalytic ORR for cathodic performance was analyzed. The investigation revealed that the coupling of WL to the SMFC brings down the alkaline pH of the native electrolyte and stabilizes its value at near neutrality, which is conducive to the proton movement in the catholyte and plant growth. Further, the conductivity of the electrolyte drastically increased (by 60%) upon cultivation of the plant in the SMFC, supporting cathodic performance by reducing the cell's internal resistance. Interestingly, a significant reduction of DO was effected by the plant, the level of which is, however, above the critical level required for the ORR in the cathode and, hence, did not affect the cathodic performance; conversely, this dropped DO level in the vicinity of the anode surface supports anodic performance by facilitating its anoxic environment, and aiding biocatalytic electron transfer to the anode. Interestingly, many WL rhizobia bacterial species were sequestered and colonized on the cathode as resilient biofilm, hosting diverse oxygen-reducing and catalase-active bacterial species and supporting ORR in the cathode. A further motivating finding is that the overall bacterial density on the biofilm was enhanced under CC operation conditions, which consequently contributed to the higher cathodic potential of the WL-SMFC. This finding highlights the prospect of inducing electrogenic biofilm by applying electrical stress to improve microbial fuel cell potential for real-world applications.

Next, the reduction of VR has been demonstrated in a stack of series-connected units of WL-SMFCs by adopting a new approach where the electrode surface size ratio of the terminal anode to the total anodic surface area was identified as the key factor to reduce the VR. It may be mentioned that the conventional macro- and micro-scale approaches to mitigate voltage reversal (VR) are challenging to implement in plant assisted sediment microbial fuel cell stacks, particularly when installed in natural, open-water environments. In this work, we developed a theoretical framework relating electrical parameters to anodic surface area, predicting that a larger anodic surface area in the terminal unit positively influences the overall voltage of a stacked microbial fuel cell system. This proposition was experimentally validated using a laboratory-scale stack of series-connected WL-SMFC units. Furthermore,

the total anode surface area was experimentally correlated with the surface capacitance and charge of the WL-SMFC stack. For optimum performance, the surface area of the terminal anode should equal the sum of the anode surface areas of all other units in the stack. However, in stacks containing more than three unit cells, this configuration should be applied intermittently, as the percentage of voltage recovery achieved by a single enlarged terminal anode decreases with increasing stack size. The decline in VR mitigation beyond this critical anode surface area ratio is attributed to limiting factors such as substrate availability and electroactive microbial population density, which govern anodic capacitance and charge. Higher capacitance and anode charge contribute to VR reduction and enhance the current discharge rate. These findings suggest that anodic surface area tuning is an effective and technically simple strategy for mitigating VR in WL-SMFC stacks. Further studies investigating the influence of bioelectrocatalytic reaction rates under varying physicochemical conditions in open environments will deepen understanding of this approach and advance the real-world application of these emerging bioelectrochemical devices.

Finally, in the context of real-world application of WL-SMFCs, the present work established a new strategy to amplify the electrical performance (voltage and power) of Water lettuce-assisted SMFC stacks by adopting a self-powered PMS. This three-step charging strategy comprising of SMFC stack to charge pump, charge pump to the capacitor, and then capacitor to supercapacitor amplified the overall electrical performance ~ seven-folds. The developed configuration also has a provision to upscale the setup by increasing the number of stacks and corresponding PMS components to increase the potential and power for high-power-consuming applications. The critical step that might limit the present strategy for some applications demanding fast power delivery is the charging time for the capacitors. An improved current production ability of the WL-SMFCs and lower output impedance of the charge pump ICs may address this issue. In addition, optimization of the switching frequency of the charge pump IC as a function of the input and output would enrich the PMS performance for its successful implementation in real-world applications. The maximum power conversion efficiency of 81.76% achieved through this PMS strategy underscores its prospect for a standalone power supply for outdoor applications such as environmental sensors, operating aeration pumps for wastewater treatment, and allied applications.

5.2 Future scope

1. The overall exciting findings described in this thesis stimulate further in-depth investigation, specifically on the seeding of the electrogenic bacteria at the cathode, their precise role in ORR, and the microbe-plant interactions that influence the pH, conductivity, and oxygen level in the catholyte for a comprehensive understanding on the WL-assisted performance of SMFC for its practical applications. Further in-depth study to correlate surface area to anode reaction kinetics would be supportive to overcome the higher mass transfer loss in the high current operation of WL-SMFC with larger anode surface area.
2. The finding on the mitigation of VR in series stacked WL-SMFCs may be comprehended with the results of further research on the effect of bioelectrocatalytic reaction rate under the changing physicochemical parametric values in open environment conditions.
3. The proposed PMS delivers a maximum power conversion efficiency of 81.76%. However, an optimization strategy for the switching frequency of the charge pump IC as a function of the input and output would enrich the PMS efficiency for its successful implementation in real-world applications.

REFERENCES

Abbas, S.Z., Rafatullah, M., Ismail, N., Syakir, M.I., 2017. A review on sediment microbial fuel cells as a new source of sustainable energy and heavy metal remediation: mechanisms and future prospective. International Journal of Energy Research 41, 1242–1264. https://doi.org/10.1002/er.3706

Abdul Quadir, M.G., Kalita, N., Goswami, P., 2025. *Spirulina* -Based Multispecies Phototrophic Biofilm Anodic Biocatalyst Endures a Prolonged Dark Phase within Light–Dark Cycle Operations and Enhances Anodic Performance in Biophotovoltaic Cells. ACS EST Eng. 5, 60–76. https://doi.org/10.1021/acsestengg.4c00447

Adami, S.-E., Degrenne, N., Vollaire, C., Allard, B., Buret, F., Costa, F., 2011. Autonomous ultra-low power DC/DC converter for Microbial Fuel Cells, in: 2011 18th IEEE International Conference on Electronics, Circuits, and Systems. Presented at the 2011 18th IEEE International Conference on Electronics, Circuits and Systems - (ICECS 2011), IEEE, Beirut, Lebanon, pp. 398–401. https://doi.org/10.1109/ICECS.2011.6122297

Aelterman, P., Rabaey, K., Pham, H.T., Boon, N., Verstraete, W., 2006. Continuous Electricity Generation at High Voltages and Currents Using Stacked Microbial Fuel Cells. Environ. Sci. Technol. 40, 3388–3394. https://doi.org/10.1021/es0525511

Aggarwal, K.K., Rajiv, J., Babu, C.R., 1999. A Rock-Iron-Solubilizing Compound from Root Exudates of Tephrosia purpurea. J Chem Ecol 25, 2327–2336. https://doi.org/10.1023/A:1020877908773

Ahmed, H.A., Yu-Xin, T., Qi-Chang, Y., 2020. Optimal control of environmental conditions affecting lettuce plant growth in a controlled environment with artificial lighting: A review. South African Journal of Botany 130, 75–89. https://doi.org/10.1016/j.sajb.2019.12.018

Alaraj, M., Radenkovic, M., Park, J.-D., 2017. Intelligent energy harvesting scheme for microbial fuel cells: Maximum power point tracking and voltage overshoot

avoidance. Journal of Power Sources 342, 726–732. https://doi.org/10.1016/j.jpowsour.2016.12.104

Alipanahi, R., Rahimnejad, M., 2018. Effect of different ecosystems on generated power in sediment microbial fuel cell. Int J Energy Res 42, 4891–4897. https://doi.org/10.1002/er.4199

Alipanahi, R., Rahimnejad, M., Najafpour, G., 2019a. Improvement of sediment microbial fuel cell performances by design and application of power management systems. International Journal of Hydrogen Energy 44, 16965–16975. https://doi.org/10.1016/j.ijhydene.2019.04.162

Alipanahi, R., Rahimnejad, M., Najafpour, G., 2019b. Improvement of sediment microbial fuel cell performances by design and application of power management systems. International Journal of Hydrogen Energy 44, 16965–16975. https://doi.org/10.1016/j.ijhydene.2019.04.162

Ammam, M., Fransaer, J., 2013. Combination of laccase and catalase in construction of H2O2–O2 based biocathode for applications in glucose biofuel cells. Biosensors and Bioelectronics 39, 274–281. https://doi.org/10.1016/j.bios.2012.07.066

An, J., Kim, B., Chang, I.S., Lee, H.-S., 2015a. Shift of voltage reversal in stacked microbial fuel cells. Journal of Power Sources 278, 534–539. https://doi.org/10.1016/j.jpowsour.2014.12.112

An, J., Kim, B., Nam, J., Ng, H.Y., Chang, I.S., 2013. Comparison in performance of sediment microbial fuel cells according to depth of embedded anode. Bioresource Technology 127, 138–142. https://doi.org/10.1016/j.biortech.2012.09.095

An, J., Kim, T., Chang, I.S., 2016. Concurrent Control of Power Overshoot and Voltage Reversal with Series Connection of Parallel-Connected Microbial Fuel Cells. Energy Tech 4, 729–736. https://doi.org/10.1002/ente.201500466

An, J., Lee, H., 2014. Occurrence and Implications of Voltage Reversal in Stacked Microbial Fuel Cells. ChemSusChem 7, 1689–1695. https://doi.org/10.1002/cssc.201300949

An, J., Nam, J., Kim, B., Lee, H.-S., Kim, B.H., Chang, I.S., 2015b. Performance variation according to anode-embedded orientation in a sediment microbial fuel cell employing a chessboard-like hundred-piece anode. Bioresource Technology 190, 175–181. https://doi.org/10.1016/j.biortech.2015.04.071

An, J., Sim, J., Lee, H.-S., 2015c. Control of voltage reversal in serially stacked microbial fuel cells through manipulating current: Significance of critical current density. Journal of Power Sources 283, 19–23. https://doi.org/10.1016/j.jpowsour.2015.02.076

Babauta, J.T., Nguyen, H.D., Istanbullu, O., Beyenal, H., 2013. Microscale Gradients of Oxygen, Hydrogen Peroxide, and pH in Freshwater Cathodic Biofilms. ChemSusChem 6, 1252–1261. https://doi.org/10.1002/cssc.201300019

Bautista, S., Eladawy, A., Mohieldin, A.N., Sanchez-Sinencio, E., 2014. Boost Converter With Dynamic Input Impedance Matching for Energy Harvesting With Multi-Array Thermoelectric Generators. IEEE Trans. Ind. Electron. 61, 5345–5353. https://doi.org/10.1109/TIE.2014.2300035

Bautista, S., Erbay, C., Han, A., Sanchez-Sinencio, E., 2015a. An Inductorless DC–DC Converter for an Energy Aware Power Management Unit Aimed at Microbial Fuel Cell Arrays. IEEE J. Emerg. Sel. Topics Power Electron. 3, 1109–1121. https://doi.org/10.1109/JESTPE.2015.2398851

Bautista, S., Erbay, C., Han, A., Sanchez-Sinencio, E., 2015b. Power Management System With Integrated Maximum Power Extraction Algorithm for Microbial Fuel Cells. IEEE Trans. Energy Convers. 30, 262–272. https://doi.org/10.1109/TEC.2014.2352654

Beygmoradi, A., Homaei, A., 2017. Marine microbes as a valuable resource for brand new industrial biocatalysts. Biocatalysis and Agricultural Biotechnology 11, 131–152. https://doi.org/10.1016/j.bcab.2017.06.013

Bjerkan, G., Witsø, E., Bergh, K., 2009. Sonication is superior to scraping for retrieval of bacteria in biofilm on titanium and steel surfaces in vitro. Acta Orthopaedica 80, 245–250. https://doi.org/10.3109/17453670902947457

Bodelier, P.L.E., 2003. Interactions Between Oxygen-Releasing Roots and Microbial Processes in Flooded Soils and Sediments, in: de Kroon, H., Visser, E.J.W. (Eds.), Root Ecology, Ecological Studies. Springer, Berlin, Heidelberg, pp. 331–362. https://doi.org/10.1007/978-3-662-09784-7_13

Bombelli, P., Iyer, D.M.R., Covshoff, S., McCormick, A.J., Yunus, K., Hibberd, J.M., Fisher, A.C., Howe, C.J., 2013. Comparison of power output by rice (Oryza sativa) and an associated weed (Echinochloa glabrescens) in vascular plant bio-photovoltaic (VP-BPV) systems. Appl Microbiol Biotechnol 97, 429–438. https://doi.org/10.1007/s00253-012-4473-6

Bora, D., Dutta, A., Mahanta, P., Goswami, P., Stom, D., Barbora, L., 2022. Membrane electrode assembly hybridized anaerobic digester for co-generation of methane enriched biogas and electricity. Fuel 316, 123315. https://doi.org/10.1016/j.fuel.2022.123315

Buzgo, M., 1994. Inflorescence development of Pistia stratiotes (Araceae). Bot. Jahrb. Syst. 115, 557–570.

Carvalho, K.M., Martin, D.F., 2001. Removal of aqueous selenium by four aquatic plants. Journal of Aquatic Plant Management 39, 33–36.

Chelikani, P., Fita, I., Loewen, P.C., 2004. Diversity of structures and properties among catalases. CMLS, Cell. Mol. Life Sci. 61, 192–208. https://doi.org/10.1007/s00018-003-3206-5

Chen, S., Tang, J., Fu, L., Yuan, Y., Zhou, S., 2016. Biochar improves sediment microbial fuel cell performance in low conductivity freshwater sediment. J Soils Sediments 16, 2326–2334. https://doi.org/10.1007/s11368-016-1452-z

Clauwaert, P., Mulenga, S., Aelterman, P., Verstraete, W., 2009. Litre-scale microbial fuel cells operated in a complete loop. Appl Microbiol Biotechnol 83, 241–247. https://doi.org/10.1007/s00253-009-1876-0

Cobine, P.A., Cruz, L.F., Navarrete, F., Duncan, D., Tygart, M., De La Fuente, L., 2013. Xylella fastidiosa Differentially Accumulates Mineral Elements in Biofilm and Planktonic Cells. PLoS ONE 8, e54936. https://doi.org/10.1371/journal.pone.0054936

Commault, A., Lear, G., Novis, P., Weld, R., 2014. Photosynthetic biocathode enhances the power output of a sediment-type microbial fuel cell. New Zealand Journal of Botany 52, 48–59. https://doi.org/10.1080/0028825X.2013.870217

Dallago, E., Lazzarini Barnabei, A., Liberale, A., Torelli, G., Venchi, G., 2016. A 300-mV Low-Power Management System for Energy Harvesting Applications. IEEE Trans. Power Electron. 31, 2273–2281. https://doi.org/10.1109/TPEL.2015.2431439

Damaschke, J.M., 1996. Design of a low input voltage converter for thermoelectric generator, in: Proceedings of Applied Power Electronics Conference. APEC ’96. Presented at the Applied Power Electronics Conference. APEC ’96, IEEE, San Jose, CA, USA, pp. 856–860. https://doi.org/10.1109/APEC.1996.500539

Danhassan, U.A., Lin, H., Lawan, I., Zhang, X., Ali, M.H., Muhammad, A.I., Sheng, K., 2023. Critical insight into sediment microbial fuel cell: Fundamentals, challenges, and perspectives as a barrier to black-odor water formation. Journal of Environmental Chemical Engineering 11, 109098. https://doi.org/10.1016/j.jece.2022.109098

De Schamphelaire, L., Boeckx, P., Verstraete, W., 2010. Evaluation of biocathodes in freshwater and brackish sediment microbial fuel cells. Appl Microbiol Biotechnol 87, 1675–1687. https://doi.org/10.1007/s00253-010-2645-9

Degrenne, N., Allard, B., Buret, F., Adami, S.-E., Labrousse, D., Vollaire, C., Morel, F., 2012a. A 140 mV Self-Starting 10 mW DC/DC Converter for Powering Low-Power Electronic Devices from Low-Voltage Microbial Fuel Cells. Journal of Low Power Electronics 8, 485–497. https://doi.org/10.1166/jolpe.2012.1209

Degrenne, N., Boileau, M., Morel, F., Khaled, F., Ondel, O., Buret, F., Allard, B., 2012b. Association of Flyback Converters to Harvest Energy from Multiple Hydraulically Connected Biofuel Cells, in: 2012 IEEE International Conference on Green Computing and Communications. Presented at the 2012 IEEE International

Conference on Green Computing and Communications (GreenCom), IEEE, Besancon, France, pp. 664–667. https://doi.org/10.1109/GreenCom.2012.106

Dickson, J.F., 1976. On-chip high-voltage generation in MNOS integrated circuits using an improved voltage multiplier technique. IEEE J. Solid-State Circuits 11, 374–378. https://doi.org/10.1109/JSSC.1976.1050739

Ding, Y.-H.R., Hixson, K.K., Giometti, C.S., Stanley, A., Esteve-Núñez, A., Khare, T., Tollaksen, S.L., Zhu, W., Adkins, J.N., Lipton, M.S., Smith, R.D., Mester, T., Lovley, D.R., 2006. The proteome of dissimilatory metal-reducing microorganism Geobacter sulfurreducens under various growth conditions. Biochimica et Biophysica Acta (BBA) - Proteins and Proteomics 1764, 1198–1206. https://doi.org/10.1016/j.bbapap.2006.04.017

Dodd, C.E.R., 2014. PSEUDOMONAS | Introduction, in: Batt, C.A., Tortorello, M.L. (Eds.), Encyclopedia of Food Microbiology (Second Edition). Academic Press, Oxford, pp. 244–247. https://doi.org/10.1016/B978-0-12-384730-0.00282-2

Domínguez-Garay, A., Berná, A., Ortiz-Bernad, I., Esteve-Núñez, A., 2013. Silica Colloid Formation Enhances Performance of Sediment Microbial Fuel Cells in a Low Conductivity Soil. Environ. Sci. Technol. 47, 2117–2122. https://doi.org/10.1021/es303436x

Donovan, C., Dewan, A., Heo, D., Beyenal, H., 2008. Batteryless, Wireless Sensor Powered by a Sediment Microbial Fuel Cell. Environ. Sci. Technol. 42, 8591–8596. https://doi.org/10.1021/es801763g

Donovan, C., Dewan, A., Peng, H., Heo, D., Beyenal, H., 2011a. Power management system for a 2.5W remote sensor powered by a sediment microbial fuel cell. Journal of Power Sources 196, 1171–1177. https://doi.org/10.1016/j.jpowsour.2010.08.099

Donovan, C., Dewan, A., Peng, H., Heo, D., Beyenal, H., 2011b. Power management system for a 2.5W remote sensor powered by a sediment microbial fuel cell. Journal of Power Sources 196, 1171–1177. https://doi.org/10.1016/j.jpowsour.2010.08.099

Dopson, M., Ni, G., Sleutels, T.H., 2016. Possibilities for extremophilic microorganisms in microbial electrochemical systems. FEMS Microbiology Reviews 40, 164–181. https://doi.org/10.1093/femsre/fuv044

Du, Y., Feng, Y., Qu, Y., Liu, J., Ren, N., Liu, H., 2014. Electricity Generation and Pollutant Degradation Using a Novel Biocathode Coupled Photoelectrochemical Cell. Environ. Sci. Technol. 48, 7634–7641. https://doi.org/10.1021/es5011994

Dutta, A., Barbora, L., Stom, D., Goswami, P., 2025. Improving power performance of sediment microbial fuel cell through Water lettuce (Pistia stratiotes) assisted boosting of cathodic activity. Renewable and Sustainable Energy Reviews 215, 115565. https://doi.org/10.1016/j.rser.2025.115565

Dutta, A., Jacob, C.A., Das, P., Corton, E., Stom, D., Barbora, L., Goswami, P., 2022a. A review on power management systems: An electronic tool to enable microbial fuel cells for powering range of electronic appliances. Journal of Power Sources 517, 230688. https://doi.org/10.1016/j.jpowsour.2021.230688

Dutta, A., Jacob, C.A., Das, P., Corton, E., Stom, D., Barbora, L., Goswami, P., 2022b. A review on power management systems: An electronic tool to enable microbial fuel cells for powering range of electronic appliances. Journal of Power Sources 517, 230688. https://doi.org/10.1016/j.jpowsour.2021.230688

Elmaadawy, K., Liu, B., Hassan, G., Wang, X., Wang, Q., Hu, J., Hou, H., Yang, J., Wu, X., 2022. Microalgae-assisted fixed-film activated sludge MFC for landfill leachate treatment and energy recovery. Process Safety and Environmental Protection 160, 221–231. https://doi.org/10.1016/j.psep.2022.02.021

Erable, B., Vandecandelaere, I., Faimali, M., Delia, M.-L., Etcheverry, L., Vandamme, P., Bergel, A., 2010. Marine aerobic biofilm as biocathode catalyst. Bioelectrochemistry, From fundamentals to microbial power plants: Electrochemically Active Biofilms 78, 51–56. https://doi.org/10.1016/j.bioelechem.2009.06.006

Erbay, C., Carreon-Bautista, S., Sanchez-Sinencio, E., Han, A., 2014. High Performance Monolithic Power Management System with Dynamic Maximum Power Point

Tracking for Microbial Fuel Cells. Environ. Sci. Technol. 48, 13992–13999. https://doi.org/10.1021/es501426j

Ewing, T., Ha, P.T., Babauta, J.T., Tang, N.T., Heo, D., Beyenal, H., 2014. Scale-up of sediment microbial fuel cells. Journal of Power Sources 272, 311–319. https://doi.org/10.1016/j.jpowsour.2014.08.070

Ewing, T., Ha, P.T., Beyenal, H., 2017. Evaluation of long-term performance of sediment microbial fuel cells and the role of natural resources. Applied Energy 192, 490–497. https://doi.org/10.1016/j.apenergy.2016.08.177

Faimali, M., Chelossi, E., Garaventa, F., Corrà, C., Greco, G., Mollica, A., 2008. Evolution of oxygen reduction current and biofilm on stainless steels cathodically polarised in natural aerated seawater. Electrochimica Acta, Special Issue BIOCORROSION OF MATERIALS Selection of papers from the International Conference (BIOCORYS 2007) 14-17 June 2007, Paris, France 54, 148–153. https://doi.org/10.1016/j.electacta.2008.02.115

Fan, Y., Sun, S., He, S., 2023. Iron plaque formation and its effect on key elements cycling in constructed wetlands: Functions and outlooks. Water Research 235, 119837. https://doi.org/10.1016/j.watres.2023.119837

Fapyane, D., Ferapontova, E.E., 2016. Enhanced electron transfer between gold nanoparticles and horseradish peroxidase reconstituted onto alkanethiol-modified hemin. Electrochemistry Communications 70, 39–42. https://doi.org/10.1016/j.elecom.2016.06.016

Feregrino-Rivas, M., Ramirez-Pereda, B., Estrada-Godoy, F., Cuesta-Zedeño, L.F., Rochín-Medina, J.J., Bustos-Terrones, Y.A., Gonzalez-Huitron, V.A., 2023. Performance of a sediment microbial fuel cell for bioenergy production: Comparison of fluvial and marine sediments|. Biomass and Bioenergy 168, 106657. https://doi.org/10.1016/j.biombioe.2022.106657

Foster, J.W., 2004. Escherichia coli acid resistance: tales of an amateur acidophile. Nat Rev Microbiol 2, 898–907. https://doi.org/10.1038/nrmicro1021

Freguia, S., Rabaey, K., Yuan, Z., Keller, J., 2007a. Non-catalyzed cathodic oxygen reduction at graphite granules in microbial fuel cells. Electrochimica Acta 53, 598–603. https://doi.org/10.1016/j.electacta.2007.07.037

Freguia, S., Rabaey, K., Yuan, Z., Keller, J., 2007b. Non-catalyzed cathodic oxygen reduction at graphite granules in microbial fuel cells. Electrochimica Acta, Selection of papers from the 5th International Conference (ECS'06) 10-14 September 2006, Kotor, Montenegro 53, 598–603. https://doi.org/10.1016/j.electacta.2007.07.037

Gadkari, S., Fontmorin, J.-M., Yu, E., Sadhukhan, J., 2020. Influence of temperature and other system parameters on microbial fuel cell performance: Numerical and experimental investigation. Chemical Engineering Journal 388, 124176. https://doi.org/10.1016/j.cej.2020.124176

Gao, H., Chen, Q., Yang, Q., 2015. Power management system for microbial fuel cell powered water quality monitoring system, in: 2015 IEEE 16th Workshop on Control and Modeling for Power Electronics (COMPEL). Presented at the 2015 IEEE 16th Workshop on Control and Modeling for Power Electronics (COMPEL), pp. 1–6. https://doi.org/10.1109/COMPEL.2015.7236522

Gao, H., Meehan, A., Lewandowski, Z., 2011. New microbial fuel cell power system for efficiency improvement, in: 2011 International Conference on Electrical Machines and Systems. Presented at the 2011 International Conference on Electrical Machines and Systems (ICEMS), IEEE, Beijing, China, pp. 1–5. https://doi.org/10.1109/ICEMS.2011.6073381

George, P., 1948. A comparison of the decomposition of hydrogen peroxide by catalase, ferrous and ferric ions, haemin and ferrous phthalocyanine. Biochemical Journal 43, 287–295. https://doi.org/10.1042/bj0430287

Grattieri, M., Minteer, S.D., 2018. Microbial fuel cells in saline and hypersaline environments: Advancements, challenges and future perspectives. Bioelectrochemistry 120, 127–137. https://doi.org/10.1016/j.bioelechem.2017.12.004

Guo, F., Luo, H., Shi, Z., Wu, Y., Liu, H., 2021. Substrate salinity: A critical factor regulating the performance of microbial fuel cells, a review. Science of The Total Environment 763, 143021. https://doi.org/10.1016/j.scitotenv.2020.143021

Gupta, S., Patro, A., Mittal, Y., Dwivedi, S., Saket, P., Panja, R., Saeed, T., Martínez, F., Yadav, A.K., 2023. The race between classical microbial fuel cells, sediment-microbial fuel cells, plant-microbial fuel cells, and constructed wetlands-microbial fuel cells: Applications and technology readiness level. Science of The Total Environment 879, 162757. https://doi.org/10.1016/j.scitotenv.2023.162757

Gurung, A., Oh, S.-E., 2012. The Performance of Serially and Parallelly Connected Microbial Fuel Cells. Energy Sources, Part A: Recovery, Utilization, and Environmental Effects 34, 1591–1598. https://doi.org/10.1080/15567036.2011.629277

Häggström, F., Delsing, J., 2018. IoT Energy Storage - A Forecast. Energy Harvesting and Systems 5, 43–51. https://doi.org/10.1515/ehs-2018-0010

Harrington, T.D., Babauta, J.T., Davenport, E.K., Renslow, R.S., Beyenal, H., 2015. Excess surface area in bioelectrochemical systems causes ion transport limitations. Biotech & Bioengineering 112, 858–866. https://doi.org/10.1002/bit.25500

Hatzell, M.C., Kim, Y., Logan, B.E., 2013. Powering microbial electrolysis cells by capacitor circuits charged using microbial fuel cell. Journal of Power Sources 229, 198–202. https://doi.org/10.1016/j.jpowsour.2012.12.006

He, Z., Shao, H., Angenent, L.T., 2007. Increased power production from a sediment microbial fuel cell with a rotating cathode. Biosensors and Bioelectronics, Chem and Biosensing Transistors: from materials to systems 22, 3252–3255. https://doi.org/10.1016/j.bios.2007.01.010

Heck, D.E., Shakarjian, M., Kim, H.D., Laskin, J.D., Vetrano, A.M., 2010. Mechanisms of oxidant generation by catalase. Annals of the New York Academy of Sciences 1203, 120–125. https://doi.org/10.1111/j.1749-6632.2010.05603.x

Hemdan, B.A., Jadhav, D.A., Dutta, A., Goswami, P., 2023. Facilitating the electrochemical characterization and biofilm enrichment through anode modification in microbial fuel

cells. Journal of Water Process Engineering 54, 104065. https://doi.org/10.1016/j.jwpe.2023.104065

Hoagland, D.R. (Dennis R., Arnon, D.I. (Daniel I., 1950. The water-culture method for growing plants without soil. Berkeley, Calif. : College of Agriculture, University of California.

Houghton, J., Santoro, C., Soavi, F., Serov, A., Ieropoulos, I., Arbizzani, C., Atanassov, P., 2016. Supercapacitive microbial fuel cell: Characterization and analysis for improved charge storage/delivery performance. Bioresource Technology 218, 552–560. https://doi.org/10.1016/j.biortech.2016.06.105

Hsu, L., Chadwick, B., Kagan, J., Thacher, R., Wotawa-Bergen, A., Richter, K., 2013. Scale up considerations for sediment microbial fuel cells. RSC Adv. 3, 15947. https://doi.org/10.1039/c3ra43180k

Huang, G., Umaz, R., Karra, U., Li, B., Wang, L., 2013. A biomass-based marine sediment energy harvesting system, in: International Symposium on Low Power Electronics and Design (ISLPED). Presented at the 2013 IEEE International Symposium on Low Power Electronics and Design (ISLPED), IEEE, Beijing, China, pp. 359–364. https://doi.org/10.1109/ISLPED.2013.6629323

Hubenova, Y., Mitov, M., 2012. Conversion of solar energy into electricity by using duckweed in Direct Photosynthetic Plant Fuel Cell. Bioelectrochemistry, International Symposium on Bioelectrochemistry and Bioenergetics, 21st BES 2011 87, 185–191. https://doi.org/10.1016/j.bioelechem.2012.02.008

Jones, P., Dunford, H.B., 1977. On the mechanism of compound I formation from peroxidases and catalases. Journal of Theoretical Biology 69, 457–470. https://doi.org/10.1016/0022-5193(77)90152-7

Kabutey, F.T., Antwi, P., Ding, J., Zhao, Q., Quashie, F.K., 2019a. Enhanced bioremediation of heavy metals and bioelectricity generation in a macrophyte-integrated cathode sediment microbial fuel cell (mSMFC). Environ Sci Pollut Res 26, 26829–26843. https://doi.org/10.1007/s11356-019-05874-9

Kabutey, F.T., Ding, J., Zhao, Q., Antwi, P., Quashie, F.K., 2020. Electrical current generation from a continuous flow macrophyte biocathode sediment microbial fuel cell (mSMFC) during the degradation of pollutants in urban river sediment. Environ Sci Pollut Res 27, 35364–35380. https://doi.org/10.1007/s11356-020-09812-y

Kabutey, F.T., Zhao, Q., Wei, L., Ding, J., Antwi, P., Quashie, F.K., Wang, W., 2019b. An overview of plant microbial fuel cells (PMFCs): Configurations and applications. Renewable and Sustainable Energy Reviews 110, 402–414. https://doi.org/10.1016/j.rser.2019.05.016

Kanakasabapathy, P., Pillai, 2014. Power processor for microbial fuel cells, in: 2014 Power and Energy Systems Conference: Towards Sustainable Energy (PESTSE). IEEE, Bangalore, India, pp. 1–6. https://doi.org/10.1109/PESTSE.2014.6805327

Karra, U., Muto, E., Umaz, R., Kölln, M., Santoro, C., Wang, L., Li, B., 2014. Performance evaluation of activated carbon-based electrodes with novel power management system for long-term benthic microbial fuel cells. International Journal of Hydrogen Energy 39, 21847–21856. https://doi.org/10.1016/j.ijhydene.2014.06.095

Kataki, S., Chatterjee, S., Vairale, M.G., Sharma, S., Dwivedi, S.K., Gupta, D.K., 2021. Constructed wetland, an eco-technology for wastewater treatment: A review on various aspects of microbial fuel cell integration, low temperature strategies and life cycle impact of the technology. Renewable and Sustainable Energy Reviews 148, 111261. https://doi.org/10.1016/j.rser.2021.111261

Kaushik, S., Goswami, P., 2018. Bacterial Membrane Depolarization-Linked Fuel Cell Potential Burst as Signal for Selective Detection of Alcohol. ACS Appl. Mater. Interfaces 10, 18630–18640. https://doi.org/10.1021/acsami.8b01838

Keilin, D., Hartree, E.F., 1955. Catalase, peroxidase and metmyoglobin as catalysts of coupled peroxidatic reactions. Biochemical Journal 60, 310–325. https://doi.org/10.1042/bj0600310

Khaled, F., Ondel, O., Allard, B., 2014. Optimal Energy Harvesting from Serially-Connected Microbial Fuel Cells. IEEE Trans. Ind. Electron. 1–1. https://doi.org/10.1109/TIE.2014.2371437

Kim, B., An, J., Fapyane, D., Chang, I.S., 2015a. Bioelectronic platforms for optimal bio-anode of bio-electrochemical systems: From nano- to macro scopes. Bioresource Technology 195, 2–13. https://doi.org/10.1016/j.biortech.2015.06.061

Kim, B., Chang, I.S., 2018. Elimination of voltage reversal in multiple membrane electrode assembly installed microbial fuel cells (mMEA-MFCs) stacking system by resistor control. Bioresource Technology 262, 338–341. https://doi.org/10.1016/j.biortech.2018.04.112

Kim, B., Lee, B.-G., Kim, B.H., Chang, I.S., 2015b. Assistance Current Effect for Prevention of Voltage Reversal in Stacked Microbial Fuel Cell Systems. ChemElectroChem 2, 755–760. https://doi.org/10.1002/celc.201402388

Kim, B., Mohan, S.V., Fapyane, D., Chang, I.S., 2020. Controlling Voltage Reversal in Microbial Fuel Cells. Trends in Biotechnology 38, 667–678. https://doi.org/10.1016/j.tibtech.2019.12.007

Kim, B.H., Chang, I.S., Gadd, G.M., 2007. Challenges in microbial fuel cell development and operation. Appl Microbiol Biotechnol 76, 485–494. https://doi.org/10.1007/s00253-007-1027-4

Kim, G., Wolfe, A., Bell, R., Bang, S., Lee, Y., Lee, I., Kim, Y., Hsu, L., Kagan, J., Arias-Thode, M., Chadwick, B., Sylvester, D., Blaauw, D., 2014. Chip-on-mud: Ultra-low power ARM-based oceanic sensing system powered by small-scale benthic microbial fuel cells, in: 2014 IEEE International Symposium on Circuits and Systems (ISCAS). Presented at the 2014 IEEE International Symposium on Circuits and Systems (ISCAS), IEEE, Melbourne VIC, Australia, pp. 1985–1988. https://doi.org/10.1109/ISCAS.2014.6865552

Kim, T., Yeo, J., Yang, Y., Kang, S., Paek, Y., Kwon, J.K., Jang, J.K., 2019. Boosting voltage without electrochemical degradation using energy-harvesting circuits and power management system-coupled multiple microbial fuel cells. Journal of Power Sources 410–411, 171–178. https://doi.org/10.1016/j.jpowsour.2018.11.010

Kim, Y., Hatzell, M.C., Hutchinson, A.J., Logan, B.E., 2011. Capturing power at higher voltages from arrays of microbial fuel cells without voltage reversal. Energy Environ. Sci. 4, 4662. https://doi.org/10.1039/c1ee02451e

Kirkman, H.N., Gaetani, G.F., 2007. Mammalian catalase: a venerable enzyme with new mysteries. Trends in Biochemical Sciences 32, 44–50. https://doi.org/10.1016/j.tibs.2006.11.003

Koffi, N.J., Okabe, S., 2020. High voltage generation from wastewater by microbial fuel cells equipped with a newly designed low voltage booster multiplier (LVBM). Sci Rep 10, 18985. https://doi.org/10.1038/s41598-020-75916-7

Koralay, N., Kara, O., Kezik, U., 2018. Effects of run-of-the-river hydropower plants on the surface water quality in the Solakli stream watershed, Northeastern Turkey. Water and Environment Journal 32, 412–421. https://doi.org/10.1111/wej.12338

Kornyshev, A.A., Kuznetsov, A.M., Spohr, E., Ulstrup, J., 2003. Kinetics of Proton Transport in Water. J. Phys. Chem. B 107, 3351–3366. https://doi.org/10.1021/jp020857d

Kouzuma, A., Kaku, N., Watanabe, K., 2014. Microbial electricity generation in rice paddy fields: recent advances and perspectives in rhizosphere microbial fuel cells. Appl Microbiol Biotechnol 98, 9521–9526. https://doi.org/10.1007/s00253-014-6138-0

Kremer, M.L., 1970. Peroxidatic activity of catalase. Biochimica et Biophysica Acta (BBA) - Enzymology 198, 199–209. https://doi.org/10.1016/0005-2744(70)90052-5

Krulwich, T.A., Sachs, G., Padan, E., 2011. Molecular aspects of bacterial pH sensing and homeostasis. Nat Rev Microbiol 9, 330–343. https://doi.org/10.1038/nrmicro2549

Kumar, R., Singh, L., Zularisam, A.W., Hai, F.I., 2018. Microbial fuel cell is emerging as a versatile technology: a review on its possible applications, challenges and strategies to improve the performances: Microbial fuel cell is emerging as a versatile technology. Int J Energy Res 42, 369–394. https://doi.org/10.1002/er.3780

Laanbroek, H.J., 2010. Methane emission from natural wetlands: interplay between emergent macrophytes and soil microbial processes. A mini-review. Annals of Botany 105, 141–153. https://doi.org/10.1093/aob/mcp201

Ladkau, N., Schmid, A., Bühler, B., 2014. The microbial cell — functional unit for energy dependent multistep biocatalysis. Current Opinion in Biotechnology 30, 178–189. https://doi.org/10.1016/j.copbio.2014.06.003

Lee, Y., Bang, S., Lee, I., Kim, Y., Kim, G., Ghaed, M.H., Pannuto, P., Dutta, P., Sylvester, D., Blaauw, D., 2013. A Modular 1 mm^{3} Die-Stacked Sensing Platform With Low Power I^{2}C Inter-Die Communication and Multi-Modal Energy Harvesting. IEEE J. Solid-State Circuits 48, 229–243. https://doi.org/10.1109/JSSC.2012.2221233

Li, R., Wang, J., Li, T., Zhou, Q., 2023. Recent advances in improving the remediation performance of microbial electrochemical systems for contaminated soil and sediments. Critical Reviews in Environmental Science and Technology 53, 137–160. https://doi.org/10.1080/10643389.2022.2040327

Li, S., Zhao, Z., Li, B., Wei, T., Jiang, H., Yan, Z., 2022. Supercapacitors accumulating energy harvesting from stacked sediment microbial fuel cells and boosting input power for power management systems. International Journal of Hydrogen Energy 47, 10689–10700. https://doi.org/10.1016/j.ijhydene.2021.11.081

Li, Xiaomin, Ding, L., Yuan, H., Li, Xiaoming, Zhu, Y., 2020. Identification of potential electrotrophic microbial community in paddy soils by enrichment of microbial electrolysis cell biocathodes. Journal of Environmental Sciences 87, 411–420. https://doi.org/10.1016/j.jes.2019.07.016

Liu, L., Yu, Y., Yan, C., Li, K., Zheng, Z., 2015. Wearable energy-dense and power-dense supercapacitor yarns enabled by scalable graphene–metallic textile composite electrodes. Nat Commun 6, 7260. https://doi.org/10.1038/ncomms8260

Logan, B.E., Hamelers, B., Rozendal, R., Schröder, U., Keller, J., Freguia, S., Aelterman, P., Verstraete, W., Rabaey, K., 2006a. Microbial Fuel Cells: Methodology and Technology. Environ. Sci. Technol. 40, 5181–5192. https://doi.org/10.1021/es0605016

Logan, B.E., Hamelers, B., Rozendal, R., Schröder, U., Keller, J., Freguia, S., Aelterman, P., Verstraete, W., Rabaey, K., 2006b. Microbial Fuel Cells: Methodology and Technology. Environ. Sci. Technol. 40, 5181–5192. https://doi.org/10.1021/es0605016

Logan, B.E., Rabaey, K., 2012. Conversion of Wastes into Bioelectricity and Chemicals by Using Microbial Electrochemical Technologies. Science 337, 686–690. https://doi.org/10.1126/science.1217412

Lund, P., Tramonti, A., De Biase, D., 2014. Coping with low pH: molecular strategies in neutralophilic bacteria. FEMS Microbiology Reviews 38, 1091–1125. https://doi.org/10.1111/1574-6976.12076

Lund, P.A., De Biase, D., Liran, O., Scheler, O., Mira, N.P., Cetecioglu, Z., Fernández, E.N., Bover-Cid, S., Hall, R., Sauer, M., O'Byrne, C., 2020. Understanding How Microorganisms Respond to Acid pH Is Central to Their Control and Successful Exploitation. Frontiers in Microbiology 11.

Ma, X., Huang, S., Jin, Y., Liao, H., Chen, S., Wang, H., Zhang, W., Wu, Y., Bi, W., Li, X., Dietrich, A.M., 2023. Domesticating aquatic plants in hydroponic systems to demonstrate and advance phytoremediation of the artificial sweetener acesulfame. Science of The Total Environment 892, 164806. https://doi.org/10.1016/j.scitotenv.2023.164806

Mamun, M.R., Keya, A.C., Alim, Mst.S., Hossen, Md.A., Mondal, Md.F., Soeb, Md.J.A., 2023. Potentiality assessment of solar based LED light trap as pest management tool in tea (Camellia sinensis L.). Smart Agricultural Technology 5, 100304. https://doi.org/10.1016/j.atech.2023.100304

Matsumoto, A., Nagoya, M., Tsuchiya, M., Suga, K., Inohana, Y., Hirose, A., Yamada, S., Hirano, S., Ito, Y., Tanaka, S., Kouzuma, A., Watanabe, K., 2020. Enhanced electricity generation in rice paddy-field microbial fuel cells supplemented with iron powders. Bioelectrochemistry 136, 107625. https://doi.org/10.1016/j.bioelechem.2020.107625

Meehan, A., Gao, H., Lewandowski, Z., 2011. Energy Harvesting With Microbial Fuel Cell and Power Management System. IEEE Trans. Power Electron. 26, 176–181. https://doi.org/10.1109/TPEL.2010.2054114

Meehan, A., Hongwei Gao, Lewandowski, Z., 2009. Energy harvest with microbial fuel cell and power management system, in: 2009 IEEE Energy Conversion Congress and Exposition. Presented at the 2009 IEEE Energy Conversion Congress and Exposition. ECCE 2009, IEEE, San Jose, CA, pp. 3558–3563. https://doi.org/10.1109/ECCE.2009.5316034

Menzel, P., Ng, K.L., Krogh, A., 2016. Fast and sensitive taxonomic classification for metagenomics with Kaiju. Nat Commun 7. https://doi.org/10.1038/ncomms11257

Milner, E.M., Popescu, D., Curtis, T., Head, I.M., Scott, K., Yu, E.H., 2016. Microbial fuel cells with highly active aerobic biocathodes. Journal of Power Sources 324, 8–16. https://doi.org/10.1016/j.jpowsour.2016.05.055

Mira, P., Yeh, P., Hall, B.G., 2022. Estimating microbial population data from optical density. PLoS ONE 17, e0276040. https://doi.org/10.1371/journal.pone.0276040

Morris, J.M., Jin, S., 2012. Enhanced biodegradation of hydrocarbon-contaminated sediments using microbial fuel cells. Journal of Hazardous Materials 213–214, 474–477. https://doi.org/10.1016/j.jhazmat.2012.02.029

Najafgholi, Z., Rahimnejad, M., 2016. Improvement of sediment microbial fuel cell performance by application of sun light and biocathode. Korean J. Chem. Eng. 33, 154–158. https://doi.org/10.1007/s11814-015-0123-x

Najafgholi, Z., Rahimnejad, M., Najafpour, G., 2015. Effect of Electrolyte Conductivity and Aeration on Performance of Sediment Microbial Fuel Cell. Journal of Renewable Energy and Environment 2, 43–48. https://doi.org/10.30501/jree.2015.70064

Nam, T., Kang, H., Pandit, S., Kim, S.-H., Yoon, S., Bae, S., Jung, S.P., 2020. Effects of vertical and horizontal configurations of different numbers of brush anodes on performance and electrochemistry of microbial fuel cells. Journal of Cleaner Production 277, 124125. https://doi.org/10.1016/j.jclepro.2020.124125

National Center for Biotechnology Information [WWW Document], n.d. URL https://www.ncbi.nlm.nih.gov/ (accessed 2.19.25).

Nguyen, C.-L., Tartakovsky, B., Woodward, L., 2019. Harvesting Energy from Multiple Microbial Fuel Cells with a High-Conversion Efficiency Power Management System. ACS Omega 4, 18978–18986. https://doi.org/10.1021/acsomega.9b01854

Nitisoravut, R., Regmi, R., 2017. Plant microbial fuel cells: A promising biosystems engineering. Renewable and Sustainable Energy Reviews 76, 81–89. https://doi.org/10.1016/j.rser.2017.03.064

Oh, S.E., Kim, J.R., Joo, J.-H., Logan, B.E., 2009. Effects of applied voltages and dissolved oxygen on sustained power generation by microbial fuel cells. Water Science and Technology 60, 1311–1317. https://doi.org/10.2166/wst.2009.444

Oh, S.-E., Logan, B.E., 2007. Voltage reversal during microbial fuel cell stack operation. Journal of Power Sources 167, 11–17. https://doi.org/10.1016/j.jpowsour.2007.02.016

Pallasser, R., Minasny, B., McBratney, A.B., 2013. Soil carbon determination by thermogravimetrics. PeerJ 1, e6. https://doi.org/10.7717/peerj.6

Papaharalabos, G., Stinchcombe, A., Horsfield, I., Melhuish, C., Greenman, J., Ieropoulos, I., 2017. Autonomous Energy Harvesting and Prevention of Cell Reversal in MFC Stacks. J. Electrochem. Soc. 164, H3047–H3051. https://doi.org/10.1149/2.0081703jes

Park, J.-D., Ren, Z., 2012. Hysteresis controller based maximum power point tracking energy harvesting system for microbial fuel cells. Journal of Power Sources 205, 151–156. https://doi.org/10.1016/j.jpowsour.2012.01.053

Park, J.-D., Ullah, M.H., Roane, T.M., Alaraj, M., Shuo, F., 2018. Optimal operating point for energy harvesting from microbial fuel cell with finite initial energy. Journal of Power Sources 400, 183–189. https://doi.org/10.1016/j.jpowsour.2018.08.011

Parot, S., Vandecandelaere, I., Cournet, A., Délia, M.-L., Vandamme, P., Bergé, M., Roques, C., Bergel, A., 2011. Catalysis of the electrochemical reduction of oxygen by bacteria

isolated from electro-active biofilms formed in seawater. Bioresource Technology, Special Issue: Biofuels - II: Algal Biofuels and Microbial Fuel Cells 102, 304–311. https://doi.org/10.1016/j.biortech.2010.06.157

Pennacchietti, E., D'Alonzo, C., Freddi, L., Occhialini, A., De Biase, D., 2018. The Glutaminase-Dependent Acid Resistance System: Qualitative and Quantitative Assays and Analysis of Its Distribution in Enteric Bacteria. Frontiers in Microbiology 9.

Phale, P.S., Sharma, A., Gautam, K., 2019. 11 - Microbial degradation of xenobiotics like aromatic pollutants from the terrestrial environments, in: Prasad, M.N.V., Vithanage, M., Kapley, A. (Eds.), Pharmaceuticals and Personal Care Products: Waste Management and Treatment Technology. Butterworth-Heinemann, pp. 259–278. https://doi.org/10.1016/B978-0-12-816189-0.00011-1

Plumeré, N., Henig, J., Campbell, W.H., 2012. Enzyme-Catalyzed O2 Removal System for Electrochemical Analysis under Ambient Air: Application in an Amperometric Nitrate Biosensor. Anal. Chem. 84, 2141–2146. https://doi.org/10.1021/ac2020883

Poli, F., Seri, J., Santoro, C., Soavi, F., 2020. Boosting Microbial Fuel Cell Performance by Combining with an External Supercapacitor: An Electrochemical Study. ChemElectroChem 7, 893–903. https://doi.org/10.1002/celc.201901876

Potter, P., MC, 1911. Electrical effects accompanying the decomposition of organic compounds. Proc. R. Soc. Lond. B. 84, 260–276. https://doi.org/10.1098/rspb.1911.0073

Prasad, J., Tripathi, R.K., 2022. Review on improving microbial fuel cell power management systems for consumer applications. Energy Reports 8, 10418–10433. https://doi.org/10.1016/j.egyr.2022.08.192

Prasad, J., Tripathi, R.K., 2021a. Effect of sediment microbial fuel cell stacks on 9 V/12 V DC power supply. International Journal of Hydrogen Energy 46, 14628–14638. https://doi.org/10.1016/j.ijhydene.2020.07.187

Prasad, J., Tripathi, R.K., 2021b. Scale-up and control the voltage of sediment microbial fuel cell for charging a cell phone. Biosensors and Bioelectronics 172, 112767. https://doi.org/10.1016/j.bios.2020.112767

Principle and Workflow of Illumina Next-generation Sequencing | CD Genomics Blog, 2018. URL https://www.cd-genomics.com/blog/principle-and-workflow-of-illumina-next-generation-sequencing/ (accessed 1.14.25).

Qiu, S., Guo, Z., Naz, F., Yang, Z., Yu, C., 2021. An overview in the development of cathode materials for the improvement in power generation of microbial fuel cells. Bioelectrochemistry 141, 107834. https://doi.org/10.1016/j.bioelechem.2021.107834

Regmi, R., Nitisoravut, R., Ketchaimongkol, J., 2018. A decade of plant-assisted microbial fuel cells: looking back and moving forward. Biofuels 9, 605–612. https://doi.org/10.1080/17597269.2018.1432272

Reimers, C.E., Tender, L.M., Fertig, S., Wang, W., 2001. Harvesting Energy from the Marine Sediment−Water Interface. Environ. Sci. Technol. 35, 192–195. https://doi.org/10.1021/es001223s

Reiner, K., 2010. Catalase Test [WWW Document]. ASM.org. URL https://asm.org:443/Protocols/Catalase-Test-Protocol (accessed 9.25.23).

Renslow, R., Donovan, C., Shim, M., Babauta, J., Nannapaneni, S., Schenk, J., Beyenal, H., 2011. Oxygen reduction kinetics on graphite cathodes in sediment microbial fuel cells. Phys. Chem. Chem. Phys. 13, 21573–21584. https://doi.org/10.1039/C1CP23200B

Reyes, A., Erbay, C., Carreon-Bautista, S., Han, A., Sánchez-Sinencio, E., 2018. A Time-Interleave-Based Power Management System with Maximum Power Extraction and Health Protection Algorithm for Multiple Microbial Fuel Cells for Internet of Things Smart Nodes. Applied Sciences 8, 2404. https://doi.org/10.3390/app8122404

Rismani-Yazdi, H., Carver, S.M., Christy, A.D., Tuovinen, O.H., 2008a. Cathodic limitations in microbial fuel cells: An overview. Journal of Power Sources 180, 683–694. https://doi.org/10.1016/j.jpowsour.2008.02.074

Rismani-Yazdi, H., Carver, S.M., Christy, A.D., Tuovinen, O.H., 2008b. Cathodic limitations in microbial fuel cells: An overview. Journal of Power Sources 180, 683–694. https://doi.org/10.1016/j.jpowsour.2008.02.074

Rossi, R., Logan, B.E., 2020. Unraveling the contributions of internal resistance components in two-chamber microbial fuel cells using the electrode potential slope analysis. Electrochimica Acta 348, 136291. https://doi.org/10.1016/j.electacta.2020.136291

Rusli, S.F.N., Abu Bakar, M.H., Loh, K.S., Mastar, M.S., 2019. Review of high-performance biocathode using stainless steel and carbon-based materials in Microbial Fuel Cell for electricity and water treatment. International Journal of Hydrogen Energy 44, 30772–30787. https://doi.org/10.1016/j.ijhydene.2018.11.145

Russell, J.B., 2007. The Energy Spilling Reactions of Bacteria and Other Organisms. Journal of Molecular Microbiology and Biotechnology 13, 1–11. https://doi.org/10.1159/000103591

Sable, S.V., Kawade, S., Ranade, S., Joshi, S., 2020. Bioreduction mechanism of silver nanoparticles. Materials Science and Engineering: C 107, 110299. https://doi.org/10.1016/j.msec.2019.110299

Santoro, C., Flores-Cadengo, C., Soavi, F., Kodali, M., Merino-Jimenez, I., Gajda, I., Greenman, J., Ieropoulos, I., Atanassov, P., 2018. Ceramic Microbial Fuel Cells Stack: power generation in standard and supercapacitive mode. Sci Rep 8, 3281. https://doi.org/10.1038/s41598-018-21404-y

Sardans, J., Lambers, H., Preece, C., Alrefaei, A.F., Penuelas, J., 2023. Role of mycorrhizas and root exudates in plant uptake of soil nutrients (calcium, iron, magnesium, and potassium): has the puzzle been completely solved? The Plant Journal 114, 1227–1242. https://doi.org/10.1111/tpj.16184

Sarma, M.K., Kaushik, S., Goswami, P., 2016. Cyanobacteria: A metabolic power house for harvesting solar energy to produce bio-electricity and biofuels. Biomass and Bioenergy 90, 187–201. https://doi.org/10.1016/j.biombioe.2016.03.043

Schievano, A., Colombo, A., Grattieri, M., Trasatti, S.P., Liberale, A., Tremolada, P., Pino, C., Cristiani, P., 2017. Floating microbial fuel cells as energy harvesters for signal transmission from natural water bodies. Journal of Power Sources 340, 80–88. https://doi.org/10.1016/j.jpowsour.2016.11.037

Schmid, R., 2000. Review of Aroids: Plants of the Arum Family. Taxon 49, 839–840. https://doi.org/10.2307/1223991

Schober, I., Koblitz, J., Sardà Carbasse, J., Ebeling, C., Schmidt, M.L., Podstawka, A., Gupta, R., Ilangovan, V., Chamanara, J., Overmann, J., Reimer, L.C., 2025. Bac *Dive* in 2025: the core database for prokaryotic strain data. Nucleic Acids Research 53, D748–D756. https://doi.org/10.1093/nar/gkae959

Schrader, P.S., Doolan, C., Reimers, C.E., Girguis, P.R., Wolf, M., Green, D., 2013. Sensors and Acoustic Modems Powered by Benthic Microbial Fuel Cells at the MARS Observatory.

Schröder, U., Harnisch, F., Angenent, L.T., 2015. Microbial electrochemistry and technology: terminology and classification. Energy Environ. Sci. 8, 513–519. https://doi.org/10.1039/C4EE03359K

Scotto, V., Cintio, R.D., Marcenaro, G., 1985. The influence of marine aerobic microbial film on stainless steel corrosion behaviour. Corrosion Science 25, 185–194. https://doi.org/10.1016/0010-938X(85)90094-0

Sharma, A., Gajbhiye, S., Chauhan, S., Chhabra, M., 2021. Effect of cathodic culture on wastewater treatment and power generation in a photosynthetic sediment microbial fuel cell (SMFC): Canna indica v/s Chlorella vulgaris. Bioresource Technology 340, 125645. https://doi.org/10.1016/j.biortech.2021.125645

Shi, X., Yang, D., Li, S., Yu, K., Yan, W., Xu, H., 2025. Research progress on coupling and stacking systems to enhance power generation performance of microbial fuel cell. Journal of Environmental Sciences 154, 784–804. https://doi.org/10.1016/j.jes.2024.10.003

Shi, Z., Luo, H., Li, Z., Xiang, Y., Wu, Y., Yang, K., Guo, F., 2021. Small boreholes embedded in the sediment layers make big difference in performance of sediment microbial fuel cells: Bioelectricity generation and microbial community. International Journal of Hydrogen Energy 46, 30124–30134. https://doi.org/10.1016/j.ijhydene.2021.06.155

Song, N., Jiang, H.-L., 2018. Effects of initial sediment properties on start-up times for sediment microbial fuel cells. International Journal of Hydrogen Energy 43, 10082–10093. https://doi.org/10.1016/j.ijhydene.2018.04.082

Song, N., Yan, Z., Xu, H., Yao, Z., Wang, Changhui, Chen, M., Zhao, Z., Peng, Z., Wang, Chunliu, Jiang, H.-L., 2019. Development of a sediment microbial fuel cell-based biosensor for simultaneous online monitoring of dissolved oxygen concentrations along various depths in lake water. Science of The Total Environment 673, 272–280. https://doi.org/10.1016/j.scitotenv.2019.04.032

Srivastava, J.K., Chandra, H., Kalra, S.J.S., Mishra, P., Khan, H., Yadav, P., 2017. Plant–microbe interaction in aquatic system and their role in the management of water quality: a review. Appl Water Sci 7, 1079–1090. https://doi.org/10.1007/s13201-016-0415-2

Stasi, F.D., 2015. Working with Boost Converters. Texas Instruments, Application report SNVA731.

Sugnaux, M., Savy, C., Cachelin, C.P., Hugenin, G., Fischer, F., 2017. Simulation and resolution of voltage reversal in microbial fuel cell stack. Bioresource Technology 238, 519–527. https://doi.org/10.1016/j.biortech.2017.04.072

Sun, F., Chen, J., Tang, M., Yang, Y., 2023. Recent research progress, challenges and future directions of sediment microbial fuel cell: A comprehensive review. International Journal of Hydrogen Energy. https://doi.org/10.1016/j.ijhydene.2023.09.112

Surhone, L.M., Timpledon, M.T., Marseken, S.F., 2010. Nernst Equation. VDM Publishing.

Tamada, K., Itoh, K., Uchida, Y., Higuchi, S., Sasayama, D., Azuma, T., 2015. Relationship between the temperature and the overwintering of water lettuce (Pistia stratiotes) at

Kowataike, a branch of Yodogawa River, Japan. Weed Biology and Management 15, 20–26. https://doi.org/10.1111/wbm.12061

Tang, N., Hong, W., Ewing, T., Beyenal, H., Kim, J.-H., Heo, D., 2015. A Self-Sustainable Power Management System for Reliable Power Scaling Up of Sediment Microbial Fuel Cells. IEEE Trans. Power Electron. 30, 4626–4632. https://doi.org/10.1109/TPEL.2015.2397931

Tavakolian, M., Ghafouri Taleghani, H., Khorshidian, M., 2020. New design of benthic microbial fuel cell for bioelectricity generation: Comparative study. International Journal of Hydrogen Energy 45, 23533–23542. https://doi.org/10.1016/j.ijhydene.2020.06.181

Tehrani, Z., Thomas, D.J., Korochkina, T., Phillips, C.O., Lupo, D., Lehtimäki, S., O'Mahony, J., Gethin, D.T., 2017. Large-area printed supercapacitor technology for low-cost domestic green energy storage. Energy 118, 1313–1321. https://doi.org/10.1016/j.energy.2016.11.019

Thakuria, A., Singh, K.K., Dutta, A., Corton, E., Stom, D., Barbora, L., Goswami, P., 2023. Phytoremediation of toxic chemicals in aquatic environment with special emphasis on duckweed mediated approaches. International Journal of Phytoremediation 25, 1699–1713. https://doi.org/10.1080/15226514.2023.2188423

Thomas, Y.R.J., Picot, M., Carer, A., Berder, O., Sentieys, O., Barrière, F., 2013. A single sediment-microbial fuel cell powering a wireless telecommunication system. Journal of Power Sources 241, 703–708. https://doi.org/10.1016/j.jpowsour.2013.05.016

Tommasi, T., Lombardelli, G., 2017. Energy sustainability of Microbial Fuel Cell (MFC): A case study. Journal of Power Sources 356, 438–447. https://doi.org/10.1016/j.jpowsour.2017.03.122

Türker, O.C., Baran, T., Yakar, A., Türe, C., Saz, Ç., 2020. Novel chitosan based smart cathode electrocatalysts for high power generation in plant based-sediment microbial fuel cells. Carbohydrate Polymers 239, 116235. https://doi.org/10.1016/j.carbpol.2020.116235

Ucar, D., Zhang, Y., Angelidaki, I., 2017. An Overview of Electron Acceptors in Microbial Fuel Cells. Frontiers in Microbiology 8, 643. https://doi.org/doi: 10.3389/fmicb.2017.00643

Umaz, R., 2020. A Power Management System for Microbial Fuel Cells With 53.02% Peak End-to-End Efficiency. IEEE Trans. Circuits Syst. II 67, 2592–2596. https://doi.org/10.1109/TCSII.2019.2951810

Umaz, R., Garrett, C., Qian, F., Li, B., Wang, L., 2017. A Power Management System for Multianode Benthic Microbial Fuel Cells. IEEE Trans. Power Electron. 32, 3562–3570. https://doi.org/10.1109/TPEL.2016.2585020

U.S. Geological Survey, U.S., 2006. Chloroethene in Ground Water, Area 2, Operable Unit 2, Naval Undersea Warfare Center, Division Keyport, WA [WWW Document]. URL https://pubs.usgs.gov/sir/2006/5030/section4.html (accessed 5.3.24).

Vo, A. -T. E., Jedlicka, J.A., 2014. Protocols for metagenomic DNA extraction and Illumina amplicon library preparation for faecal and swab samples. Molecular Ecology Resources 14, 1183–1197. https://doi.org/10.1111/1755-0998.12269

Walter, X.A., Santoro, C., Greenman, J., Ieropoulos, I., 2020. Scaling up self-stratifying supercapacitive microbial fuel cell. International Journal of Hydrogen Energy 45, 25240–25248. https://doi.org/10.1016/j.ijhydene.2020.06.070

Walter, X.A., Stinchcombe, A., Greenman, J., Ieropoulos, I., 2017. Urine transduction to usable energy: A modular MFC approach for smartphone and remote system charging. Applied Energy 192, 575–581. https://doi.org/10.1016/j.apenergy.2016.06.006

Wang, A., Cheng, H., Ren, N., Cui, D., Lin, N., Wu, W., 2012. Sediment microbial fuel cell with floating biocathode for organic removal and energy recovery. Front. Environ. Sci. Eng. 6, 569–574. https://doi.org/10.1007/s11783-011-0335-1

Wang, C.-T., Lee, Y.-C., Ou, Y.-T., Yang, Y.-C., Chong, W.-T., Sangeetha, T., Yan, W.-M., 2017. Exposing effect of comb-type cathode electrode on the performance of

sediment microbial fuel cells. Applied Energy 204, 620–625. https://doi.org/10.1016/j.apenergy.2017.07.079

Wang, G., Yu, M., Xie, K., Zhao, R., Fu, Y., Chen, T., 2019. Graphene modified polyacrylonitrile fiber as high-performance cathode for marine sediment microbial fuel cells. Journal of Power Sources 438, 227002. https://doi.org/10.1016/j.jpowsour.2019.227002

Wang, H., Park, J.-D., Ren, Z.J., 2015. Practical Energy Harvesting for Microbial Fuel Cells: A Review. Environ. Sci. Technol. 49, 3267–3277. https://doi.org/10.1021/es5047765

Wang, H., Ye, Y., Zhang, J., Ning, H., Xiang, Y., Song, X., Zhao, W., Guo, F., 2023. Power performance improvement in sediment microbial fuel cells: Recent advances and future challenges. International Journal of Hydrogen Energy 48, 24426–24446. https://doi.org/10.1016/j.ijhydene.2023.03.291

Winfield, J., Chambers, L.D., Stinchcombe, A., Rossiter, J., Ieropoulos, I., 2014. The power of glove: Soft microbial fuel cell for low-power electronics. Journal of Power Sources 249, 327–332. https://doi.org/10.1016/j.jpowsour.2013.10.096

Wohlgemuth, R., 2010. Asymmetric biocatalysis with microbial enzymes and cells. Current Opinion in Microbiology 13, 283–292. https://doi.org/10.1016/j.mib.2010.04.001

Wu, M., Si, M., Li, X., Song, L., Liu, J., Zhai, R., Cong, L., Yue, R., Yang, C., Ma, F., Xu, L., Wang, Z., 2019. PbCOP1.1 Contributes to the Negative Regulation of Anthocyanin Biosynthesis in Pear. Plants 8, 39. https://doi.org/10.3390/plants8020039

Wu, S., Li, H., Zhou, X., Liang, P., Zhang, X., Jiang, Y., Huang, X., 2016. A novel pilot-scale stacked microbial fuel cell for efficient electricity generation and wastewater treatment. Water Research 98, 396–403. https://doi.org/10.1016/j.watres.2016.04.043

Xiao, Y., Chen, L., Li, C., Ma, J., Chen, R., Yang, B., Liu, G., Liu, S., Fang, J., 2023. Role of the rhizosphere bacterial community in assisting phytoremediation in a lead-zinc area. Frontiers in Plant Science 13, 1106985. https://doi.org/doi: 10.3389/fpls.2022.1106985

Xu, J.-Y., Xu, H., Yang, X.-L., Singh, R.P., Li, T., Wu, Y., Song, H.-L., 2021. Simultaneous bioelectricity generation and pollutants removal of sediment microbial fuel cell combined with submerged macrophyte. International Journal of Hydrogen Energy 46, 11378–11388. https://doi.org/10.1016/j.ijhydene.2020.06.007

Yang, F., Wang, K.-C., Huang, Y., 2015. Energy-Neutral Communication Protocol for Very Low Power Microbial Fuel Cell Based Wireless Sensor Network. IEEE Sensors J. 15, 2306–2315. https://doi.org/10.1109/JSEN.2014.2377031

Yang, X., Chen, S., 2021. Microorganisms in sediment microbial fuel cells: Ecological niche, microbial response, and environmental function. Science of The Total Environment 756, 144145. https://doi.org/10.1016/j.scitotenv.2020.144145

Yaqoob, A.A., Ibrahim, M.N.M., Rodríguez-Couto, S., 2020. Development and modification of materials to build cost-effective anodes for microbial fuel cells (MFCs): An overview. Biochemical Engineering Journal 164, 107779. https://doi.org/10.1016/j.bej.2020.107779

Yeruva, D.K., Chiranjeevi, P., Butti, S.K., Mohan, S.V., 2018. Self-sustained photocatalytic power generation using eco-electrogenic engineered systems. Bioresource Technology 260, 23–29. https://doi.org/10.1016/j.biortech.2018.03.063

You, S., Gong, X., Wang, W., Qi, D., Wang, X., Chen, X., Ren, N., 2016. Enhanced Cathodic Oxygen Reduction and Power Production of Microbial Fuel Cell Based on Noble-Metal-Free Electrocatalyst Derived from Metal-Organic Frameworks. Advanced Energy Materials 6, 1501497. https://doi.org/10.1002/aenm.201501497

Yu, B., Feng, L., He, Y., Yang, L., Xun, Y., 2021. Effects of anode materials on the performance and anode microbial community of soil microbial fuel cell. Journal of Hazardous Materials 401, 123394. https://doi.org/10.1016/j.jhazmat.2020.123394

Zabihallahpoor, A., Rahimnejad, M., Talebnia, F., 2015. Sediment microbial fuel cells as a new source of renewable and sustainable energy: present status and future prospects. RSC Adv. 5, 94171–94183. https://doi.org/10.1039/C5RA15279H

Zámocký, M., Koller, F., 1999. Understanding the structure and function of catalases: clues from molecular evolution and in vitro mutagenesis. Progress in Biophysics and Molecular Biology 72, 19–66. https://doi.org/10.1016/S0079-6107(98)00058-3

Zhang, F., Cheng, S., Pant, D., Bogaert, G.V., Logan, B.E., 2009. Power generation using an activated carbon and metal mesh cathode in a microbial fuel cell. Electrochemistry Communications 11, 2177–2179. https://doi.org/10.1016/j.elecom.2009.09.024

Zhang, L., Li, J., Zhu, X., Ye, D., Fu, Q., Liao, Q., 2017. Response of stacked microbial fuel cells with serpentine flow fields to variable operating conditions. International Journal of Hydrogen Energy 42, 27641–27648. https://doi.org/10.1016/j.ijhydene.2017.04.205

Zhang, L., Lv, P., Wang, Y., Lv, S., Liu, Y., Wang, R., Liu, L., 2024. Response of different plants to ecological floating bed-microbial fuel cells: Decontamination and power generation. Journal of Cleaner Production 458, 142474. https://doi.org/10.1016/j.jclepro.2024.142474

Zhao, F., Harnisch, F., Schröder, U., Scholz, F., Bogdanoff, P., Herrmann, I., 2006. Challenges and Constraints of Using Oxygen Cathodes in Microbial Fuel Cells. Environ. Sci. Technol. 40, 5193–5199. https://doi.org/10.1021/es060332p

Zhao, L., Deng, J., Hou, H., Li, J., Yang, Y., 2019. Investigation of PAH and oil degradation along with electricity generation in soil using an enhanced plant-microbial fuel cell. Journal of Cleaner Production 221, 678–683. https://doi.org/10.1016/j.jclepro.2019.02.212

Zhao, M., Ren, C.E., Ling, Z., Lukatskaya, M.R., Zhang, C., Van Aken, K.L., Barsoum, M.W., Gogotsi, Y., 2015. Flexible MXene/Carbon Nanotube Composite Paper with High Volumetric Capacitance. Advanced Materials 27, 339–345. https://doi.org/10.1002/adma.201404140

Zhao, Q., Ji, M., Li, R., Ren, Z.J., 2017. Long-term performance of sediment microbial fuel cells with multiple anodes. Bioresource Technology 237, 178–185. https://doi.org/10.1016/j.biortech.2017.03.002

Zhao, Q., Li, R., Ji, M., Ren, Z.J., 2016. Organic content influences sediment microbial fuel cell performance and community structure. Bioresource Technology 220, 549–556. https://doi.org/10.1016/j.biortech.2016.09.005

LIST OF PUBLICATIONS

Communicated/communicating

Dutta A, Kalita N, Barbora L, Goswami P. An approach to eliminate voltage reversal in series connected plant-assisted sediment microbial fuel cells through surface area tuning of the anode. (Submitted)

Dutta A, Barbora L, Goswami P. Design and fabrication of a self-powered voltage-booster for enabling real-time applications of Water lettuce-Assisted Sediment Microbial Fuel Cell. (Communicating)

Published

Dutta A, Barbora L, Stom D, Goswami P. Improving Power Performance of Sediment Microbial Fuel Cell through Water Lettuce (*Pistia stratiotes*) Assisted Boosting of Cathodic Activity. Renewable and Sustainable Energy Reviews 2025; 215:115565

Dutta A, Jacob CA, Das P, Corton E, Stom D, Barbora L, Goswami P. A review on power management systems: An electronic tool to enable Microbial Fuel Cells for powering range of electronic appliances. Journal of Power Sources 2022; 517:230688.

Collaborative publications

Bachu V, Mili M, Dutta A, Thungon PD, Goswami P. Electrochemiluminescence-Based Lateral Flow Assay for Detection of Cardiac Troponin T Using Aptamers Developed through a Modified SELEX Technique. ACS Applied Optical Materials 2024; 2 (8): 1688-1698.

Hemdan BA, Jadhav DA, Dutta A, Goswami P. Facilitating the electrochemical characterization and biofilm enrichment through anode modification in microbial fuel cells. Journal of Water Process Engineering 2023; 54:104065.

Bora D, Dutta A, Mahanta P, Goswami P, Stom D, Barbora L. Membrane electrode assembly hybridized anaerobic digester for co-generation of methane enriched biogas and electricity. Fuel 2022; 316:123315.

Das P, Bachu V, Barbora L, Dutta A, Sarma MK, Goswami P. Passive fuel delivery and efficient anoxic condition in anode improve performance of methanol biofuel cell. Applied Energy 2022; 305:117824.

Conferences

Dutta A, Barbora L, Thakuria A, Goswami P, Stom D. Duckweed assisted sediment microbial fuel cell for powering small scale devices. International Conference on Recent Trends in Developments of Thermo-fluids and Renewable Energy (TFRE) 2020.

Patents

Barbora L, Bora D, Dutta A, Mahanta P, Kalita JM, Deori SK. Title of invention: Anaerobic Digester-Membrane Electrode Assembly (ADMEA) System for Producing Enriched Biogas and Electricity. Grant No. - 401901 (2021)

Goswami P, Das P, Borbora L, Dutta A, Sarma MK. Title of the invention: Enzymatic Biofuel Cell. Grant No. - 550361 (2019).

Journal of Power Sources 517 (2022) 230688

Contents lists available at ScienceDirect

Journal of Power Sources

journal homepage: www.elsevier.com/locate/jpowsour

A review on power management systems: An electronic tool to enable microbial fuel cells for powering range of electronic appliances

Arup Dutta [a], Caraline Ann Jacob [a], Priyanki Das [a], Eduardo Corton [c], Devard Stom [d,e,f], Lepakshi Barbora [a], Pranab Goswami [b,*]

[a] School of Energy Science and Engineering, Indian Institute of Technology Guwahati, India
[b] Department of Biosciences and Bioengineering, Indian Institute of Technology Guwahati, India
[c] Laboratorio de Biosensores y Bioanálisis IQUIBICEN-CONICET, UBA, Argentina
[d] Irkutsk National Research Technical University, Russia
[e] Baikal Museum of the Irkutsk Scientific Center of the Siberian Branch of the Russian Academy of Sciences, Russia
[f] Irkutsk State University, Russia

HIGHLIGHTS

- Microbial fuel cells (MFCs) produce only limited amount of electrical energy.
- The application of MFCs is restricted due to their low energy.
- Coupling a power management system (PMS) could enhance the output power of MFC.
- PMS mainly consists a charge pump, a super capacitor, and a boost converter.

GRAPHICAL ABSTRACT

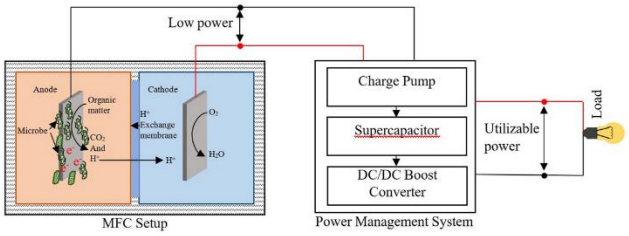

ARTICLE INFO

Keywords:
Bioelectrochemistry
Charge pump
DC/DC converter
Microbial fuel cells
Power management system (PMS)
Supercapacitor (SC)

ABSTRACT

Microbial fuel cells (MFCs) receive substantial research interest for their eco-friendly and energy conversion ability. Along with the production of electrical energy, a synergistic benefit of MFCs is also gained from their capability to reduce organic contaminant load in polluted water. The sub-categories of MFCs such as Sediment MFC and Plant MFC also have great prospects for bioremediation and energy conversion processes. However, the efficiency of these renewable energy-producing systems needs significant improvement for their real world application through commercial paradigm. This review mainly focuses on the power management systems (PMSs) that can be used in conjunction with the MFCs to improve its energy output for powering various ranges of electronic appliances. A PMS is a device that is constituted of some electronic components to work together in order to convert a low electrical input into a utilizable power output. The basic configuration of PMS mainly entails a charge pump, a supercapacitor, and a boost converter. Integration of these basic power management systems enables the enhancement of the output characteristic of MFCs to intermittently power small-scale appliances.

* Corresponding author. Department of Biosciences and Bioengineering, Indian Institute of Technology Guwahati, India.
E-mail addresses: lopab@iitg.ac.in (L. Barbora), pgoswami@iitg.ac.in (P. Goswami).

https://doi.org/10.1016/j.jpowsour.2021.230688
Received 30 July 2021; Received in revised form 8 October 2021; Accepted 23 October 2021
Available online 3 November 2021

Renewable and Sustainable Energy Reviews 215 (2025) 115565

Contents lists available at ScienceDirect

Renewable and Sustainable Energy Reviews

journal homepage: www.elsevier.com/locate/rser

Improving power performance of sediment microbial fuel cell through Water lettuce (*Pistia stratiotes*) assisted boosting of cathodic activity

Arup Dutta [a], Lepakshi Barbora [a,*], Devard Stom [c], Pranab Goswami [b,**]

[a] School of Energy Science and Engineering, Indian Institute of Technology Guwahati, Assam, 781039, India
[b] Department of Biosciences and Bioengineering, Indian Institute of Technology Guwahati, Assam, 781039, India
[c] Faculty of Biology and Soil, Irkutsk State University, Irkutsk, Russia

ARTICLE INFO

Keywords:
Cathode potential
Dissolved oxygen
Ionic conductivity
pH
Self-sustainable
Water lettuce
Biofilm

ABSTRACT

Sediment microbial fuel cells (SMFCs) are emerging as a promising green energy technology with enormous application potential for wastewater treatment and linked electrical energy production. However, the practical application of these devices is challenged by their low-performance factors pertaining to the imbalanced electrolyte and oxygen levels and weak cathodic functions in open environment conditions. This study explored to address the poor performance of the SMFC by coupling it with a free-floating aquatic plant, Water lettuce. Growth of the plant balanced the catholyte pH in the range of 7.2–7.6, increased the ionic conductivity by 60 %, stabilized the sub-surface water oxygen level, and boosted the cathodic potential by ~102 mV and ~49 mV in open and close circuit operations mode, respectively. The cumulative effect of these inputs led to producing a power density of 22.45 mW/m^2 and a current density of 136.84 mA/m^2 at 2 kΩ and 50 Ω loads, respectively. The enhanced cathodic performance was also attributed to the colonization of Water lettuce root bacteria as biofilm on the cathode that supported catalytic oxygen reduction on the graphite electrode. Metagenonic analysis indicated the biofilm is created mostly by aerobic microbes such as *Ferrovibrio terrae, Comamonas aquatic, Achromobacter xylosoxidans, Hydrogenophaga taeniospiralis* etc. bearing catalase enzyme, *Pannonibacter phragmitetus, Streptococcus pyogenes, Streptococcus mutans* etc. bearing heme enzyme and these microbes synergistically catalysed cathodic reduction reactions. This study demonstrated the positive role of Water lettuce in boosting the power performance of SMFC mainly by activating the cathodic functions of the setup.

Nomenclature

Abbreviations		*Notations/symbols*	
SMFC	Sediment Microbial Fuel Cell	E	Reduction potential
WL	Water Lettuce (*Pistia stratiotes*)	C	DO concentration
WL-SMFC	Water Lettuce assisted SMFC	p	Partial pressure of DO
C-SMFC	Control SMFC (SMFC without WL)	E^0	Standard reduction potential
OC	Open circuit	ΔH_r^0	Standard molar enthalpy of reduction
CC	Close circuit	ΔH_{sol}	Molar enthalpy change of solution
SMFC(CC)	WL-SMFC operated in CC condition	K_H^0	Henry's law constant
WL-SMFC (OC)	WL-SMFC operated in OC condition	R	Universal gas constant
C-SMFC (CC)	C-SMFC operated in CC condition	n	Number of e−(s)
C-SMFC (OC)	C-SMFC operated in OC condition	F	Faraday constant
DO	Dissolved oxygen	T	Normal temperature
OCP	Open circuit potential	T^0	Standard state temperature
NGS	Next Generation Sequencing	*Units*	
CV	Cyclic voltammetry	g/L	Gram per liter
DPV	Differential pulse voltammetry	mS/cm	MilliSiemens per centimeter
GCE	Glassy carbon electrode	mW/m^2	MilliWatt per square meter

(*continued on next column*)

(*continued*)

(*continued on next page*)

* Corresponding author.
** Corresponding author.
E-mail addresses: lopab@iitg.ac.in (L. Barbora), pgoswami@iitg.ac.in (P. Goswami).

https://doi.org/10.1016/j.rser.2025.115565
Received 19 March 2024; Received in revised form 23 February 2025; Accepted 26 February 2025
Available online 7 March 2025